Thesis

# (411)A super-flat interfaces in InGaAs-related III-V heterostructures grown by molecular beam epitaxy

Takahiro Kitada

OSAKA UNIVERSITY
Graduate School of Engineering Science
Department of Physical Science
Toyonaka Osaka

May 1999

Thesis

# (411)A super-flat interfaces in InGaAs-related III-V heterostructures grown by molecular beam epitaxy

Takahiro Kitada

OSAKA UNIVERSITY
Graduate School of Engineering Science
Department of Physical Science
Toyonaka Osaka

May 1999

## Abstract

Physical properties of InGaAs-related III-V heterostructures grown on (411)A-oriented substrates by molecular beam epitaxy (MBE) have been investigated. Effectively atomically flat heterointerfaces over a wafer-size area ["(411)A super-flat interfaces"] were found to be formed in these heterostructures, and pseudomorphic $In_{0.7}Ga_{0.3}As/In_{0.52}Al_{0.48}As$ modulation-doped quantum wells (MD-QWs) with higher electron mobilities were successfully grown on (411)A InP substrates by MBE.

The (411)A super-flat interfaces could be successfully formed in pseudomophic $In_xGa_{1-x}As$/AlGaAs QWs with $x$ up to 0.27 grown on (411)A GaAs substrates. A single and very sharp peak was observed in low-temperature photoluminescence (PL) from each of the (411)A InGaAs/AlGaAs QWs. PL (11 K) properties of $In_{0.25}Ga_{0.75}As$/AlGaAs single QWs also show much larger critical thickness ($\sim$ 20 nm) of a (411)A $In_{0.25}Ga_{0.75}As$ layer compared with that ($\sim$ 12 nm) of a conventional (100) $In_{0.25}Ga_{0.75}As$, which is probably due to much stable InGaAs growing surfaces. Enhanced In surface segregation was observed in (411)A InGaAs/(Al)GaAs superlattices (SLs) and QWs by HRXRD and PL measurements compared with that of the (100) SLs and QWs because of larger surface migration of group III atoms, nevertheless, degradation of the superior interface flatness in the (411)A QWs due to the enhanced In surface segregation was not observed, and the (411)A super-flat InGaAs/AlGaAs interfaces could be formed at a wide substrate temperature range of 450–540°C.

The (411)A super-flat interfaces could be also formed in InGaAs/InAlAs QWs lattice-matched to (411)A InP substrates by MBE. High-quality InGaAs and InAlAs epitaxal layers were successfully grown on (411)A InP substrates at optimized MBE growth conditions. A single and very sharp PL peaks at 4.2 K were observed from the (411)A InGaAs/InAlAs QWs over a wafer-size area, and the PL linewidths of the (411)A QWs are almost comparable to those of splitted peaks of (100) growth-interrupted InGaAs/InAlAs QWs. Furthermore, interface flatness in the (411)A InGaAs QWs could be slightly improved by using $(InGaAs)_2(InAlAs)_m$ short-period SL barriers with $m \leq 4$.

Based on these results, the pseudomorphic $In_{0.7}Ga_{0.3}As/In_{0.52}Al_{0.48}As$ MD-QWs with the (411)A super-flat interfaces were successfully grown on InP substrates by MBE. Higher two-dimensional electron gas (2DEG) mobilities were observed in the (411)A MD-QWs with well widths ($L_w$) of 12–18 nm compared with the corresponding (100) MD-QWs due to (1) the (411)A super-flat interfaces for $L_w$ = 12–16 nm and (2) larger critical thickness of the (411)A $In_{0.7}Ga_{0.3}As$ for $L_w$ = 18 nm. The 2DEG in the (411)A MD-QW with $L_w$ = 12 nm shows 27% higher mobility ($\mu$ = 108,000 $cm^2/Vs$) with 2DEG concentration of 1.5 $\times$ $10^{12}$ $cm^{-2}$ at T = 77 K than that ($\mu$ = 85,000 $cm^2/Vs$) of the corresponding (100) MD-QW in this study, and the $\mu$ of the (411)A MD-QW is the highest mobility in the previously reported ones. Theoretical analysis of the low-temperature (24 K) 2DEG mobilities confirms that the enhanced 2DEG mobilities in the (411)A MD-QWs are caused by reduced interface roughness scattering due to the (411)A super-flat interfaces.

# Contents

# Chapter 1

# Introduction

## 1.1 Introduction

Heterostructures consisting of III-V compound semiconductors have been widely studied because of their suitable structures for physical topics of low-dimensional electrons or excitons and electrical- and optical-device applications. Advanced progress of growth technologies of III-V compound semiconductor thin layers, such as molecular beam epitaxy (MBE) or metal organic chemical vapor deposition (MOCVD), enable us to obtain high-quality epitaxial layers with precisely controlled layer thickness in atomic scale, and they have supported development in research fields of III-V heterostructures (GaAs/AlGaAs, InGaAs/InAlAs). In addition, high-quality devices with the use of the III-V heterostructures, such as high electron mobility transistors (HEMTs) [1] or quantum well (QW) lasers [2], are successfully fabricated by MBE or MOCVD, and they are used in satellite broadcasting systems, mobile phones and optical communication systems, and so on.

InGaAs-related III-V heterostructures, such as InGaAs/InAlAs system lattice-matched to InP substrates, are the most interesting materials, because of their superior physical properties (larger conduction band offset and lighter electron effective mass) for low-noise and high-frequency devices [3, 4, 5] compared with those of conventional GaAs/AlGaAs system. In addition, an energy gap of $In_{0.53}Ga_{0.47}As$ lattice-matched to InP is 0.75 eV, which is suitable for 1.5 $\mu$m optical devices [6, 7] used for optical communication networks. Pseudomorphic epitaxial growth of InGaAs-related III-V heterostructures, such as InGaAs/AlGaAs system on GaAs substrates and InGaAs/InAlAs system on InP substrates with lattice-mismatch, is one of the most interesting technologies, because

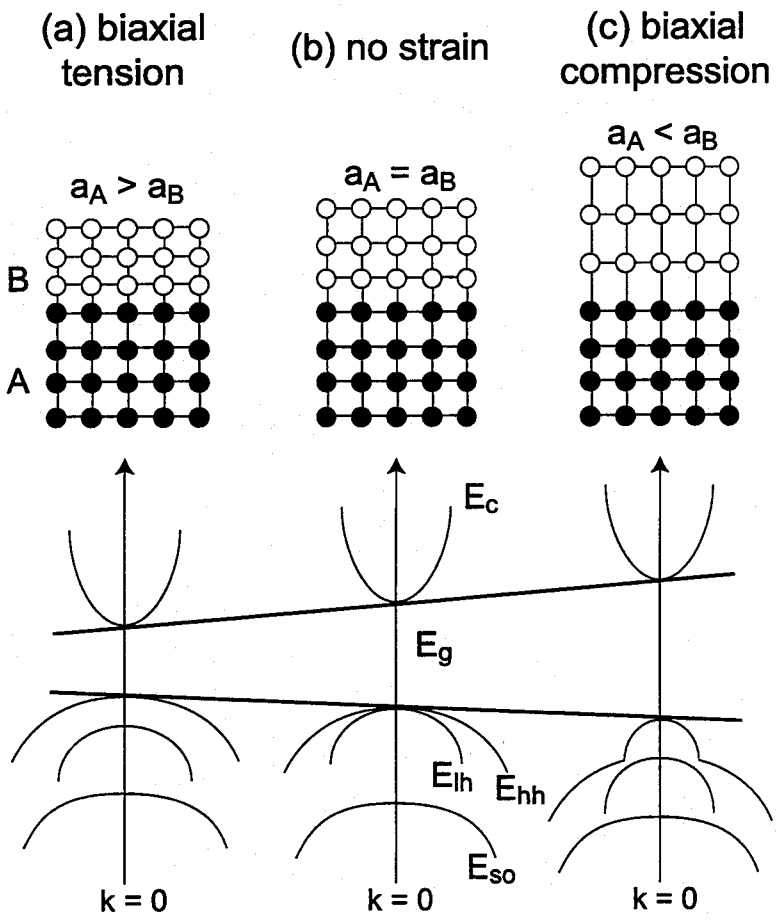


Figure 1.1: Schematic illustration of III-V heterostructures with (a) biaxial tensile strain, (b) no strain and (c) biaxial compression strain, and the corresponding conduction- and valence-band structures.

conduction- and valence-band structures are modulated by an elastic strain (biaxial compression or biaxial tensile strain) in the pseudomorphic layer as shown in Fig. 1.1. These pseudomorphic heterostructures without dislocations due to lattice-mismatch between III-V materials with different lattice constants can be obtained by MBE or MOCVD under a certain layer thickness so called "critical layer thickness". [8]

One of the most important factor to achieve high performance in III-V heterostrucute devices is improvement in heterointerface flatness. Roughness at heterointerfaces degrades optical gain in QW lasers because of degradation of uniformity in the QW layer thickness, and it also degrades electron mobility in HEMT structures because of electrons scattered by interface fluctuation. Therefore, it is very important to realize atomically flat interfaces over a whole device-size area in InGaAs-related III-V heterostructures to achieve various

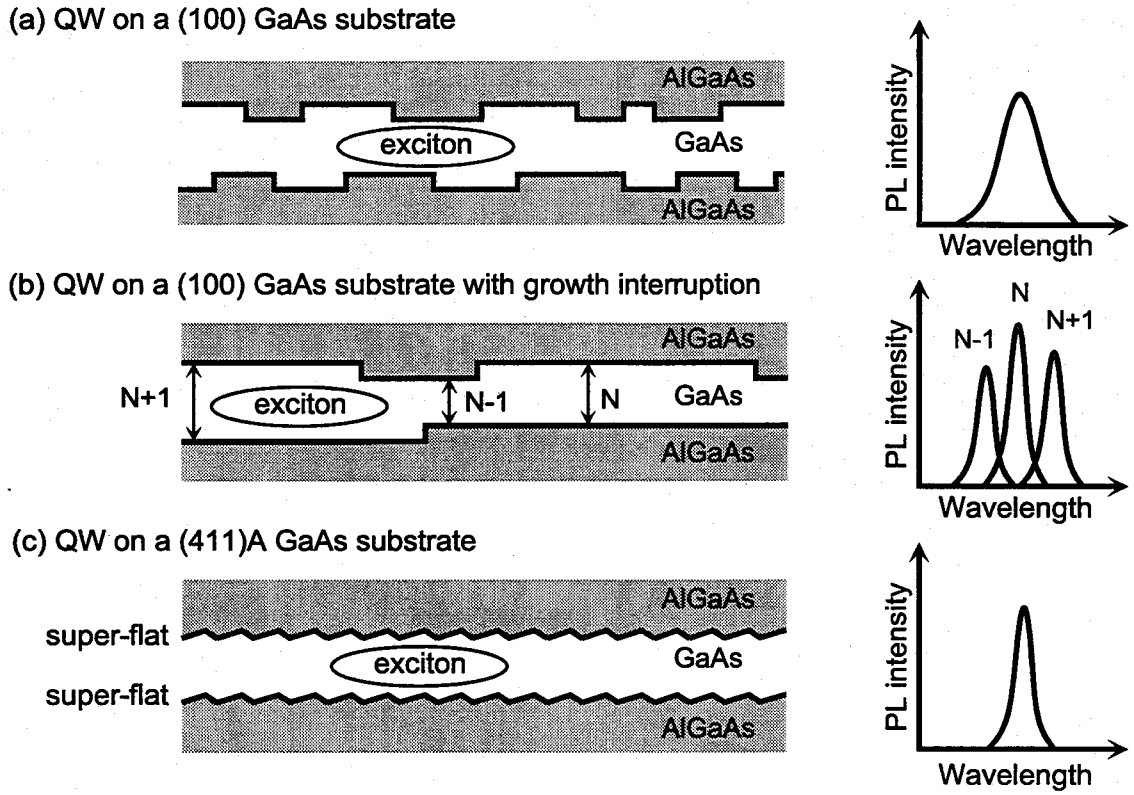


Figure 1.2: Schematic illustration of the cross sections of GaAs/AlGaAs QWs grown on (a) a (100) GaAs substrates without interruption and on (b) a (100) GaAs substrate with growth interruption and on (c) a (411)A GaAs substrate, and the corresponding photoluminescence spectra at low temperatures.

kinds of the quantum devices with better performance.

In 1993, Shimomura et al. proposed that extremely flat heterointerfaces can be formed in GaAs/AlGaAs QWs grown on (411)A-oriented GaAs substrates by MBE [9]. Linewidths of low-temperature photoluminescence (PL) peaks from the (411)A QWs are much narrower than those of the conventional (100) QWs, which have $\pm$ one-monolayer fluctuation at heterointerfaces [Fig. 1.2(a)], and they are as narrow as those of growth-interrupted (100) QWs. The growth-interruption at heterointerfaces is one of most interesting technique to achieve atomically flat interfaces [10, 11], however, they are formed only in a very small area of about a few $\mu m^2$, because size of atomic steps at heterointerfaces are limited by surface migration length of Ga atoms. Therefore, two or three PL peaks with narrow linewidths are observed from the growth-interrupted (100) QWs [Fig. 1.2(b)]. In contrast, the (411)A QWs exhibit single PL peaks with narrow linewidths

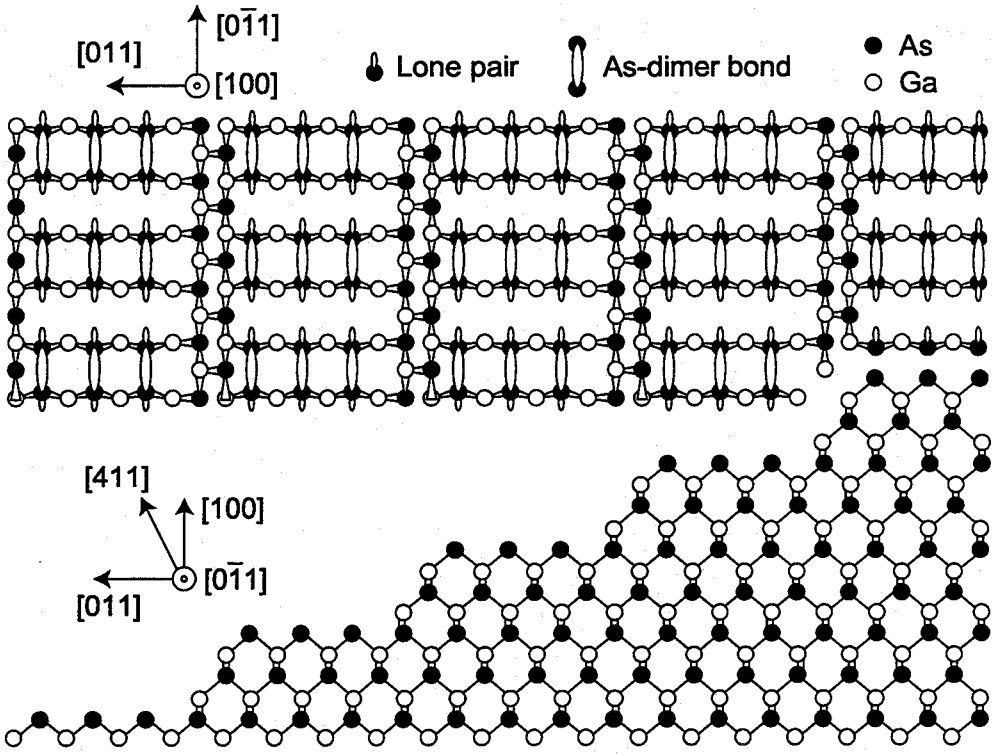


Figure 1.3: Atomic model of (411)A GaAs surface.

over an extraordinarily large area ($\sim$ 1 cm$^2$) [Fig. 1.2(c)] [12], indicating that effectively atomically flat interfaces are formed in the (411)A GaAs/AlGaAs QWs over a wafer-size area ["(411)A super-flat interfaces"]. An atomic model of the (411)A GaAs surface [the (0$\bar{1}$1) cross section] is shown in Fig. 1.3(a), which consists of (100) terraces with three As-dimer rows in the [011] direction and (111)A steps with a two-monolayer height. The period of the surface corrugation is 1.69 nm in the [$\bar{1}$22] direction. The exciton radius (12 $\sim$ 15 nm) for a GaAs/AlGaAs QW [13] is about one order of magnitude larger than this period. Therefore, this atomic-size corrugation along the [$\bar{1}$22] direction is almost completely averaged out over a size of the exciton. This leads to very narrow PL peak widths of the (411)A GaAs/AlGaAs QWs, which are better than or equal to those of splitted peaks of the GaAs/AlGaAs QWs grown with the growth interruption on the (100) substrates. In addition, GaAs/AlGaAs HEMT structures and resonant tunneling diodes with (411)A super-flat interfaces exhibit much improved electron mobility [14] and peak-to-valley current ratio [15], respectively, compared with those structures with conventional (100) interfaces. Therefore, InGaAs-related III-V heterostructures grown on

(411)A-oriented substrates are considered to be suitable for fabrication of electrical- and optical-devices with improved performance, because they are expected to have extremely flat heterointerfaces.

The purposes of this work are investigation of interface flatness in (1) pseudomorphic InGaAs/AlGaAs system on (411)A GaAs substrates and (2) InGaAs/InAlAs lattice-matched to (411)A InP substrates , and (3) an application of the (411)A super-flat interfaces to pseudomorphic InGaAs/InAlAs HEMT structures grown on InP substrates in order to achieve better performance in low-noise and high-frequency devices. In chapter 2, MBE system and characterization methods are described. Optical and structural properties of pseudomorphic InGaAs/AlGaAs QWs and superlattices grown on (411)A GaAs substrates by MBE are given in chapter 3. Interface flatness in pseudomorphic (411)A InGaAs/AlGaAs QWs, critical layer thickness of pseudomorphic (411)A InGaAs and effect of surface segregation of In atoms are discussed. In chapter 4, optical and structural properties of InGaAs and InAlAs epitaxial layer and InGaAs/InAlAs QWs lattice-matched to (411)A InP substrates are described. Improved crystalline structure and interface flatness in (411)A InGaAs/InAlAs system are presented there. Electrical properties of pseudomorphic InGaAs/InAlAs modulation-doped QWs (MD-QWs) grown on (411)A InP substrates by MBE are presented in chapter 5. Enhanced electron mobilities of (411)A InGaAs/InAlAs MD-QWs are discussed in terms of their superior interface flatness. Finally, conclusions are give in Chapter 6.

# Bibliography


[1] T. Mimura, S. Hiyamizu, T. Fujii, and K. Nanbu: Jpn. J. Appl. Phys. **19** (1980) L225.

[2] W. T. Tsang: Appl. Phys. Lett. **39** (1981) 786.

[3] L. D. Nguyen, A. S. Brown, M. A. Thompson and L. M. Jelloian: IEEE Trans. Electron. Devices **ED-39** (1992) 2007.

[4] N. Iwata, M. Tomita and M. Kuzuhara: Electon. Lett **29** (1993) 628.

[5] K. B. Chough, T. Y. Chang, M. D. Feuer, N. J. Sauer and B. Lalevic: IEEE Electron. Device Lett. **ED-13** (1992) 451.

[6] W. T. Tsang: Appl. Phys. Lett. **49** (1986) 1010.

[7] H. Temkin, K. Alavi, W. R. Wagner, T. P. Pearsall and A. Y. Cho: Appl. Phys. Lett. **42** (1983) 845.

[8] J. W. Mathews and A. E. Blakesee: J. Vac. Sci. Technol. **14** (1977) 989.

[9] S. Shimomura, A. Wakejima, A. Adachi, Y. Okamoto, N. Sano, K. Murase, and S. Hiyamizu: Jpn. J. Appl. Phys. **32** (1993) L1728.

[10] M. Tanaka, H. Sakaki, J. Yoshino, and T. Furuta: Surf. Sci. **174** (1986) 65.

[11] J. H. Neave, B. A. Joyce, P. J. Dobson, and N. Norton: Appl. Phys. **A31** (1983) 1.

[12] S. Hiyamizu, S. Shimomura, A. Wakejima, S, Kaneko, A. Adachi, Y. Okamoto, N. Sano, and K. Murase: J. Vac. Sci. Technol. **B12** (1994) 1043.

[13] Y. Shinozuka, and M. Matsuura: Phys. Rev. **B29** (1984) 3717.

[14] S. Shimomura, K. Shinohara, K. Kasahara and S. Hiyamizu: Microelectron. Eng. **43–44** (1998) 213.

[15] K. Shinohara, K. Kasahara, S. Shimomura, A. Adachi, N. Sano and S. Hiyamizu: J. Cryst. Growth **175/176** (1997) 924.

# Chapter 2

# Experimental techniques

This chapter describes experimental techniques used in this study. Details of MBE systems, substrate preparation procedures and characterization methods employed in this study are shown here.

## 2.1 MBE system

All samples used in this study were grown by a Nissin RB 2001G or a VG semicon V80H MK-II MBE system.

### 2.1.1 Nissin RB 2001G MBE system

The Nissin RB 2001G MBE system consists of two vacuum chambers (the growth chamber and the loading chamber) and the pumping system. The growth chamber is evacuated by an ion getter pump (ANELVA; PIC-400IP) during normal operation. The basic pressure of the growth chamber is less than $3 \times 10^{-11}$ Torr. The growth chamber is equipped with a liquid nitrogen shroud to trap impurities during MBE growth. The loading chamber is evacuated by a turbo molecular pump (SEIKO; STP-200). The basic pressure of the loading chamber is less than $3 \times 10^{-8}$ Torr. The conventional effusion cells are used for Ga, Al, In, As, Si, and Be as group III, V, and dopant sources. Group III and V fluxes are measured by a beam flux monitor with a nude ion gauge at the growth position. Substrate temperature is monitored with an optical pyrometer calibrated with the melting points of Al sheets (660°C) and InSb substrates (525°C). Reflection high-energy electron diffraction (RHEED) and quadrupole mass spectrometer (QMS, ANELVA;

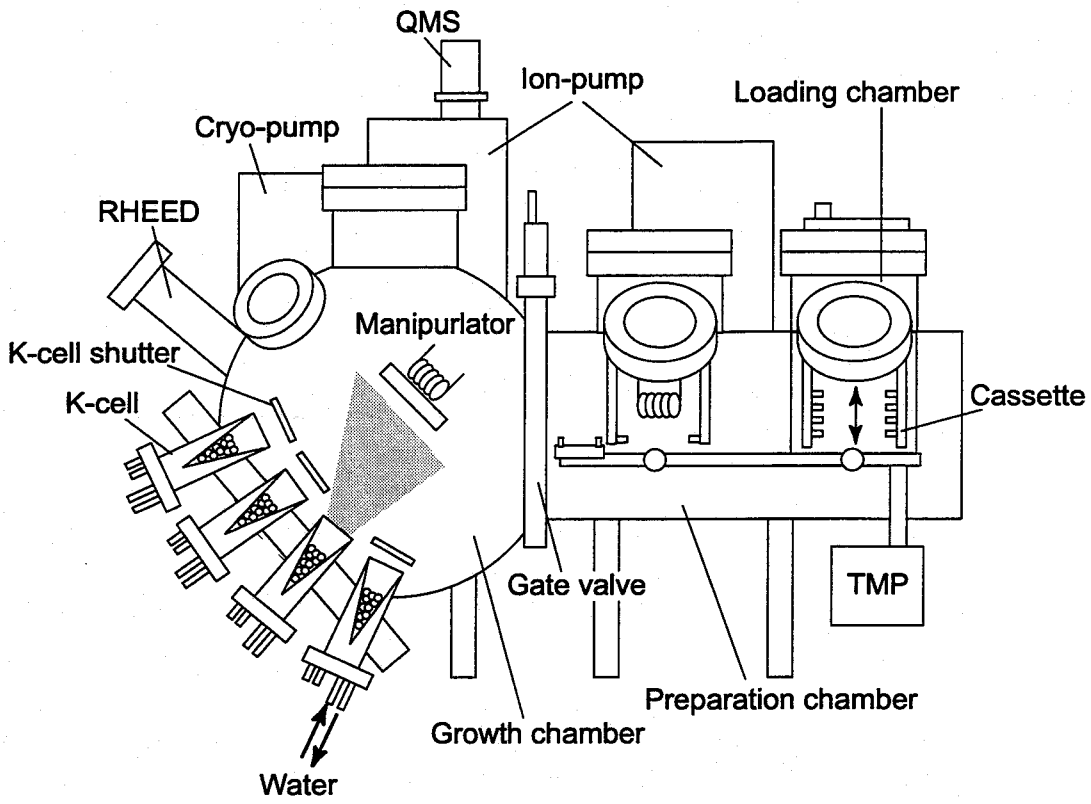


Figure 2.1: Schematic illustration of the VG semicon V80H MK-II MBE system.

AQA-360) are used as *in situ* monitoring system to control the MBE growth.

### 2.1.2 VG semicon V80H MK-II MBE system

A schematic illustration of the VG semicon V80H MK-II MBE system is shown in Fig. 2.1. The VG semicon V80H MK-II MBE system consists of three vacuum chamber (the growth chamber, the preparation chamber and the loading chamber) and these chamber is separately evacuated by the pumping system. The growth chamber is evacuated by an ion getter pump (VARIAN; 400 $l/s$ Triode VacIon Pump), a cryo-pump (CTI-CRYOGENICS; Cryo-Torr 8) and a liquid nitrogen shroud during MBE growth. The basic pressure of the growth chamber is less than $5 \times 10^{-11}$ Torr. The preparation chamber ($< 5 \times 10^{-10}$ Torr) and the loading chamber ($< 1 \times 10^{-7}$ Torr) are evacuated by an ion getter pump (VARIAN; 220 $l/s$ Triode VacIon Pump) and a turbo molecular pump (BLAZERS; TPU-180H), respectively. The growth chamber has nine conventional effusion cells used as group III sources (two Ga, two Al and In), group V sources (two As) and dopants (Si, Be). Temperatures of the effusion cells and positions ("OPEN" or "CLOSE") of the

mechanical shutters are operated by a computer control system. Group III and V fluxes are measured by a beam flux monitor with a nude ion gauge at the growth position. Substrate temperature is monitored with an optical pyrometer calibrated with the melting points of Al sheets (660°C) and InSb substrates (525°C). RHEED and QMS are used as *in situ* monitoring system to control the MBE growth.

## 2.2 Substrate preparation

Process of the substrate preparation before MBE growth is very important to obtain a high-quality epitaxial layer. Here, we describe the preparation methods of (1) GaAs substrates and (2) InP substrates.

### 2.2.1 (411)A-oriented GaAs substrates

(411)A- and (100)-oriented GaAs substrates were degreased by boiled-trichloroethylene and they were cleaned by methanol in an ultrasonic bath. After rinsing by distilled water, they were etched by sulfuric acid etchant solution ($H_2SO_4 : H_2O_2 : H_2O = 5 : 1 : 1$) at a temperature of approximately 100°C, or etched by "Semico-Clean" (Furuuchi Chemical Corp., Japan) at room temperature. These substrates were soldered on molybdenum substrate holders with indium after rinsing by distilled water, and they were put in the loading chamber of the MBE system. After predegasing at 300°C in the loading chamber or the preparation chamber, the native oxides on the GaAs substrates were removed by heating up to 650°C in $As_4$ atmosphere ($\sim 10^{-6}$ Torr) in the MBE growth chamber.

### 2.2.2 (411)A-oriented InP substrates

(411)A- and (100)-oriented InP substrates were degreased by boiled-trichloroethylene and they were cleaned by methanol in an ultrasonic bath. After rinsing by methanol or distilled water, they were etched by 0.05% by volume $Br_2 : CH_3OH$ etchant or etched by "Semico-Clean" (Furuuchi Chemical Corp., Japan) at room temperature. These substrates were soldered on molybdenum substrate holders with indium after rinsing by methanol and distilled water, and they were put in the loading chamber of the MBE system. After

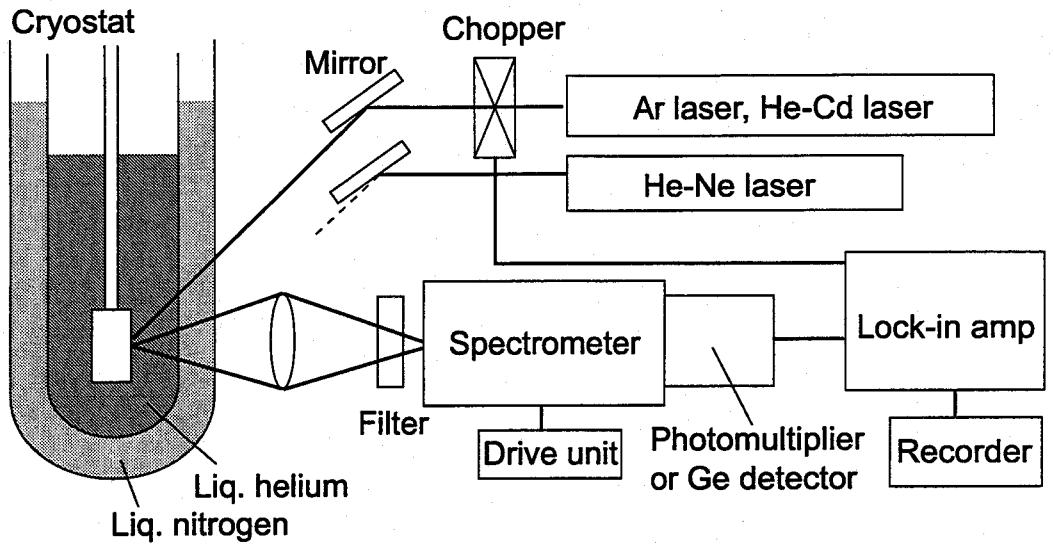


Figure 2.2: Block diagram of the photoluminescence equipment.

predegasing at 300°C in the loading chamber or the preparation chamber, the native oxides on the InP substrates were removed by heating up to 520°C in $As_4$ atmosphere ($\sim 10^{-6}$ Torr) in the MBE growth chamber.

## 2.3 Characterization methods

### 2.3.1 Photoluminescence measurements

Photoluminescence (PL) was used to characterize optical properties of the samples. Fig. 2.2 shows a block diagram of the PL equipment. The wavelength of the excitation laser was 514.5 nm ($Ar^+$ laser) or 325 nm (He-Cd laser) and the excitation power was changed from sample to sample (1 mW $\sim$ 7 mW). The excitation laser beam was focused on an area of a sample surface with a diameter of about 200 $\mu$m. Luminescence from the sample was monochromated and detected by a photomultiplier or a cooled Ge detector. The samples were cooled down by liquid helium (4.2K) or by a helium-gas closed-cycle cryostat ($\sim$ 10K).

### 2.3.2 Hall measurements

Hall measurements were carried out using the van der Pauw technique under a magnetic field of 0.5 T. Ohmic contacts to the samples were formed by AuGeNi metals. The

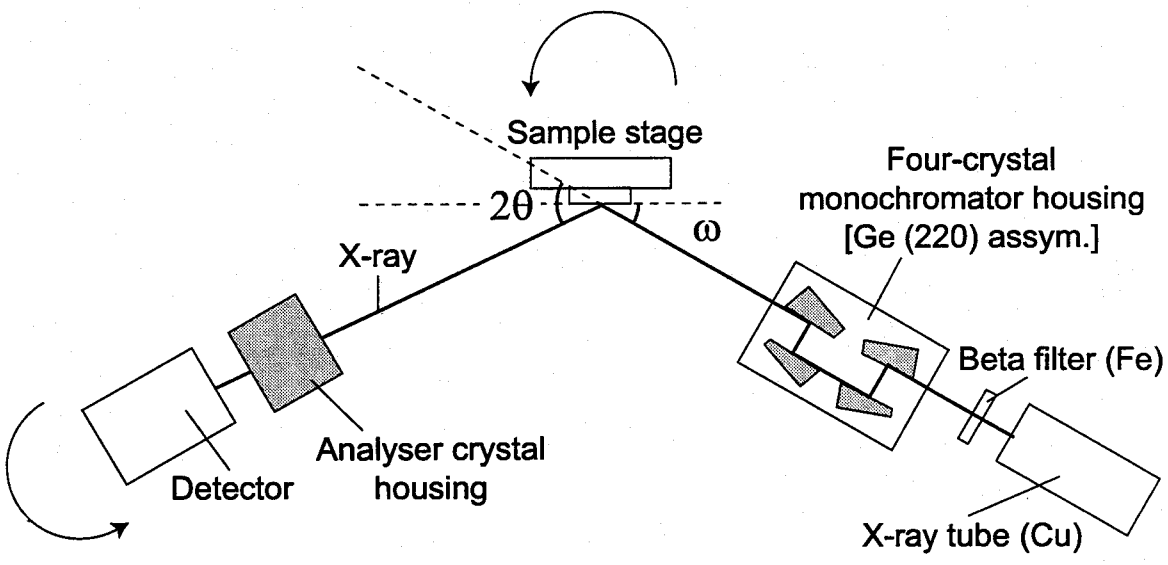


Figure 2.3: Block diagram of the HRXRD system.

samples were cooled to a temperature range of 24–300 K by using a helium-gas closed cycle cryostat or liquid nitrogen.

### 2.3.3 High-resolution X-ray diffraction measurements

High-resolution X-ray diffraction (HRXRD) system of a Phillips X'Pert MRD was used to characterize structural properties of the samples. Fig. 2.3 shows a block diagram of the HRXRD system. An incident X-ray beam with a wavelength ($\lambda = 0.15406$ nm) of Cu K$\alpha$1 was monochromated by a (220)-oriented Ge asymmetric four-crystal system. The samples were mounted on a computer-controlled goniometer stage. Rocking curves of the samples were measured by $\omega$-2$\theta$ scan (where $\omega$ and 2$\theta$ are the angles of the sample and detector relative to the incident X-ray beam) with a detector angular acceptance of $\sim 1°$. The reciprocal space maps of the samples were obtained by measuring a series of $\omega$-2$\theta$ scan curves with slightly changed $\omega$ values by using three (220) Ge reflection analyser crystals, which makes a detector angular acceptance to $\sim$ 12 sec.

### 2.3.4 Atomic force microscopy observations

Atomic force microscopy (AFM, type NANOSCOPE III) was used to observe cross-sectional structures or surface morphologies of the samples. In this study, the AFM was used in a 'Tapping mode' to reduce mechanical damage of a sample.

# Chapter 3

# Pseudmorphic InGaAs/AlGaAs system on (411)A GaAs substrates

## 3.1 Pseudomorphic InGaAs/AlGaAs QWs

Pseudomorphic InGaAs/AlGaAs heterostructures have attracted much interest for optical and electrical device applications such as high electron mobility transistors (HEMTs) and strained QW lasers. [1, 2, 3, 4] The (411)A super-flat interfaces can be achieved in lattice-matched GaAs/$Al_{0.3}Ga_{0.7}As$ heterostructures, however it is not clear whether the super-flat interfaces can be also realized in pseudomorphic heterostructures such as InGaAs/AlGaAs QWs, because formation of the (411)A super-flat interfaces depends sensitively on MBE growth conditions. In this section, we study MBE growth of pseudomorphic InGaAs/AlGaAs QWs with various In contents grown on (411)A GaAs substrates and characterize flatness of InGaAs/AlGaAs heterointerfaces by low-temperature photoluminescence measurements.

### 3.1.1 MBE growth of InGaAs/AlGaAs QWs

(411)A-oriented GaAs substrates were etched by sulfuric acid etchant solution ($H_2SO_4$ : $H_2O_2$ : $H_2O = 5 : 1 : 1$) after degreasing and were then loaded into a growth chamber of a Nissin RB-2001G MBE system. $In_xGa_{1-x}As/Al_yGa_{1-y}As$ QWs with well widths ($L_w$) of 1.2–12.0 nm and a barrier width of 20 nm on $GaAs/Al_yGa_{1-y}As$ buffer layers were grown on (411)A and (100) GaAs substrates at a substrate temperature ($T_s$) of 520°C. The V/III pressure ratios were 8.5 for the (411)A QWs and 10.5 for the (100) QWs which are the optimized V/III pressure ratios for corresponding samples. Growth rates of

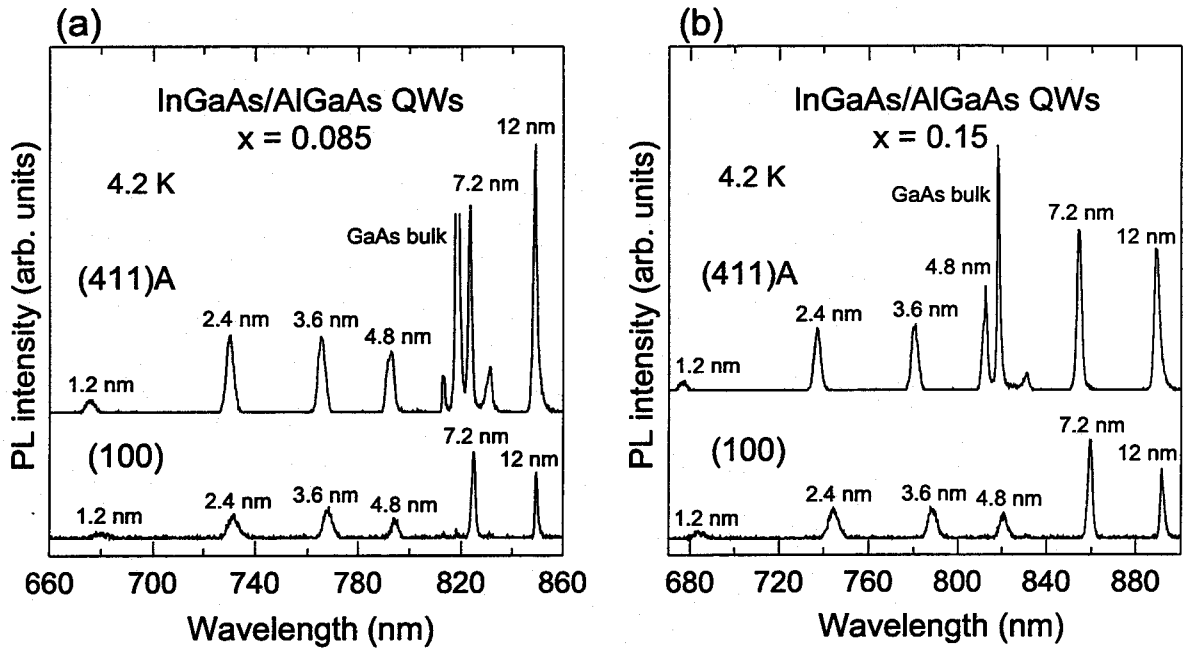


Figure 3.1: Photoluminescence spectra at 4.2 K from pseudomorphic $In_xGa_{1-x}As/Al_{0.28}Ga_{0.72}As$ QWs with In contents of (a) $x = 0.085$ and (b) $x = 0.15$ grown on (411)A and (100) GaAs substrates.

GaAs and AlAs were 1.0 $\mu$m/h and 0.39–0.4 $\mu$m/h, respectively, as determined from layer thicknesses of GaAs and AlGaAs of GaAs/AlGaAs superlattice buffer layers observed by cross-sectional scanning electron microscopy (SEM). The Al content ($y = 0.28$–$0.3$) of AlGaAs was determined by reflection high energy electron diffraction (RHEED) oscillations for GaAs and AlAs layers. An In content ($x = 0$–$0.35$) of each sample was determined by PL peak energy (4.2 K) of the (100) and (411)A QWs with $L_w = 12$ nm, or high resolution X-ray diffraction measurements of 100-nm-thick InGaAs grown on the (411)A and (100) GaAs substrats. In contents of the (411)A sample were the same as those of the (100) samples. The substrates were rotated at 30 rpm during MBE growth.

### 3.1.2 Photoluminesce measurements

Figure 3.1 shows PL spectra at 4.2 K from the pseudomorphic $In_xGa_{1-x}As/Al_{0.28}Ga_{0.72}As$ QWs with (a) $x = 0.085$ and (b) $x = 0.15$ grown on (411)A and (100) GaAs substrates. The wavelength of an excitation laser was 514.5 nm and the excitation power was 5 mW. The excitation laser beam was focused on an area, approximately 200 $\mu$m in diameter of the sample surface. Weak and broad peaks at 680.0, 731.4, 767.8, 794.2, 824.8 and

849.4 nm in Fig. 3.1(a) correspond to the luminescences from the (100) QWs of $L_w$ = 1.2, 2.4, 3.6, 4.8, 7.2 and 12.0 nm, respectively. On the other hand, PL peaks from the (411)A QWs are observed at 675.4, 729.8, 765.2, 792.8, 823.4 and 849.0 nm. The peak at 818 nm is from GaAs of the buffer layer. The most characteristic feature is a much smaller linewidth of each PL peak of the (411)A QWs. This result shows improved flatness of the (411)A $In_{0.085}Ga_{0.915}As/Al_{0.28}Ga_{0.72}As$ interfaces. A slight blue-shift of the luminescence peaks was observed in the case of all the (411)A QWs compared with those of the corresponding (100) QWs. This is probably due to differently strain-induced band gap shift of the (411)A QWs. [8] Figure 3.1(b) shows PL spectra from the $In_{0.15}Ga_{0.85}As/Al_{0.28}Ga_{0.72}As$ QWs with $L_w$ = 1.2–12 nm grown on (411)A and (100) GaAs substrates. The (411)A QWs also show apparently narrower PL peaks than the (100) QWs, especially for thin QWs with $L_w$ = 1.2, 2.4, 3.6 and 4.8 nm. Figure 1 also demonstrates that the integrated PL intensities of the (411)A QWs are much stronger than those of the (100) QWs, which suggests much better optical quality of the (411)A InGaAs/AlGaAs QWs.

Figure 3.2 illustrates full widths at half maximum (FWHMs) of the PL peaks from the $In_xGa_{1-x}As/Al_{0.28}Ga_{0.72}As$ QWs grown on (411)A and(100) GaAs substrates with (a) $x$ = 0.085 and (b) $x$ = 0.15 as a function of wavelength. In the case of the lower In content ($x$ = 0.085), the FWHM (7.3 meV) of the narrow (411)A QW ($L_w$ = 2.4 nm) is about 30% smaller than that (10.5 meV) of the (100) QW, although the FWHMs of the wide (411)A QWs ($L_w$ = 7.2, 12 nm) are almost comparable to those of (100) QWs. In the case of the QW of $L_w$ = 4.8 nm, however, PL FWHM from the (411)A QW is larger than that from the (100) QW. This is probably because of a double-peaked PL line due to the free and bound excitons in the (411)A QW. In the case of the higher In content ($x$ = 0.15), the narrow (411)A QW ($L_w$ = 2.4 nm) revealed FWHM (7.3 meV) which is about 40% smaller than that (11.9 meV) of the (100) QW [Fig. 3.2(b)]. On the other hand, the PL FWHM of the wide (411)A QW ($L_w$ = 12 nm) is a little larger than that of (100) QW, which is probably due to a slightly larger alloy disorder in the InGaAs QW layer of the (411)A QW. The observed FWHM values (2–4 meV) of the (411)A and (100) QWs ($L_w$ = 12 nm, $x$ = 0.085–0.15) in this study are smaller than a previously reported value (6.7

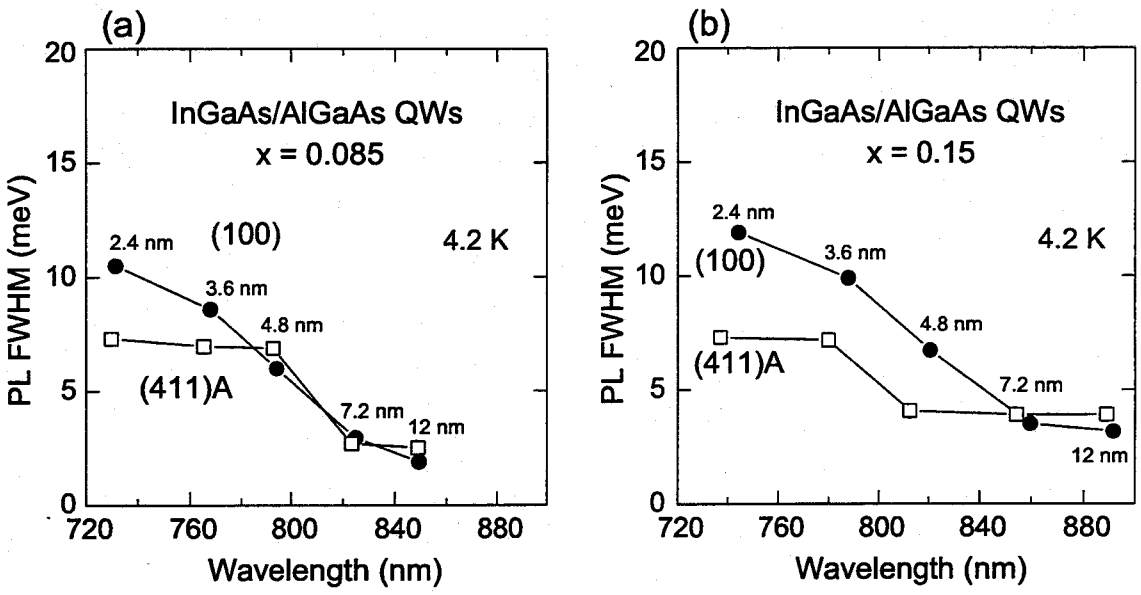


Figure 3.2: FWHMs of PL peaks at 4.2 K from pseudomorphic $In_xGa_{1-x}As/Al_{0.28}Ga_{0.72}As$ QWs with (a) $x = 0.085$ and (b) $x = 0.15$ grown on (411)A and (100) GaAs substrates as a function of wavelength.

meV at 4.2 K) for a $GaAs/In_{0.11}Ga_{0.89}As/Al_{0.23}Ga_{0.77}As$ QW ($L_w$ = 15 nm) on a (100) GaAs substrate. [5]

### 3.1.3 Excited position dependence of photoluminescence

In order to observe uniformity of QW thickness over a macroscopic area, we measured the lateral variation of the PL peak energy and FWHM at 4.2 K for the $In_xGa_{1-x}As/Al_{0.3}Ga_{0.7}As$ QW ($x = 0.07$) with $L_w$ = 2.4 nm grown on (411)A GaAs substrate by changing the excitation position on the wafer surface with an area of 8 mm × 5 mm. Observed positions are at the distances of $z$ = 1, 2, 3, 4, 5, 6, 7 mm from the edge of the wafer. Peak energy and FWHM of the luminescence from the (411)A QW with $L_w$ = 2.4 nm are plotted as a function of distance ($z$) in Fig. 3.3. The peak energy varies continuously from 1.6906 to 1.6933 eV with increasing $z$. This corresponds to a lateral variation of only 0.03 nm [1% of $L_w$ = 2.4 nm and much smaller than 1 ML thickness (0.28 nm) of (100) GaAs layer] in the thickness of the InGaAs well layer over a distance of 6 mm, which reflects the thickness variation of an InGaAs layer grown by our MBE system. This is due to the continuous growth of InGaAs and AlGaAs layers by the step-flow growth mode on an atomically corrugated (411)A surface as described

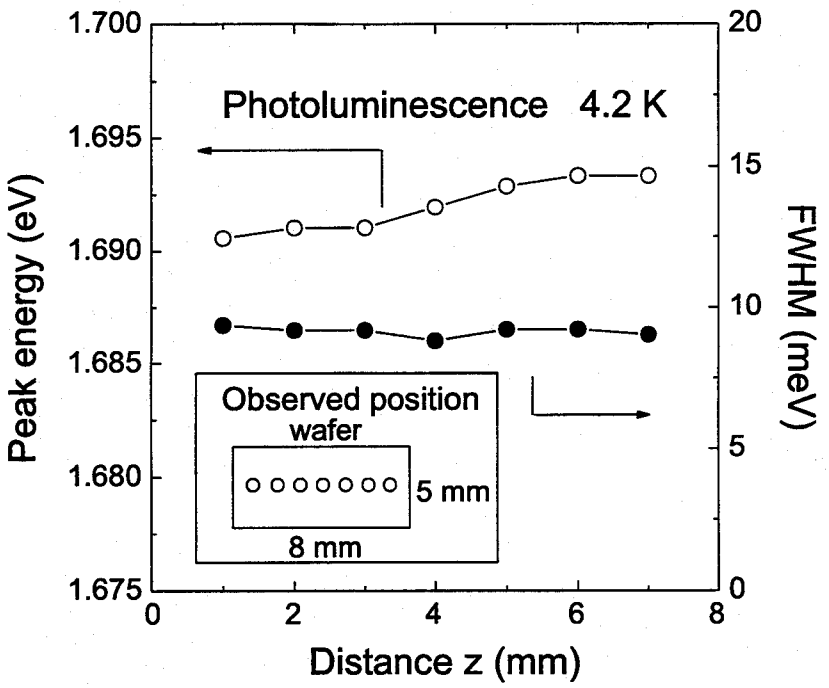


Figure 3.3: Peak energy and FWHM of PL peak (4.2 K) from $In_xGa_{1-x}As/Al_{0.3}Ga_{0.7}As$ QW ($x = 0.07$) with $L_w = 2.4$ nm grown on (411)A GaAs substrate as a function of distance.

in the case of GaAs/AlGaAs QWs on (411)A substrate. [7] In contrast, observed values of FWHM are almost constant (8.8 meV $\sim$ 9.3 meV) which is similar to the case of the $GaAs/Al_{0.3}Ga_{0.7}As$ QWs on the (411)A GaAs substrate. [7] These results indicate that effectively atomically flat interfaces over a macroscopic area of 8 mm $\times$ 5 mm [(411)A super-flat interfaces] are realized even in pseudomorphic $In_xGa_{1-x}As/Al_{0.3}Ga_{0.7}As$ QWs with an In content of $x = 0.07$ grown on the (411)A GaAs substrates similarly to the lattice-matched case of $GaAs/Al_{0.3}Ga_{0.7}As$ QWs on the (411)A GaAs substrates. [6, 7]

### 3.1.4 In content dependence

Photoluminescence FWHMs of the $In_xGa_{1-x}As$/AlGaAs QWs with the well width of $L_w = 2.4$ nm ($x = 0$–$0.15$) and 1.9 nm ($x = 0.22$–$0.38$) grown on (411)A and (100) GaAs substrates are plotted as a function of In content ($x$) in Fig. 3.4. A only one PL peak was observed for each corresponding (411)A or (100) QW, indicating that lateral size of microsteps in the (411)A and (100) heterointerfaces is much smaller than exciton size. PL FWHMs of the (411)A QWs are approximately 30–40% smaller than those of the

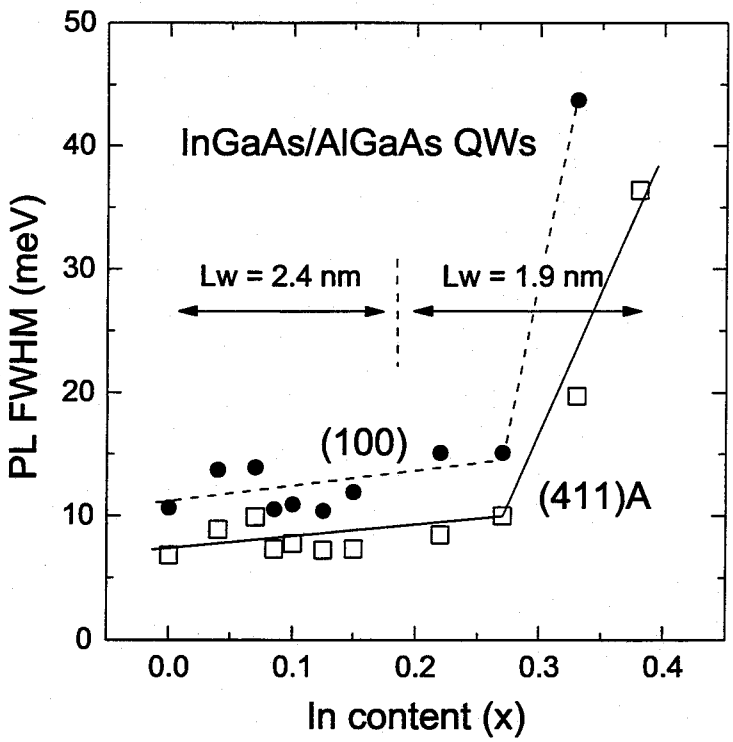


Figure 3.4: FWHMs of low-temperature PL peaks from $In_xGa_{1-x}As$/AlGaAs QWs with the well width of $L_w = 2.4$ nm ($x = 0$–$0.15$) and 1.9 nm ($x = 0.22$–$0.38$) grown on (411)A and (100) GaAs substrates as a function of In content ($x$).

(100) QWs in the range of $0 \leq x \leq 0.27$. Full width at half maximum of PL is mainly determined by both the alloy disorder of an InGaAs QW layer and the interface roughness in the case of the pseudomorphic InGaAs/AlGaAs QWs. The interface roughness influences the PL FWHMs more sensitively for narrower QWs. Therefore, the much reduced FWHMs achieved for the (411)A QWs with $L_w = 2.4$ nm indicate the superior flatness of the (411)A InGaAs/AlGaAs interfaces. PL FWHMs of the (411)A and (100) QWs drastically increases with increasing $x > 0.27$, because thickness of the InGaAs QW exceeds their critical thickness. However, PLFWHMs of the (411)A QWs are much narrower than those of the (100) QWs for $x > 0.3$, indicating that superior flatness of the (411)A heterointerfaces in pseudomorphic InGaAs/AlGaAs QWs with higher In contents, even if dislocations are induced in the QWs due to the lattice-mismatch. These results indicate that atomically flat interfaces over a macroscopic portion (200 $\mu$m diameter) of the laser excitation area [(411)A super-flat interfaces] can be also formed in pseudomorphic $In_xGa_{1-x}As$/AlGaAs QWs with In content $x$ up to 0.27 grown on the (411)A GaAs

substrates, as previously demonstrated in lattice-matched GaAs/AlGaAs QWs grown on (411)A GaAs substrates. [6, 7]

### 3.1.5 Summary

Optical properties of pseudomorphic $In_xGa_{1-x}As/Al_yGa_{1-y}As$ QWs ($x$ = 0–0.35, $y$ = 0.28–0.3) grown on (411)A-oriented GaAs substrates by MBE were investigated by low-temprature PL measurements. Single and very sharp PL peaks were observed at 4.2 K from the InGaAs/AlGaAs QWs with the well widths of $L_w$ = 1.2–12.0 nm grown on the (411)A GaAs substrates at $T_s$ = 520°C over a macroscopic are of 8 mm × 5 mm. PL FWHMs from the (411)A QWs with $L_w$ = 2.4 nm (1.9 nm), which are very sensitive to interface roughness, are 30–40% smaller than those of the (100) QWs for $x$ up to 0.27, indicatindg that "(411)A super-flat interfaces" can be formed in pseudomorphic InGaAs/AlGaAs QWs with In content up to 0.27. Therefore, (411)A pseudomorphic InGaAs/AlGaAs heterostructures can be expected to have high potential for applications to various kinds of quantum devices because of the (411)A super-flat interfaces.

## 3.2 Pseudomorphic InGaAs/GaAs strained-layer superlattices

In this section, structural and optical properties of an $In_{0.08}Ga_{0.92}As$/GaAs strained-layer superlattice (SLS) grown on the (411)A GaAs substrate by MBE were characterized by high resolution X-ray diffraction measurements (HRXRD) and PL measurements, and much improved crystalline quality of the (411)A InGaAs/GaAs SLS was achieved compared with that of a conventional $In_{0.08}Ga_{0.92}As$/GaAs SLS grown on a (100) GaAs substrate.

### 3.2.1 MBE growth of InGaAs/GaAs SLS

A (411)A-oriented GaAs substrate was degreased and etched by a sulfuric acid etchant solution to remove residual impurities on the surface. This (411)A substrate was mounted side by side with a (100) GaAs substrate on a 2-inch Mo substrate holder. After loading into a growth chamber of a Nissin RB-2001G MBE system, native GaAs oxides on their surfaces were removed by raising a substrate temperature ($T_s$) up to 630°C under $As_4$ beam flux. A 30-periods $In_{0.08}Ga_{0.92}As$ (5.7 nm) / GaAs (8.7 nm) SLS was grown at $T_s$= 550°C and V/III = 7 (in pressure ratio) on a 0.5 $\mu$m thick GaAs buffer layer. Growth rates of GaAs and InAs were 1.0 and 0.09 $\mu$m/h, respectively. The substrates were rotated at 30 rpm during MBE growth.

### 3.2.2 HRXRD measurements

Structural properties of the $In_{0.08}Ga_{0.92}As$/GaAs SLS grown on the (411)A GaAs substrate were characterized by high resolution X-ray diffraction (HRXRD) measurements. An incident X-ray beam with a wavelength of Cu K$\alpha$1 ($\lambda$ = 0.15406 nm) was monochromated by (220)-oriented Ge asymmetric four crystals. Rocking curves of the (411)A and (100) SLSs were measured by $\omega$-2$\theta$ scan (where $\omega$ and 2$\theta$ are the angles of the sample and detector relative to the incident X-ray beam) with a detector angular acceptance of $\sim$ 1°.

Figure 3.5 shows HRXRD rocking curves around a low-incidence asymmetric (511) reflection of the (411)A $In_{0.08}Ga_{0.92}As$/GaAs SLS and around a symmetric (400) reflection

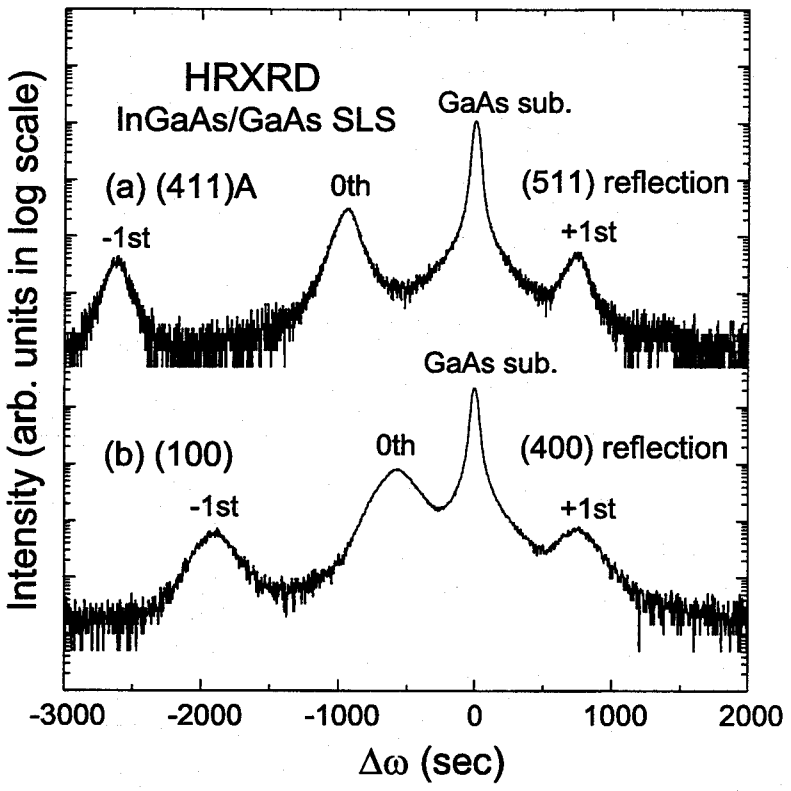


Figure 3.5: HRXRD rocking curves around a low-incidence asymmetric (511) reflection of the 30-periods $In_{0.08}Ga_{0.92}As$ (5.7 nm) / GaAs (8.5 nm) SLS grown on a (411)A GaAs substrate (a), and a symmetric (400) reflection of the same InGaAs/GaAs SLS grown on a (100) GaAs substrate (b).

of the (100) SLS. Sharp -1st, 0th, and +1st order reflections of the (411)A SLS are clearly observed at $\Delta\omega$ = -2615 sec (full width at half maximum, FWHM of 140 sec), -935 sec (FWHM = 135 sec), and 750 sec (FWHM = 155 sec) apart from the (511) reflection of GaAs, respectively. In contrast with this, broader peaks of -1st, 0th, and +1st order reflections of the (100) SLS are observed at $\Delta\omega$ = -1900 sec (FWHM = 280 sec), -575 sec (FWHM = 260 sec), and 750 sec (FWHM = 315 sec). In contents ($x$) of the $In_xGa_{1-x}As$ layers, thicknesses of InGaAs and GaAs layer of the (411)A and (100) SLSs were deduced from these reflection angles, which are summarized in Table. 3.1. These structural parameters were determined by comparing observed reflection angles with calculated ones of the (411)A SLS and the (100) SLS taking into account of the strain components in an epitaxial-layer on a high index substrate. [9] Average lateral lattice constants ($a_{||}$) of the (411)A and (100) SLSs were obtained by reciprocal space map measurements as describing below. Structural parameters (In content, thicknesses

Table 3.1: Structural parameters of the (411)A and (100) SLSs determined by HRXRD rocking curves

| Sample | Thickness (nm) | | In content | Relaxation |
|---|---|---|---|---|
| | InGaAs | GaAs | (x) | (%) |
| (411)A | 5.7 | 8.5 | 0.082 | 0 |
| (100) | 5.7 | 8.5 | 0.089 | 10 |

of the InGaAs and GaAs layers) were almost the same in the (411)A and (100) SLSs. Most prominent feature of the rocking curves of the SLSs is that FWHMs of the all reflection peaks from the (411)A SLS are approximately 50% smaller than that from the (100) SLS. This indicates that much improved crystalline quality is achieved in the (411)A InGaAs/GaAs SLS compared with a conventional (100) SLS.

In order to investigate the most dominant origin of the broadening of the reflection peaks, $\omega$ and $\omega$-$2\theta$ scan measurements for the (411)A and (100) SLSs were performed with the use of three (220) Ge reflection analyser crystals, which makes a detector angular acceptance to $\sim$ 12 sec. In case of using analyser crystals, a linewidth of a $\omega$ scan curve is sensitive to fluctuation of tilting angles of local crystal planes of the SLS samples, and a linewidth of a $\omega$-$2\theta$ scan curve is sensitive to fluctuation of layer thickness of the samples. Figure 3.6 shows $\omega$ and $\omega$-$2\theta$ scan curves around the (511) 0th order reflection of the (411)A SLS and around the (400) 0th order reflection of the (100) SLS measured with the use of the analyser crystals. FWHMs {100 sec [Fig. 3.6(b)] and 220 sec [Fig. 3.6(e)]} of $\omega$ scan curves of the (411)A and (100) SLSs are almost comparable to those {135 sec [Fig. 3.6(a)] and 260 sec [Fig. 3.6(d)]} of the rocking curves, so broadening of the reflection peaks in the rocking curves is mainly due to the fluctuation of tilting angles in the SLSs. FWHM of the $\omega$ scan curve of the (411)A SLS is less than half of that of the (100) SLS, indicating that fluctuation of tilting angles of local crystal planes in the (411)A SLS are much suppressed compared with the (100) SLS. FWHMs of the $\omega$-$2\theta$ curves of the (411)A and (100) SLSs are almost the same {75 sec [Fig. 3.6(c)] and 80 sec [Fig. 3.6(f)]}, which suggests that the fluctuation of layer thickness of both SLS samples are comparable.

Figure 3.7 shows reciprocal space maps around an asymmetric (400) reflection of the

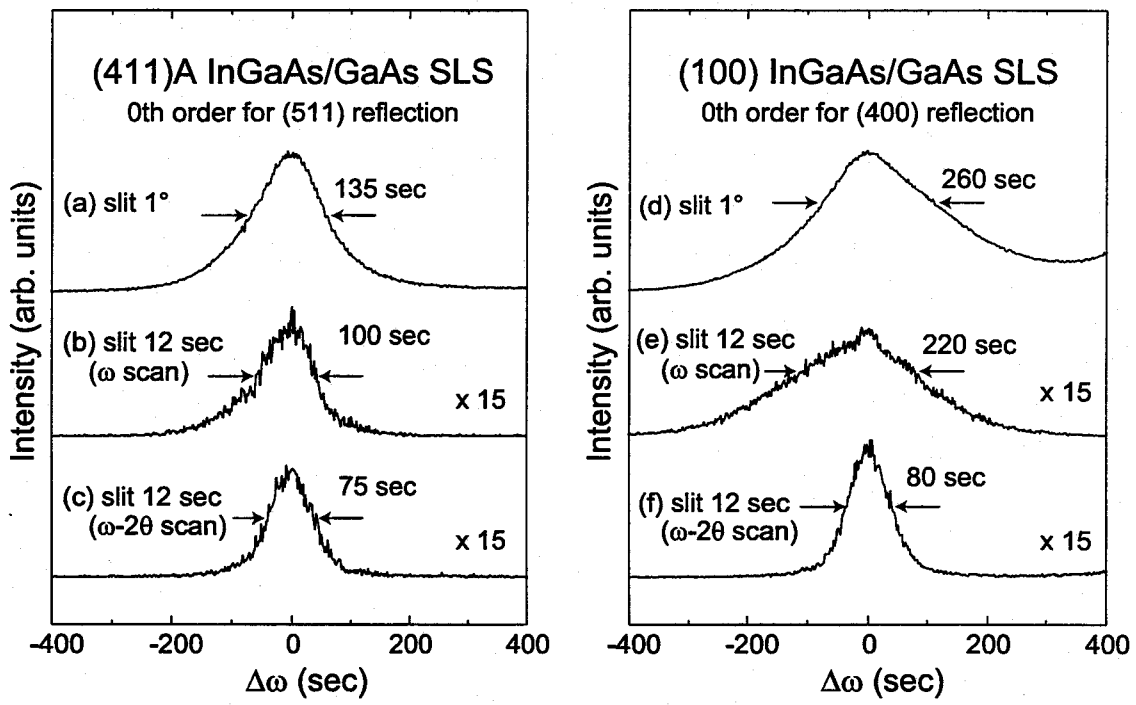


Figure 3.6: $\omega$ and $\omega$-$2\theta$ scan curves around 0th order peaks for a (511) reflection of the (411)A SLS [(a) - (c)], and for a (400) reflection of the (100) SLS [(d) - (f)]. (a), (d) are $\omega$-$2\theta$ scan curves without (220) Ge analyser crystals, (c), (f) are those with analyser crystals, and (b), (e) are $\omega$ scan curves with analyser crystals.

(411)A SLS and an asymmetric (511) reflection of the (100) SLS. The reciprocal space maps were obtained by measuring a series of $\omega$-$2\theta$ scan curves with slightly changed $\omega$ values by using the analyser crystals. For the (411)A SLS sample, the 0th and +1st order reflection spots and the (400) spot of the GaAs substrate are on the same line parallel to [411], indicating that the average lattice constant of the (411)A SLS layer parallel to the (411)A interface is the same as that of the GaAs substrate (no lattice relaxation). On the other hand, in the case of the (100) SLS sample, the 0th and +1st order reflection spots of the (100) SLS layer are on a line parallel to [100], but the (511) spot of the GaAs substrate does not locate on this line connecting the 0th and +1st spots, and it approximately shifts from the line by $\Delta$ toward [011] as indicated in Fig. 3.7(b). This result indicates that considerable amount of relaxation of the lattice-mismatch in the direction parallel to the (100) interface occurs between the (100) SLS layer and the GaAs substrate. An average lattice constant parallel to the (100) interface ($a_{\parallel}$) of the (100) SLS was determined to be 0.09% larger than that of the GaAs substrate, and the

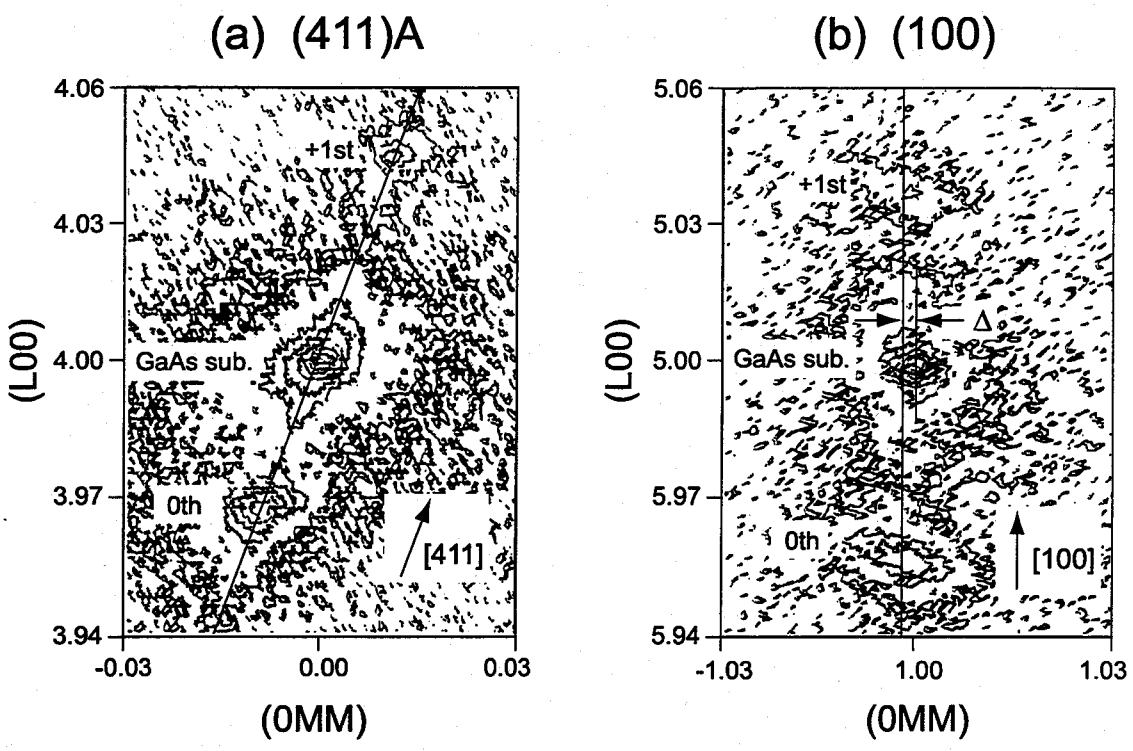


Figure 3.7: Reciprocal space maps around a (400) reflection of the (411)A SLS (a) and a (511) reflection of the (100) SLS (b).

degree of relaxation, $R$ [$\equiv (a_{\parallel} - a_{InGaAs})/(a_{InGaAs} - a_{GaAs})$], was 10%, where $a_{InGaAs}$ and $a_{GaAs}$ are intrinsic cubic lattice constants of InGaAs and GaAs. This relaxation of the (100) SLS may cause some fluctuation of tilting angles of local crystal planes in the (100) SLS and resulted in the broad reflection curves of the (100) SLS, which is similar to previously reported results for (100) InGaAs/AlAs SLSs with high In contents ($x$ = 0.15) [10]. The suppressed relaxation of lattice-mismatch in the (411)A InGaAs/GaAs SLS probably implies that a surface energy density of a growing surface of the (411)A SLS during MBE growth is much lower than that of the (100) SLS, and generation of misfit dislocations is suppressed in the (411)A SLS, even if a strain energy density of the (411)A SLS is almost the same as that of the (100).

### 3.2.3 Photoluminescence measurements

Optical properties of the $In_{0.08}Ga_{0.92}As$/GaAs SLSs were characterized by photoluminescence (PL) measurements at 12 K. Excitation laser was a He-Cd laser with a wavelength of 325 nm and an excitation power of 2 mW. The excitation beam was focused on an area

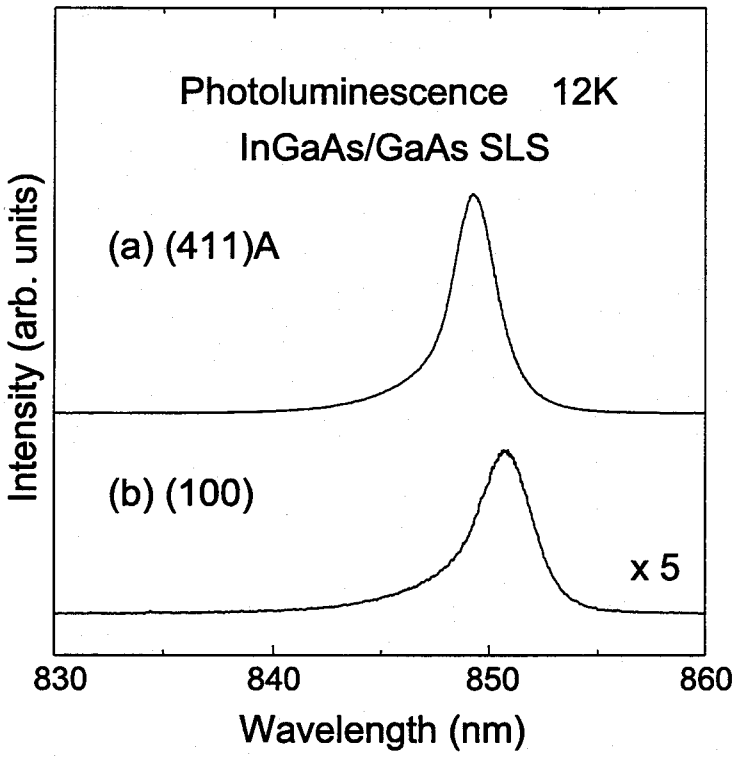


Figure 3.8: Photoluminescence spectra at 12 K from the (411)A $In_{0.08}Ga_{0.92}As/GaAs$ SLS (a) and the (100) InGaAs/GaAs SLS (b).

of about 200 $\mu$m diameter of the sample surface.

Figure 3.8 shows PL spectra at 12 K from the (411)A and (100) SLSs. PL peaks from the (411)A and (100) SLSs are clearly observed at 849.2 nm (FWHM = 4.2 meV) and 850.9 nm (5.2 meV), respectively. A slight blue-shift (2.9 meV in energy) of the luminescence peak was observed for the (411)A SLS compared with that of the (100) SLS. This blue-shift for the (411)A SLS is probably due to slight difference of In content, surface segregation of In atoms [11], and strain-induced band gap shift [8], which is caused by different strain components in the (411)A SLS as observed in HRXRD measurements. Future investigation such as a quantitative observation of surface segregation of In atoms on the (411)A plane is necessary to determine the main cause of the blue-shift for the (411)A SLS. FWHM (4.2 meV) of the PL peak from the (411)A SLS is approximately 20% smaller than that (5.2 meV) of the (100) SLS. Furthermore, integrated PL intensity of the (411)A SLS is about 5 times larger than that of the (100)SLS. These results indicate that superior uniformity and suppressed non-radiative centers in the (411)A SLS compared

with the (100) SLS. The improved optical quality of the (411)A SLS is probably due to much reduced relaxation of lattice-mismatch in this sample. Therefore, this PL result also supports the higher crystalline quality of the (411)A SLS than that of the (100) SLS.

### 3.2.4 Summary

An extremely uniform $In_{0.08}Ga_{0.92}As/GaAs$ strained-layer superlattice (SLS) was grown on a (411)A GaAs substrate by molecular beam epitaxy (MBE). High resolution X-ray diffraction (HRXRD) measurements revealed that fluctuation of tilting angles of local crystal planes in the (411)A SLS was much reduced than that of a simultaneously grown (100) $In_{0.08}Ga_{0.92}As/GaAs$ SLS, which is due to difference of relaxation of lattice-mismatch between InGaAs and GaAs layers for these two SLSs. Photoluminescence (PL) properties also exhibited the superior crystalline quality of the (411)A SLS (a higher PL intensity and a smaller FWHM of the PL peak) compared with the (100) SLS. Hence, improved quantum devices such as optical modulators can be expected by using InGaAs/GaAs SLS structures grown on (411)A GaAs substrates.

## 3.3 Critical thickness of InGaAs

For the psduomorphic InGaAs/AlGaAs system, critical thickness of the InGaAs layer is one of the most important material parameters for device applications. This section describes the critical thicknesses of pseudomorphic $In_{0.25}Ga_{0.75}As/Al_{0.32}Ga_{0.68}As$ QWs grown on the (411)A GaAs substrates by molecular beam epitaxy (MBE) which were determined by PL measurements at 11 K and the surface morphologies of $In_{0.25}Ga_{0.75}As$ layers observed by atomic force microscopy (AFM).

### 3.3.1 MBE growth of InGaAs/AlGaAs single QWs

(411)A- and (100)-oriented GaAs substrates were degreased and chemically etched by "Semico-Clean" prior to MBE growth. Six kinds of $In_{0.25}Ga_{0.75}As/Al_{0.32}Ga_{0.68}As$ single QW (SQW) structures were grown on the (411)A and (100) GaAs substrates mounted side-by-side on a Mo block in a MBE system. At first, a 6-period GaAs (50 nm)/ $Al_{0.32}Ga_{0.68}As$ (20 nm) superlattice buffer layer was grown at a substrate temperature ($T_s$) of 610°C. Then, after a short growth interruption for decreasing $T_s$ from 610°C to 480°C, $In_{0.25}Ga_{0.75}As/Al_{0.32}Ga_{0.68}As$ SQW with well width ($L_w$) of 13, 15, 17, 19, 21 or 23 nm and 100 - nm thick $Al_{0.32}Ga_{0.68}As$ barrier layers were grown at $T_s$ = 480°C. An $In_{0.25}Ga_{0.75}As$ top layer with the same thickness of $L_w$ was grown on each SQW sample for the AFM observations. The growth rates of GaAs and InGaAs were 1.0 $\mu$m/h and 0.87 $\mu$m/h, respectively. The V/III ratio ($As_4$/Ga, flux ratio) was 11. In contents ($x$) of $In_xGa_{1-x}As$ well layers were approximately 0.26 for the (411)A SQWs and 0.24 for (100) SQWs, which were determined by X-ray diffraction of thick InGaAs layers (100 nm) grown on (411)A and (100) GaAs substrates under the same growth condition of the SQWs. The substrates were not rotated during MBE growth.

### 3.3.2 Photoluminescence measurements

Figure 3.9 shows PL spectra at 11 K from the six kinds of pseudomorphic $In_{0.25}Ga_{0.75}As/$ $Al_{0.32}Ga_{0.68}As$ SQW structures simultaneously grown on the (411)A and (100) GaAs substrates. An excitation laser beam with the wavelength of 325 nm (He-Cd laser) and power

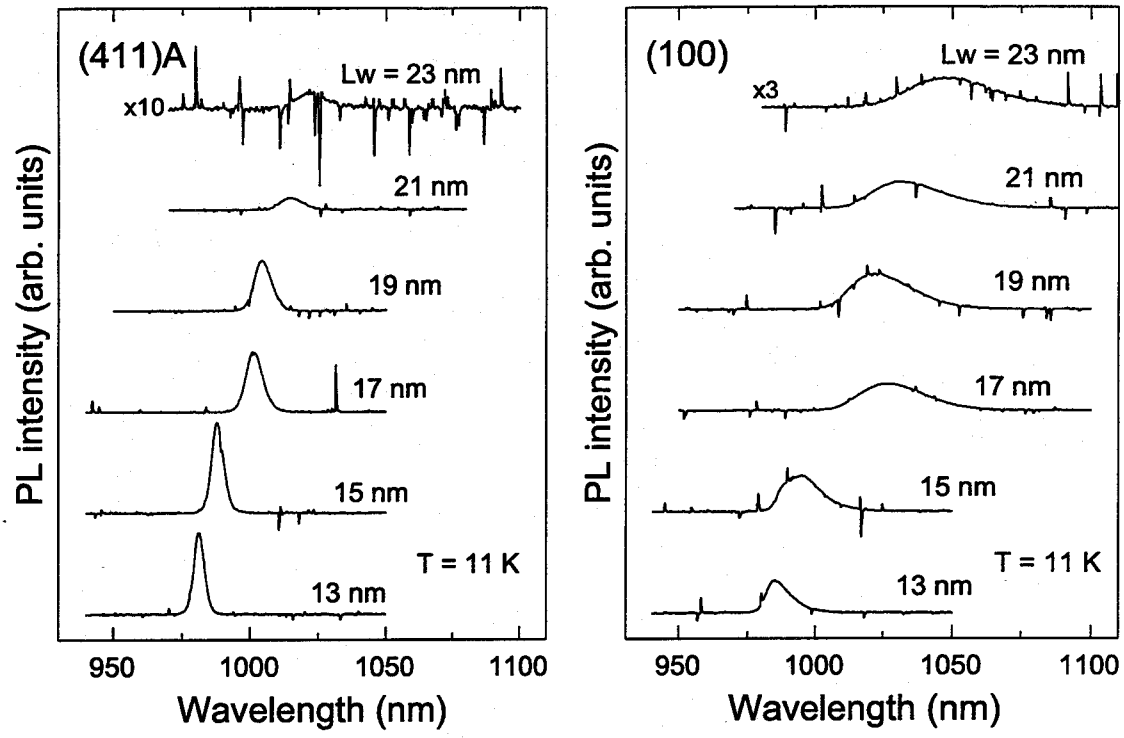


Figure 3.9: Photoluminescence spectra at 11 K of pseudomorphic $In_{0.25}Ga_{0.75}As/Al_{0.32}Ga_{0.68}As$ QWs with $L_w$ = 13–23 nm simultaneously grown on (411)A and (100) GaAs substrates

of 2 mW was focused on an area of a sample surface with a diameter of about 200 $\mu$m. Generally speaking, PL peaks of (100) SQWs are red-shifted, especially for large $L_w$, compared with those of corresponding (411)A SQWs. This is probably due to the different InGaAs/AlGaAs interface between (411)A and (100) samples, which results from different growth mode between the (411)A and (100) surface. This is also discussed later with AFM images of the InGaAs top layers. One prominent feature is a much smaller linewidth of each PL peak observed for the (411)A SQWs compared with those of the (100) SQWs, indicating much improved crystalline quality and flat interfaces of (411)A SQWs. In the case of (411)A SQWs, sharp and strong PL peaks were observed for $L_w$ = 13–19 nm, but when $L_w$ exceeded 21 nm, the PL intensity apparently decreased and the linewidth increased.

Figure 3.10 shows the full width at half maximum (FWHM) of PL peaks observed for the (411)A and (100) $In_{0.25}Ga_{0.75}As/Al_{0.32}Ga_{0.68}As$ SQWs at 11 K as a function of well width. PL-FWHM (5.7 meV) of the (411)A SQW with $L_w$ = 13 nm is as small as 44

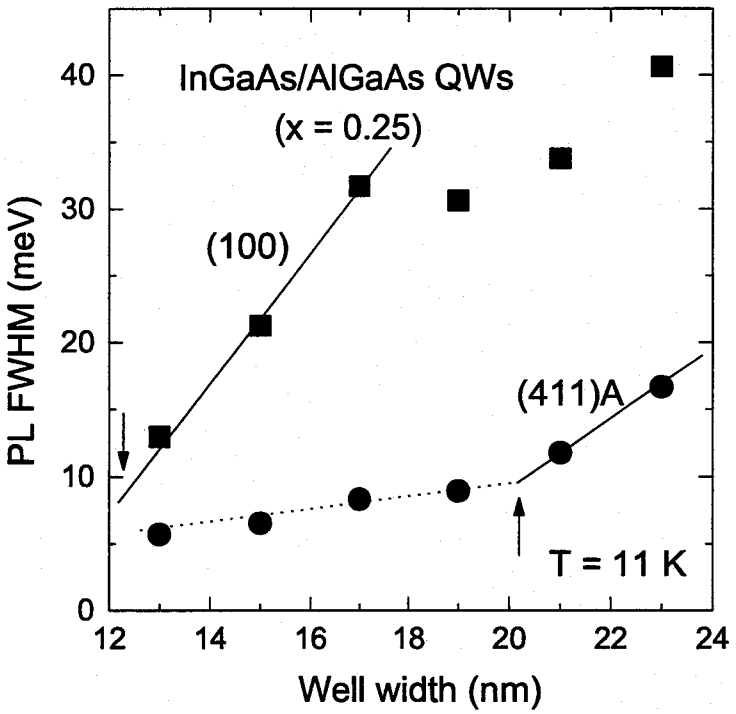


Figure 3.10: FWHM of PL peaks at 11 K of the (411)A and (100) pseudomorphic $In_{0.25}Ga_{0.75}As/Al_{0.32}Ga_{0.68}As$ QWs as a function of well width. The solid and dotted lines indicate the tendency of the variation of FWHM and the arrow sign indicates the point around the critical thickness.

% of that (13 meV) of the corresponding (100) SQW. PL-FWHM of the (411)A SQWs remained small (< 10 meV) until $L_w = 19$ nm and it increased slowly for $L_w \geq 21$ nm (12 $\sim$ 17 meV). On the other hand, broadening of PL peaks already started (13 $\sim$ 32 meV) even at $L_w = 13$ nm for the (100) SQWs. Broadening of PL peaks in thick QW layer arises from many factors, for example strain relaxation, segregation, and so on. But at this low growth temperature ($T_s = 480°C$), the segregation length is small (about 1 nm for (100) QW [11]). So the effect of In segregation is very small in these thick QWs and the main factor is the strain relaxation. These results suggest that the critical thickness of the (411)A $In_{0.25}Ga_{0.75}As/Al_{0.32}Ga_{0.68}As$ QWs determined by PL is approximately 20 nm, which is more than 60 % larger than that (around 12 nm) of the (100) SQWs.

Figure 3.11 shows the critical thicknesses in the (411)A and (100) $In_{0.25}Ga_{0.75}As/Al_{0.32}Ga_{0.68}As$ QWs determined in this study and the calculated critical thicknesses used by the mechanical equilibrium model [12] for (100) InGaAs/GaAs QWs. The critical thickness of the present (100) QWs shows good agreement with the calculated value and

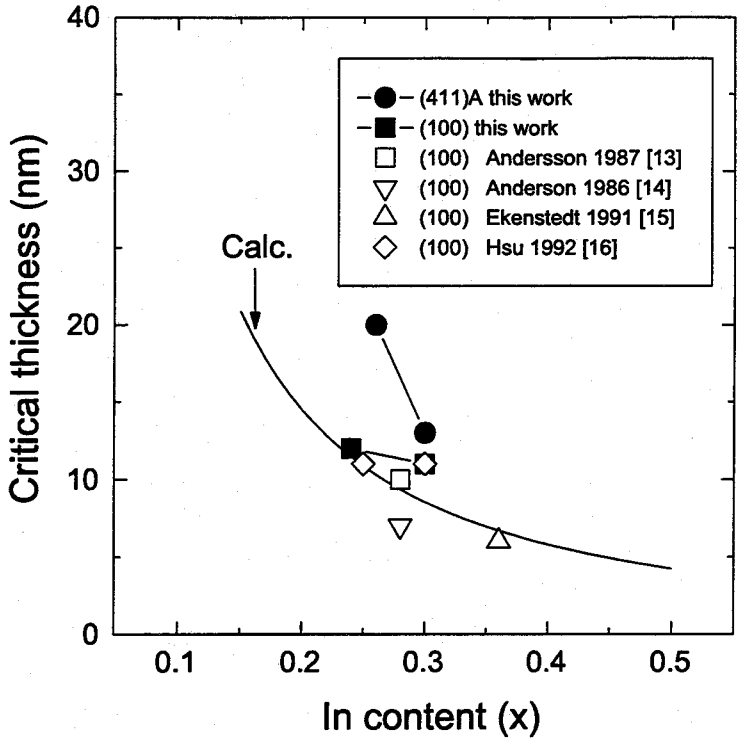


Figure 3.11: The critical thickness of the $In_xGa_{1-x}As$ layers in (411)A and (100) $In_{0.25}Ga_{0.75}As/Al_{0.32}Ga_{0.68}As$ QWs plotted as a function of In content ($x$), together with previously reported data for similar (100) $In_xGa_{1-x}As/GaAs$ QWs.[13–16]

also with observed data for (100) InGaAs/GaAs QWs determined by PL. [13, 14, 15, 16] The observed critical thickness of the (411)A QWs is significantly larger than the calculated and observed value for the (100) QWs.

### 3.3.3 Surface morphology of $In_{0.25}Ga_{0.75}As$ layer

Figure 3.12 shows AFM images of surface morphologies of the $In_{0.25}Ga_{0.75}As$ top layers with the thickness of $L_w$ grown on the (411)A (a) and the (100) (b) SQWs. The scan area was 5 $\mu$m $\times$ 5 $\mu$m . There was no cross-hatch pattern on the (411)A $In_{0.25}Ga_{0.75}As$ for $L_w$ = 13 - 15 nm. A few cross-hatch lines began to appear on the surface for the $L_w$ = 17 nm and with further increasing $L_w$, number of the cross-hatch lines increased. This indicates that misfit dislocations start to be introduced at around $L_w$ = 17 nm for the pseudomorphic (411)A InGaAs layers, which is slightly smaller than the critical thickness ($\sim$ 20 nm) determined by the PL measurements. These dislocations did not affect the PL property of the QWs with $L_w$ = 17 and 19 nm. The roughness of the (411)A $In_{0.25}Ga_{0.75}As$

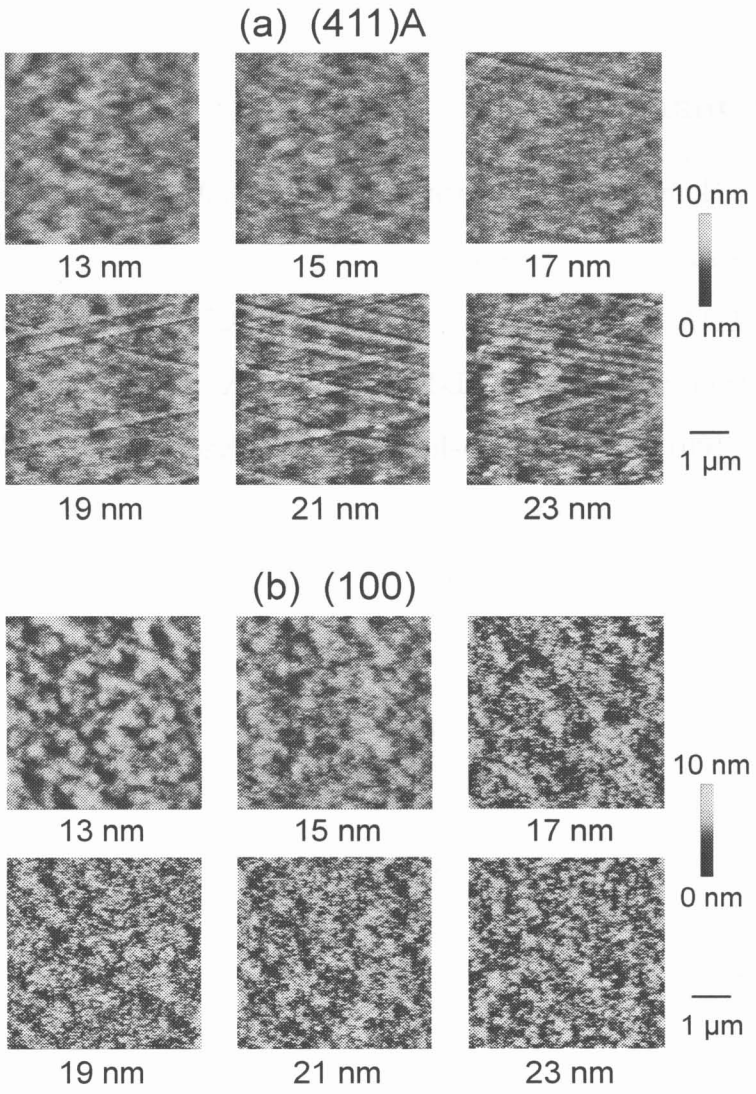


Figure 3.12: AFM images of (a) the (411)A and (b) (100) $In_{0.25}Ga_{0.75}As$ top layer with thickness of $L_w$ (13 - 23 nm). The scan area is 5 $\mu$m $\times$ 5 $\mu$m.

texture, however, was very small in the regions except for the cross-hatch lines. For the (100) $In_{0.25}Ga_{0.75}As$ layers, no cross-hatch pattern was observed for all samples, but small islands and rough texture were seen on the surface, particularly for $L_w \geq 17$ nm, and this roughness of the surface texture was much larger than that of the (411)A $In_{0.25}Ga_{0.75}As$. It is thought that the thick (100) QW was grown in 3D growth mode which was caused by strain relaxation (Stranski-Krastanov growth mode), and the 3D islands may be more easily formed on the strained (100) InGaAs than (411)A InGaAs. It will be due to the difference of the surface stability between the (411)A and the (100). The (411)A surface is more stable than the (100) surface during MBE growth. This is one of the main factor

of large critical thickness of (411)A QW.

### 3.3.4 Summary

The critical thickness of MBE-grown $In_{0.25}Ga_{0.75}As/Al_{0.32}Ga_{0.68}As$ SQWs on the (411)A and (100) GaAs substrates was investigated by PL and AFM measurements. The critical thickness of (411)A $In_{0.25}Ga_{0.75}As/Al_{0.32}Ga_{0.68}As$ SQWs was determined to be approximately 20 nm from the observed PL-FWHM at 11 K, which is much larger than that ($\sim$ 12 nm) of the (100) SQWs. We believe that this lager critical thickness should be another advantage of the (411)A pseudomorphic InGaAs/AlGaAs QWs besides the (411)A super-flat interfaces for device applications of this material.

## 3.4 Surface segregation of In atoms

For the MBE growth of the pseudomorphic InGaAs/AlGaAs heterostructures, surface segregation of In atoms, which degrades compositional abruptness of heterointerfaces, was significantly observed by *in-situ* surface-sensitive experiments such as Auger electron spectroscopy (AES), X-ray photoemission spectroscopy (XPS) [17] and reflection high-energy diffraction (RHEED) [18]. Therefore, the In surface segregation makes a large influence on a quantization energy level in the QW, which was studied by secondary ion mass spectroscopy (SIMS) and PL measurements. [11, 19] In this section, we studied substrate temperature ($T_s$) dependence of In surface segregation during MBE growth of InGaAs on (411)A GaAs substrates. In surface segregations were characterized by high resolution X-ray diffraction (HRXRD) measurements of (411)A InGaAs/GaAs SLs and PL measurements of (411)A InGaAs/AlGaAs QWs. We discuss the mechanism of In surface segregation on the (411)A growth-layer plane and its correlation with heterointerface flatness of (411)A InGaAs/AlGaAs QWs.

### 3.4.1 Experimental details

All samples used in this study were grown by a VG semicon V80H MK-II MBE system. (411)A and (100)-oriented GaAs substrates were prepared by conventional chemical treatments and they were mounted side by side on a Mo substrate holder. Native oxides on the GaAs substrates were removed by heating up to a substrate temperature ($T_s$) of 650°C under $As_4$ atmosphere in the MBE growth chamber. For HRXRD measurements, 15-periods pseudomorphic $In_xGa_{1-x}As$ (6.8 nm) /GaAs (9 nm) SLs ($x \simeq 0.08$) were grown at $T_s$ = 450, 480, 510 and 540°C under V/III pressure ratio of 14. Growth rates of InGaAs and GaAs were 0.76 and 0.7 $\mu$m/h, respectively. Layer-thicknesses of InGaAs and GaAs layers and In contents ($x$) in $In_xGa_{1-x}As$ were characterized by HRXRD rocking curves of the samples. For PL measurements, pseudomorphic $In_xGa_{1-x}As/Al_{0.28}Ga_{0.72}As$ QWs ($x \simeq 0.2$) with various well widths ($L_w$ = 1.5–14.8 nm) were grown at $T_s$ = 450–540°C under V/III = 10. AlGaAs barriers were 20 nm thick and growth rates of InGaAs and AlGaAs were about 0.98 and 1.0 $\mu$m/h, respectively. The substrates were not rotated

during MBE growth.

High resolution X-ray diffraction measurements were performed with an incident X-ray beam (Cu K$\alpha$1) monochromated by a (220)-oriented Ge asymmetric four crystal system. Rocking curves of the InGaAs/GaAs SLs were measured by $\omega$-$2\theta$ scans (where $\omega$ and $2\theta$ are the angles of the sample and detector relative to the incident X-ray beam) around low-incidence asymmetric (511) reflections for the (411)A samples, and those around symmetric (400) reflections for the (100) samples. Photoluminescence from the InGaAs/AlGaAs QWs were measured at 12 K with a He-Cd laser as an excitation source. The excitation laser beam was focused on an area approximately 200 $\mu$m in diameter of the sample surface and the exception power was 5 mW.

### 3.4.2 Results and discussion

#### HRXRD measurements of InGaAs/GaAs SLs

Figure 3.13 shows HRXRD rocking curves of the InGaAs/GaAs SLs simultaneously grown on the (411)A and (100) GaAs substrates at various substrate temperatures. In Fig. 3.13, intensities of HRXRD rocking curves are normalized at intensities of 0th-order reflections $I(0)$ observed around $\Delta\omega \simeq$ - 1000 sec for the (411)A SLs and $\Delta\omega \simeq$ - 620 sec for the (100) SLs apart from reflections of GaAs substrates. The 0th-order reflection peaks of the (411)A SLs grown at $T_s$ = 450–510°C were observed at almost the same angle ($\Delta\omega \simeq$ - 1000 sec) as shown in Figs 3.13(b)–3.13(d), while that of the (411)A SLs grown at $T_s$ = 540°C was observed at $\Delta\omega$ = - 900 sec as shown in Fig 3.13(a). On the other hand, peak angles of the 0th-order reflections of the (100) SLs are almost the same ($\Delta\omega \simeq$ - 620 sec) for $T_s$ = 450–540°C [Figs. 3.13(e)–3.13(g)]. This indicates that a significant amount of In atoms were desorbed at $T_s$ = 540°C on the (411)A InGaAs growth-layer plane, which did not occurred on the (100) plane. Most prominent feature in Fig. 3.13 is that normalized-intensities of -1st and 1st-order reflections [$I(-1)/I(0)$ and $I(1)/I(0)$] decreases with increasing substrate temperature for both the (411)A and (100) SL samples. This is due to degradation of InGaAs/GaAs heterointerfaces in their abruptness caused by In surface segregation effect, which is the same effect as interdiffusion of Ga and Al

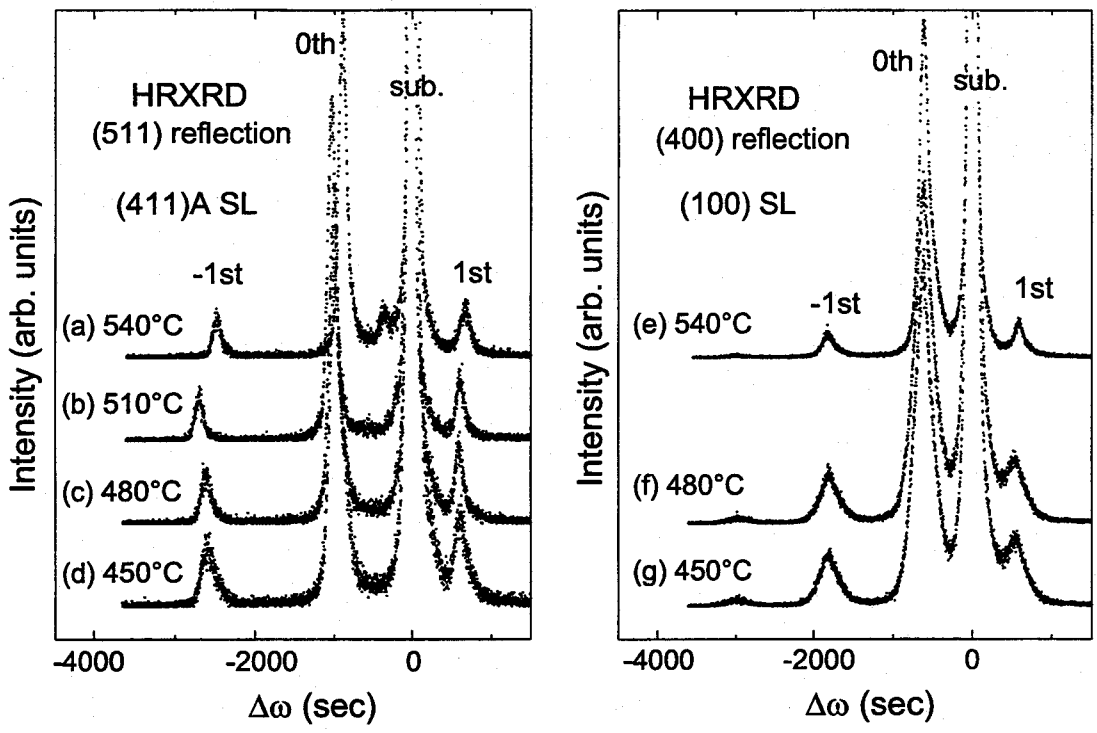


Figure 3.13: HRXRD rocking curves around low-incidence asymmetric (511) reflections of the (411)A InGaAs/GaAs SLs grown at $T_s$ = (a) 540, (b) 510, (c) 480 and (d) 450°C, and those around symmetric (400) reflections of the (100) SLs grown at $T_s$ = (e) 540, (f) 480 and (g) 450°C.

atoms in a GaAs/AlAs SL. [20]

For a quantitative analysis of the In surface segregation, we calculated angles of the satellite peaks and an an intensity ratio of the -1st-order peak relative to the 0th-order peak $[I(-1)/I(0)]$ of the InGaAs/GaAs SL. In order to determine a profile of the In content along the growth direction, we used In segregation model during MBE proposed by Muraki et al. [11, 19] In their segregation model, it is assumed that a certain fraction $R$ of the In atoms on the growing surface segregate to the next growing surface with a nominal In content of $x_0$. According to this model, In content of the $n$th layer $(x_n)$ in a primitive unit cell of the InGaAs/GaAs SL is given by

$$x_n = \begin{cases} x_0(1-R)^n & (1 \leq n \leq N) \\ x_0(1-R^n)R^{n-N} & (n > N) \end{cases}, \tag{3.1}$$

where $N$ is thickness of the InGaAs layer in monolayers. The segregation probability $R$ can be calculated from In segregation length $\lambda$ using a relation given by

$$R = \exp\left(-\frac{d}{\lambda}\right), \tag{3.2}$$

where $d$ is monolayer thickness of GaAs. Assuming this profile of In content in the InGaAs/GaAs SL, we calculated reciprocal lattice points $\mathbf{q}$ around (511) reflections for the (411)A InGaAs/GaAs SLs taking into account of strain components on high index substrates. [9] We also calculated those around (400) reflections for the (100) SLs. Thus, we obtained angles of satellite peaks of the SLs from the calculated $\mathbf{q}$. The scattering amplitude $F(\mathbf{q})$ at the reciprocal lattice point of $\mathbf{q}$ is given by the usual sum over lattice points in the SL, which is written as

$$F(\mathbf{q}) = m \cdot \sum_j f_j(\mathbf{q}) \exp(-i\mathbf{q} \cdot \mathbf{r}_j), \tag{3.3}$$

where $m$ is superlattice periods, $f_j(\mathbf{q})$ is the atomic scattering factor for the $j$th lattice point in the primitive unit cell of the SL, and $\mathbf{r}_j$ is the position of the $j$th lattice point. Then, the intensity ratio of the -1st-order peak relative to the 0th-order peak is given by

$$\frac{I(-1)}{I(0)} = \left| \frac{F(\mathbf{q}_{-1\mathrm{st}})}{F(\mathbf{q}_{0\mathrm{th}})} \right|^2, \tag{3.4}$$

where $\mathbf{q}_{0\mathrm{th}}$ and $\mathbf{q}_{-1\mathrm{st}}$ are reciprocal lattice points of 0th- and -1st-order satellite peaks of the SL. We calculated $I(-1)/I(0)$ around the (511) reflection for the (411)A SL and that around the (400) reflection for the (100) SL.

Figure 3.14 shows calculated results of the 0th-order peak angle (a broken line) and $I(-1)/I(0)$ (a solid line) in the low-incidence diffraction pattern around the (511) reflection for the (411)A InGaAs (6.8 nm) / GaAs (9 nm) SL with $x_0 = 0.08$ plotted as a function of In segregation length $\lambda$. It can be clearly seen that the calculated $I(-1)/I(0)$ is almost the constant for $\lambda < 0.5$ nm, while $I(-1)/I(0)$ drastically decreases from 0.22 to 0.08 with an increase in the In segregation length from 0.5 nm to 3 nm. On the other hand, the calculated 0th-order peak angle is almost the constant ($\Delta\omega \simeq 980$ sec) for $0 \leq \lambda \leq 3$ nm. Therefore, the intensity ratio of the -1st-order peak relative to the 0th-order peak is very sensitive to the In segregation length for $\lambda \geq 0.5$ nm. Thus, we determined $x_0$ and $\lambda$ in the SL samples by comparing observed HRXRD results and calculated ones, which are summarized in Table 3.2.

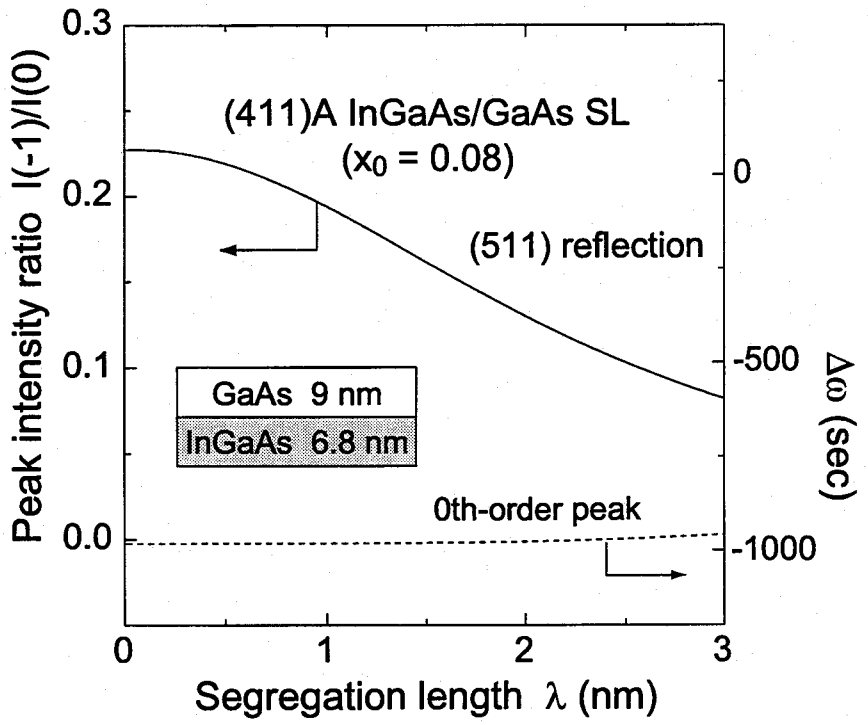


Figure 3.14: Calculated results for the intensity ratio of -1st-order peak relative to 0th-order peak (a solid line) and the angle of the 0th-order peak (a broken line) in the low-incidence diffraction pattern around the (511) reflection of the (411)A InGaAs (6.8 nm)/GaAs (9nm) SL with $x_0 = 0.08$ plotted as a function of In segregation length.

Table 3.2: In segregation length ($\lambda$) and nominal In content ($x_0$) of the InGaAs/GaAs SLs grown at various substrate temperature ($T_s$) determined from HRXRD results.

| Substrate orientation | $T_s$ (°C) | $\lambda$ (nm) | $x_0$ |
|---|---|---|---|
| (411)A | 450 | 1.40 | 0.081 |
| | 480 | 1.94 | 0.082 |
| | 510 | 2.36 | 0.083 |
| | 540 | 1.79 | 0.073 |
| (100) | 450 | 0.53 | 0.080 |
| | 480 | 0.67 | 0.080 |
| | 540 | 2.84 | 0.080 |

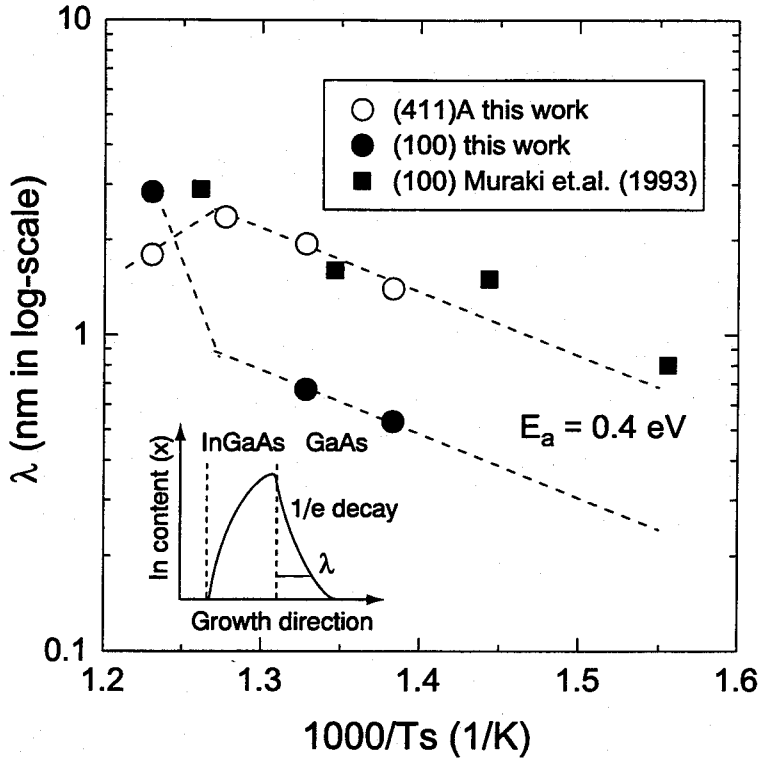


Figure 3.15: Substrate temperature dependence of In segregation length ($\lambda$) in the (411)A samples (open circles) and the (100) samples (closed circles) determined by HRXRD results. Reported In segregation lengths for (100) InGaAs/GaAs QWs (closed squares), which were characterized by SIMS measurements are also plotted.

Figure 3.15 shows determined In segregation lengths for the (411)A and (100) samples as a function of substrate temperature. Reported In segregation lengths for (100) InGaAs/ GaAs QWs, which were characterized by SIMS measurements [11, 19], are also plotted in Fig. 3.15. In the temperature range of $T_s$ = 450–510°C, the In segregation lengths of both the (411)A and (100) samples have a temperature dependence of the thermal activation type with the same activation energy ($E_a$) of 0.4 eV. However, the values of $\lambda$ of the (411)A samples are about three times larger than those of the (100) samples. This can be explained by a surface segregation model based on the surface migration of group III atoms. Surface migration lengths of In and Ga atoms on the (411)A crystal-plane is much larger than those on the (100) plane [6, 21], in other words, incorporation life-times ($\tau_c$) of In and Ga atoms on the (411)A plane are much longer than those on the (100). Probability of In atoms climbing to the growing surface, i.e. In segregation probability, should be larger for the longer $\tau_c$, which is the same as that reported for segregations

of Ga and Sb dopants during Si-MBE on (100) and (111) Si substrates. [22] It is also worth mentioning that potential energy for In atoms climbing to the next layers is the same for both the (411)A and (100) samples, indicating that the potential energy for In segregation should have no dependence on the substrate orientation. The activation energy of $\lambda$ studied by SIMS is almost the same as that of our results, however, values of $\lambda$ are larger than those of the (100) samples in this study. This is probably due to lower growth rates of InGaAs and GaAs, which give lower $\tau_c$ of InGaAs and GaAs, and different V/III pressure ratio during MBE compared with those for our (100) samples. $\lambda$ of the (411)A sample decreases with increasing $T_s$ from 510°C to 540°C. This is because a significant amount of In atoms desorbs from the InGaAs growing surface at $T_s = 540$°C. In fact, nominal In content of the (411)A sample grown at $T_s = 540$°C ($x_0 = 0.073$) is 12% smaller than that of the sample grown at $T_s = 510$°C ($x_0 = 0.083$) as shown in Table 3.2. It have been reported that desorption of In atoms, which reduces surface population of In atoms, apparently suppresses In surface segregation [19]. In contrast with this, $\lambda$ of the (100) sample drastically increases with increasing $T_s$ from 510°C to 540°C, which is probably due to no In desorption from the (100) surface and much rough InGaAs growing surface as describing below.

### PL measurements of InGaAs/AlGaAs QWs

Figure 3.16 shows PL spectra at 12 K from the pseudomorphic $In_xGa_{1-x}As$/ $Al_{0.28}Ga_{0.72}As$ QWs ($x \simeq 0.2$) grown at $T_s = 450$ and 510°C simultaneously on (411)A and (100) GaAs substrates. PL peaks around 733 nm observed in Figs. 3.16(a)–3.16(d) correspond to luminesceneces from GaAs/$Al_{0.28}Ga_{0.72}As$ QWs with $L_w \simeq 2.8$ nm, which are grown on pseudomorphic InGaAs/AlGaAs QWs in order to determine thicknesses of GaAs layers. A slight variation of PL peak wavelengths (732–735 nm) of the GaAs/ AlGaAs QWs is due to a variation of GaAs thicknesses, which is caused by no substrate rotations during MBE. Luminescences from the InGaAs/AlGaAs QWs grown at $T_s = 510$°C [Figs 3.16(a) and 3.16(b)] were observed at higher energy sides compared with those from the corresponding QWs grown at $T_s = 450$°C [Figs 3.16(c) and 3.16(d)] for

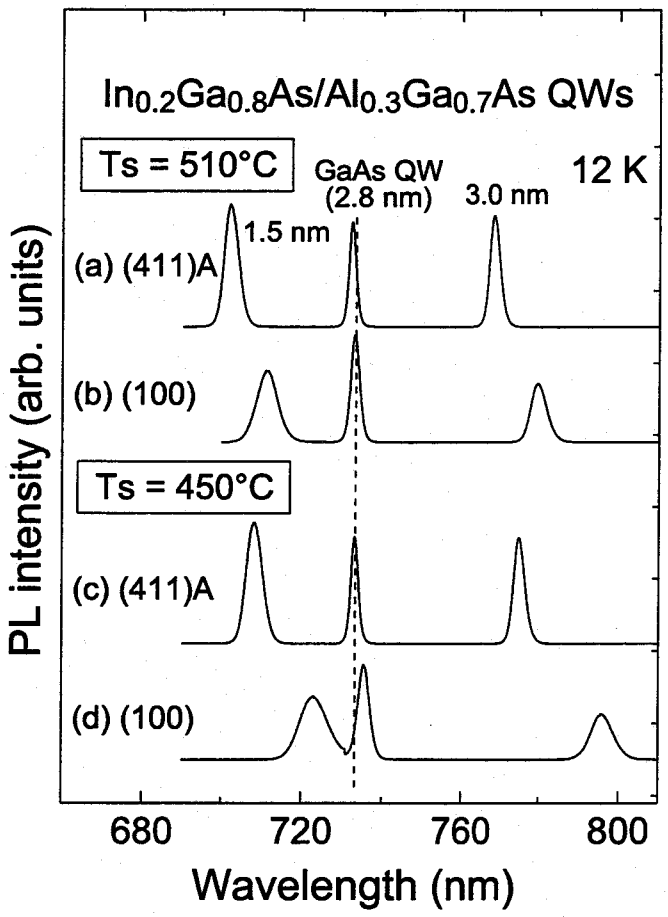


Figure 3.16: PL spectra at 12 K from the (411)A and (100) InGaAs/AlGaAs QWs grown at $T_s$ = 450 and 510°C.

both the (411) and (100) samples, while, such blue-shifts were not observed for luminescences from GaAs/AlGaAs QWs. These blue-shifts of PL peaks were due to In surface segregation effect as shown in HRXRD results. Furthermore, much narrower PL peaks from the (411)A QWs were observed at higher energy sides compared with those of the corresponding (100) QWs for both the substrate temperature ($T_s$ = 450 and 510°C).

In order to investigate the blue-shifts of PL peaks from the (411)A QWs compared with those of the corresponding (100) QWs, we calculate PL peak energies of the QWs taking into account of In surface segregation effects. Potential profiles of the QWs were assumed to be obtained by using In content profiles given by eq. (3.1), thus lowest quantization energies for an electron and a hole were calculated. For a calculation, we also took into account of a strain-induced InGaAs band-gap energy shift ($\Delta E_g$), which is determined by strain components in the InGaAs layer [8], and a band offset ratio was taken to be

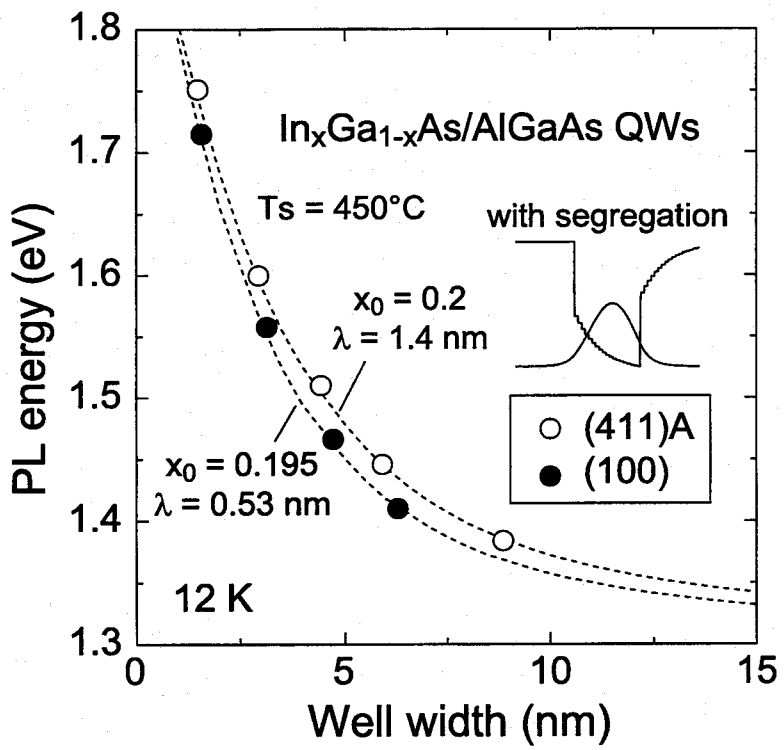


Figure 3.17: PL peak energies of the (411)A and (100) InGaAs/AlGaAs QWs grown at $T_s$ = 450°C plotted as a function of well widths. Broken lines are calculated ones taking into account of In surface segregation effect.

0.6. In segregation length $\lambda$ determined by the HRXRD result was used, and $x_0$ was used as a fitting parameter. In Fig. 3.17, observed PL peak energies from the (411)A (open circles) and (100) QWs (closed circles) grown at $T_s$ = 450°C and calculated ones (broken lines) were plotted as a function of well width. Thicknesses of InGaAs well widths of the (411)A and (100) QWs were calibrated by $x_0$ and thickness of GaAs determined by PL peaks from GaAs/AlGaAs QWs. Observed PL peak energies of the (411)A and (100) QWs were well fitted by almost the same $x_0$ ($x_0$ = 0.200 for the (411)A QWs and $x_0$ = 0.195 for the (100) QWs), which is good agreement with HRXRD results. Thus, the observed blue-shifts of PL peaks from the (411)A QWs compared to the corresponding (100) QWs can be well explained by differences of $\Delta E_g$ and In segregation length.

Figure 3.18 illustrates substrate temperature dependence of full widths at half maximums (FWHMs) of the PL peaks from the (411)A and (100) InGaAs/AlGaAs QWs plotted as a function of wavelength. PL FWHMs of the (411)A QWs have almost no dependence on $T_s$ [Fig. 3.18(a)], while those of the (100) QWs strongly depends on $T_s$

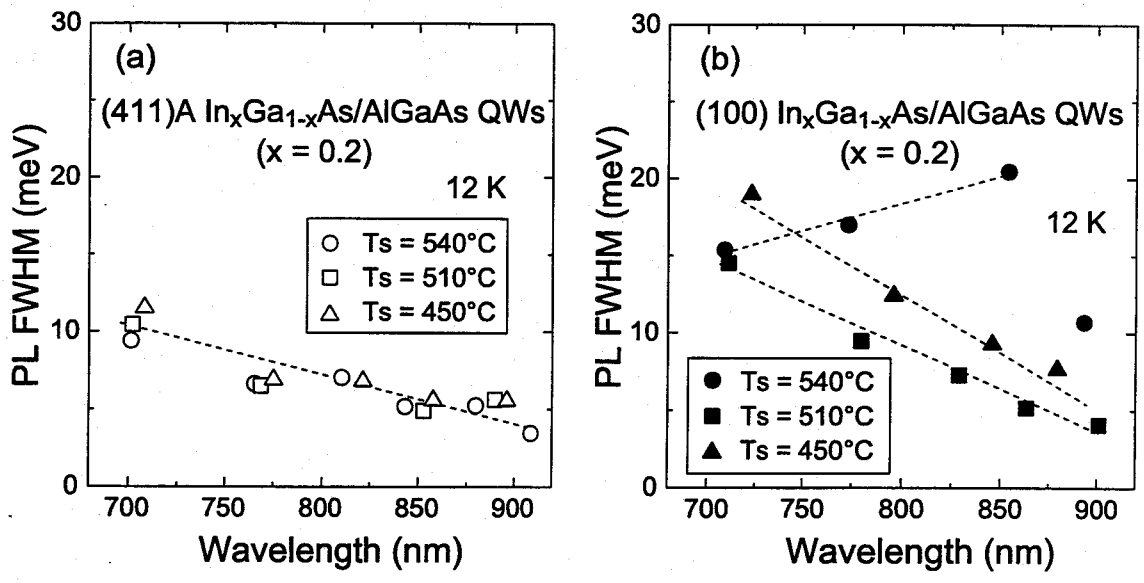


Figure 3.18: Substrate temperature dependence of PL FWHMs at 12 K of the (a) (411)A and (b) (100) InGaAs/AlGaAs QWs plotted as a function of wavelength.

[Fig. 3.18(b)]. In case of the (100) QWs grown at $T_s$ = 540°C, the PL FWHM degraded as increasing well width, indicating that roughness of the (100) InGaAs growing surface increased consistently with their thickness at high $T_s$ of 540°C. In contrast with this, PL FWHMs of the (411)A QWs grown at $T_s$ = 540°C did not degrade as increasing well width, indicating that a flat InGaAs growing surface was achieved even at high $T_s$ of 540°C. Furthermore, PL FWHMs of all the (411)A QWs are 20–30% smaller than those of the corresponding (100) QWs grown at $T_s$ = 510°C, which have the smallest PL FWHMs in the (100) samples. These results indicate that interface flatness in the (411)A QWs does not degrade even at higher $T_s$ which makes In surface segregation more enhanced, and superior interface flatness in the (411)A QWs compared with those of the (100) QWs can be achieved at a wide substrate temperature range. No degradation of PL FWHMs from the (411)A QWs grown at high $T_s$ also indicates that the In surface segregation uniformly proceeds in the (411)A growth-layer plane. As a result, "(411)A super-flat interfaces" (effectively atomically flat interfaces over a wafer-size are) can be formed in pseudomorphic InGaAs/AlGaAs QWs at a wide substrate temperature range ($T_s$ = 450–510°C).

### 3.4.3 Summary

We investigated that In surface segregation during InGaAs growth on (411)A GaAs substrates by MBE and its correlation with interface flatness in the pseudomorphic (411)A InGaAs/AlGaAs QWs. Values of In segregation lengths of the (411)A InGaAs are about three times larger than those of simultaneously grown (100) InGaAs, however, the activation energy of the In segregation length for the (411)A InGaAs is the same as that for the (100) InGaAs. This behavior of the In segregation length can be well explained by a surface segregation model base on surface migration of group III atoms. PL peak energies at 12 K of the pseudomorphic (411)A and (100) InGaAs/AlGaAs QWs were well explained by calculated ones taking into account of the In surface segregation, which were characterized by HRXRD measurements. Much narrower PL linewidths of the (411)A QWs compared with conventional (100) QWs have almost no dependence on the substrate temperature, indicating that superior interface flatness does not degrade even if In surface segregation is enhanced by an increase in the substrate temperature in the range of $T_s$ = 450–510°C. Therefore, In surface segregation uniformly proceeds in the (411)A growth-layer plane and (411)A super-flat InGaAs/AlGaAs interfaces can be formed at a wide substrate temperature range. These results are important information for fabricating pseudomorphic InGaAs/AlGaAs quantum devices with (411)A super-flat interfaces.

# Bibliography


[1] L. D. Nguyen, P. J. Tasker, D. C. Radulescu and L. F. Eastman: IEEE Trans. Electron Devices **36** (1989) 2243.

[2] P. P. Ruden, M. Shur, D. K. Arch, R. R. Daniels, D. E. Grider and T. E. Nahova: IEEE Trans. Electron Devices **36** (1989) 2371.

[3] M. Fukuda, M. Okayasu, J. Temmyo and J. Nakano: IEEE J. Quantum Electron. **30** (1994) 471.

[4] U. Strau$\beta$, D. Bernklau, H. Riechert and S. Finkbeiner: J. Appl. Phys. **80** (1996) 322.

[5] P. B. Kirby, J. A. Constable and R. S. Smith: Phys. Rev. **B40** (1989) 3013.

[6] S. Shimomura, A. Wakejima, A. Adachi, Y. Okamoto, N. Sano, K. Murase and S. Hiyamizu: Jpn. J. Appl. Phys. **32** (1993) L1728.

[7] S. Hiyamizu, S. Shimomura, A. Wakejima, S. Kaneko, A. Adachi, Y. Okamoto, N. Sano and K. Murase: J. Vac. Sci. & Technol. **B12** (1994) 1043.

[8] S.Yamakawa, M. Hisada, S. Shimomura, Y. Yuba, S. Namba, Y. Okamoto, M. Shigeta, T. Yamamoto, K. Kobayashi, N. Sano and S. Hiyamizu: Surf. Sci. **267** (1992) 21

[9] K. Yang, T. Anan and L. J. Schowalter,: Appl. Phys. Lett. **65** (1994) 2789.

[10] L. Hart, M. Ghisoni, P. Stavrinou and G. Party: Mat. Sci. and Technol. **11** (1995) 50.

[11] Muraki, K., Fukatsu, S., Shiraki, Y. and Ito, R., Appl. Phys. Lett. **61** (1992) 557.

[12] J. W. Matthews and A. E. Blakeslee: J. Cryst. Growth. **27** (1974) 118.

[13] T. G. Andersson, Z. G. Chan, V. D. Kulakovskii, A. Uddin and J. T. Vallin: Appl. Phys. Lett. **51** (1987) 752.

[14] N. G. Anderson, W. D. Laidig, R. M. Kolbas and Y. C. Lo: J. Appl. Phys. **60** (1986) 2361.

[15] M. J. Ekenstedt, S. M. Wang and T. G. Andersson: Appl. Phys. Lett. **58** (1991) 854.

[16] W. C. Hsu, S. Z. Chang and W. Lin: Jpn. J. Appl. Phys. **31** (1992) 26.

[17] J. M. Moison, C. Guille, F. Houzay, F. Barthe and M. Van Rompay: Phys. Rev. **B40** (1989) 6149.

[18] J. M. Gerard: Appl. Phys. Lett. **61** (1992) 2096.

[19] K. Muraki, S. Fukatsu, Y. Shiraki and R. Ito: J. Cryst. Growth **127** (1993) 546.

[20] R. M. Fleming, D. B. McWhan, A. C. Gossard, W. Wiegmann and R. A. Logan: J. Appl. Phys. **51** (1980) 357.

[21] A. Wakejima, A. Inoue, T. Kitada, N. Tomita, S. Shimomura, M. Fujii, T. Yaamoto, K. Kobayashi, N.Sano, and S. Hiyamizu: J. Vac. Sci. & Technol. **B12** (1994) 1102.

[22] K. Nakagawa, M. Miyao, Y. Shiraki: Thin Solid Films **183** (1989) 315.

# Chapter 4

# InGaAs/InAlAs system on (411)A InP substrates

## 4.1 Properties of InGaAs layer on (411)A InP

In this section, we investigated structural and optical properties of $In_xGa_{1-x}As$ layers ($0.505 \leq x \leq 0.545$) grown on (411)A InP substrates by MBE. High-resolution X-ray diffraction (HRXRD) and low-temperature PL measurements were used for characterization.

### 4.1.1 MBE growth procedures

(411)A and (100)-oriented InP substrates were degreased and etched by $Br_2/CH_3OH$ etchants to remove residual impurities on the surfaces, and they were mounted side by side on a 2 in Mo block of a substrate holder. After loading into a growth chamber of a Nissin RB-2001G MBE system, native oxides on the InP substrate surfaces were removed by increasing substrate temperature ($T_s$) up to 520°C under $As_4$ beam flux. $In_xGa_{1-x}As$ layers ($x$ = 0.505–0.545, about 800 nm thick) were grown simultaneously on (411)A and (100) substrates under two growth conditions [(1) $T_s$ = 490°C, V/III = 10 (in pressure ratio) or (2) $T_s$ = 520°C, V/III = 15]. Growth rate of the InGaAs layers was about 1 $\mu$m/h and the substrates were rotated at 30 rpm during MBE growth. In contents ($x$) of the $In_xGa_{1-x}As$ layers were observed by HRXRD measurements. Variations of In contents in the (411)A and (100) samples with sized 10 $mm^2$ were less than 0.5%. HRXRD and PL measurements were performed at the center of the (411)A and (100) samples, which were mounted side by side at the center of the Mo substrate holder. This indicates that

the observed In contents of the (411)A samples were the same as those of simultaneously grown (100) samples. Surfaces of all samples observed by a Nomarski-type microscope were featureless, and any cross-hatch pattern or cracking due to lattice mismatch was not observed.

### 4.1.2 HRXRD measurements

Structural properties of the $In_xGa_{1-x}As$ layers grown on (411)A InP substrates were characterized by HRXRD measurements. An incident X-ray beam with a wavelength ($\lambda$ = 0.15406 nm) of Cu K$\alpha$1 was monochromated by a (220)-oriented Ge asymmetric four-crystal system. InGaAs samples were mounted on a computer-controlled goniometer stage, and the diffracted X-ray intensity was counted as a function of the incident beam angle.

Figure 4.1 shows HRXRD rocking curves around the (400) reflection of $In_xGa_{1-x}As$ layers ($x$ = 0.505) grown at $T_s$ = 520°C and V/III = 15 on (411)A and (100) InP substrates. The (400) reflection is an asymmetric reflection for the (411)A samples, so HRXRD rocking curves around the low- and high-incidence angle (400) reflections are shown in Figs. 4.1(a) and 4.1(b), respectively. Peak angle difference between the InGaAs epitaxial layer and the InP substrate for the low-incidence angle (400) reflection was 655 sec, which is much different from that (173 sec) for the high-incidence angle (400) reflection. This result indicates that the [400] direction of the (411)A InGaAs crystals is different from that of the (411)A InP substrate due to a small amount of strain caused by lattice mismatch. Full-widths at half maximum (FWHMs) of the low- and high-incidence angle (400) peaks of the (411)A InGaAs layer were 44 sec and 33 sec, respectively, which are better than or comparable to that (44 sec) of the (100) InGaAs layer [Fig. 4.1(c)]. Hence, crystal uniformity of the (411)A InGaAs is almost the same or slightly better than that of the (100) InGaAs.

In order to evaluate the magnitude of the strain in the (411)A InGaAs layers, we calculated the peak angle difference between the InGaAs layer and the InP substrate by taking into account elastic strain in the InGaAs layer on (411)A InP substrate. Yang

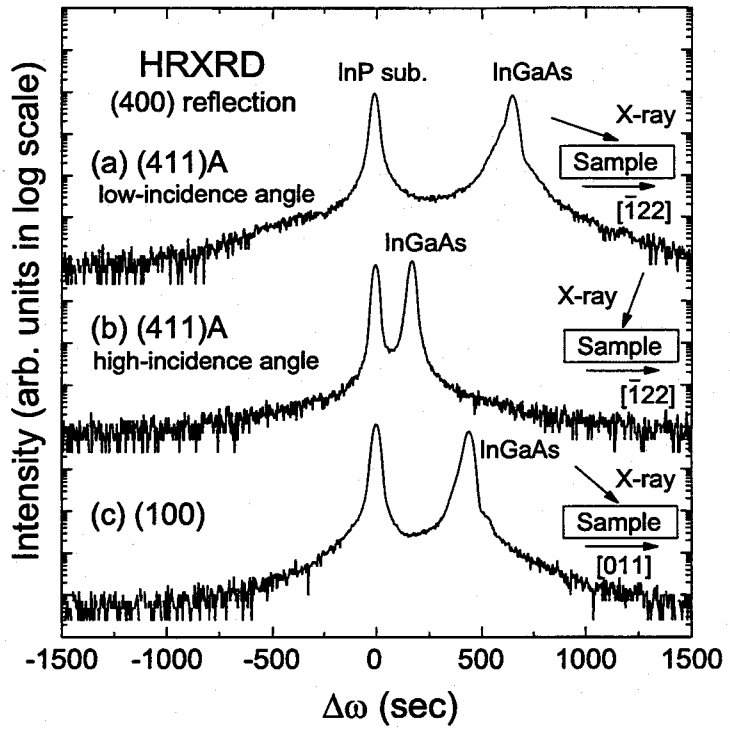


Figure 4.1: HRXRD rocking curves around the (400) reflection of an $In_xGa_{1-x}As$ layer ($x$ = 0.505) on a (411)A InP substrate for (a) low-incidence and (b) high-incidence angles, and (c) a rocking curve around the (400) reflection of an $In_xGa_{1-x}As$ ($x$ = 0.505) layer on a (100) InP substrate. These InGaAs layers were simultaneously grown at $T_s$ = 520°C and V/III = 15.

et al. [1] reported a model in which the strain components of a pseudomorphic layer grown on an arbitrarily oriented substrate can be calculated. In this model, the strain components of the pseudomorphic layer were derived by minimizing the elastic strain energy density under the "constrained" condition where all vectors connecting any two lattice points on a crystal plane parallel to the interface in a pseudomorphic layer should be equal to the corresponding vectors in the substrate crystal, as illustrated in Fig. 4.2. We calculated unit reciprocal vectors of the pseudomorphic $In_xGa_{1-x}As$ layer on the (411)A InP substrate using calculated strain components. A lattice constant ($a_{InGaAs}$) of $In_xGa_{1-x}As$ without any strain was assumed to be given by Vegard's law. Then, the difference ($\Delta\omega$) in peak angle between the InGaAs layer and the InP substrate in a HRXRD rocking curve around a low-incidence angle (400) reflection is given by

$$\Delta\omega = \omega_{InGaAs} - \omega_{InP} - \Delta\theta, \quad \text{for } \omega_{InGaAs} \leq \omega_{InP}, \tag{4.1}$$

$$\Delta\omega = \omega_{InGaAs} - \omega_{InP} + \Delta\theta, \quad \text{for } \omega_{InGaAs} > \omega_{InP}, \tag{4.2}$$

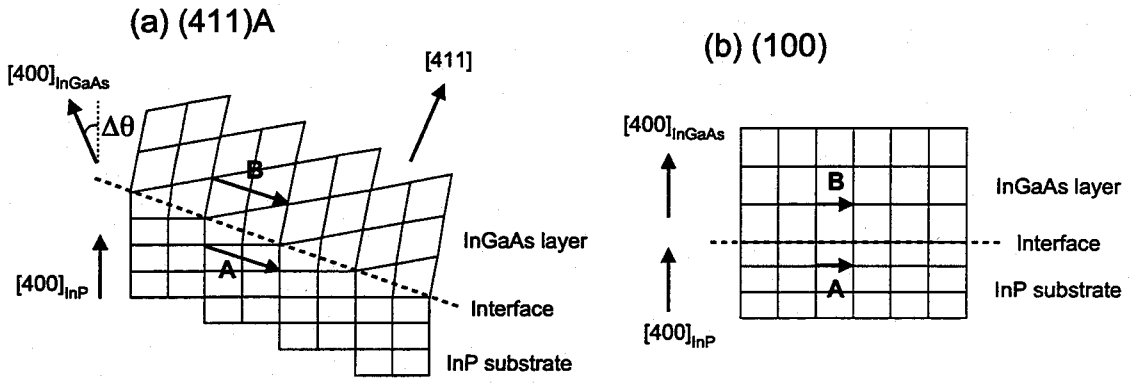


Figure 4.2: Illustration of pseudomorphic "constraint" requirements of an InGaAs layer grown on (a) (411)A and (b) conventional (100) InP substrates. All vectors connecting any two lattice points on a crystal plane parallel to the InGaAs/InP interface in the InGaAs layer should be equal to the corresponding vectors of the InP substrate. For instance, vector **A** is equal to vector **B**.

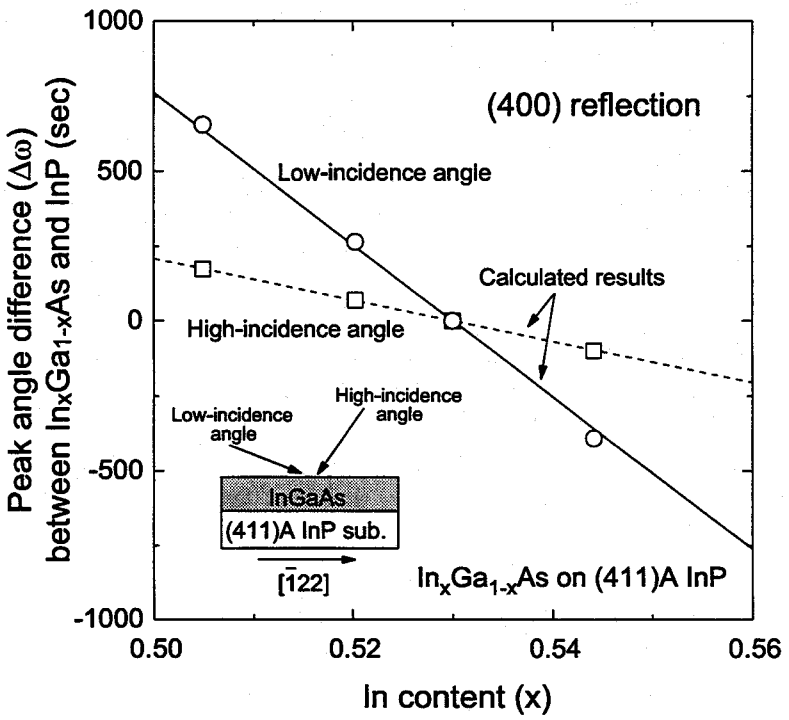


Figure 4.3: Difference ($\Delta\omega$) in peak angle between the $In_xGa_{1-x}As$ layer and the InP substrate in the HRXRD rocking curves around the (400) reflection of the (411)A samples as a function of In content ($x$). Open circles and a solid line (open squares and a dotted line) are the observed and calculated results, respectively, for low-incidence angle diffraction (for high-incidence angle diffraction). Observed results are in good agreement with the calculated ones.

and $\Delta\omega$ for the high-incidence angle case is given by

$$\Delta\omega = \omega_{InGaAs} - \omega_{InP} + \Delta\theta, \quad \text{for } \omega_{InGaAs} \leq \omega_{InP}, \tag{4.3}$$

$$\Delta\omega = \omega_{InGaAs} - \omega_{InP} - \Delta\theta, \quad \text{for } \omega_{InGaAs} > \omega_{InP}, \tag{4.4}$$

where $\omega_{InGaAs}$ and $\omega_{InP}$ are the (400) Bragg diffraction angles of InGaAs and InP, and $\Delta\theta$ is the angle difference between the (400) reciprocal vectors of the InGaAs layer and the InP substrate.

Observed $\Delta\omega$ of the (400) reflection as a function of In content of the $In_xGa_{1-x}As$ layers is shown in Fig. 4.3. Open circles and open squares show observed $\Delta\omega$ for the low- and high-incidence angle (400) reflections, respectively, and solid and dotted lines illustrate calculated $\Delta\omega$ using eqs. (4.1)–(4.4). In contents ($x$) of the (411)A $In_xGa_{1-x}As$ layers were determined from the (400) HRXRD curves of the $In_xGa_{1-x}As$ layers simultaneously grown on the (100) InP substrates. The calculated results showed good agreement with the experimental results, as can be seen in Fig. 4.3. These results indicate that there is no relaxation of lattice mismatch in the $In_xGa_{1-x}As$ layers grown on (411)A-oriented InP substrates for $0.505 \leq x \leq 0.545$.

### 4.1.3 PL measurements

Optical properties of the (411)A InGaAs layers were characterized by low temperature PL measurements (T = 12–50 K). The excitation laser used was a He-Cd laser ($\lambda$ = 325 nm) with an excitation power of 5 mW. The excitation beam was focused on an area of the substrate surface measuring approximately 200 $\mu$m diameter. Figure 4.4 shows temperature dependence of the PL spectra of the $In_{0.53}Ga_{0.47}As$ layers grown at $T_s$ = 490°C and V/III = 10 on (411)A and the (100) InP substrates. A PL peak at 12 K of the (411)A InGaAs layer was observed at a wavelength of 1562 nm with a small tail at the low-energy side. Line shapes of PL peaks of the (411)A InGaAs layer were almost the same over the whole temperature range of 12–50 K as shown in Fig. 4.4(a), while a PL peak of the (100) InGaAs layer has a double-peak feature ($\lambda$ = 1563 nm and 1576 nm), and the high-energy peak increases in intensity with increasing temperature from 12 K

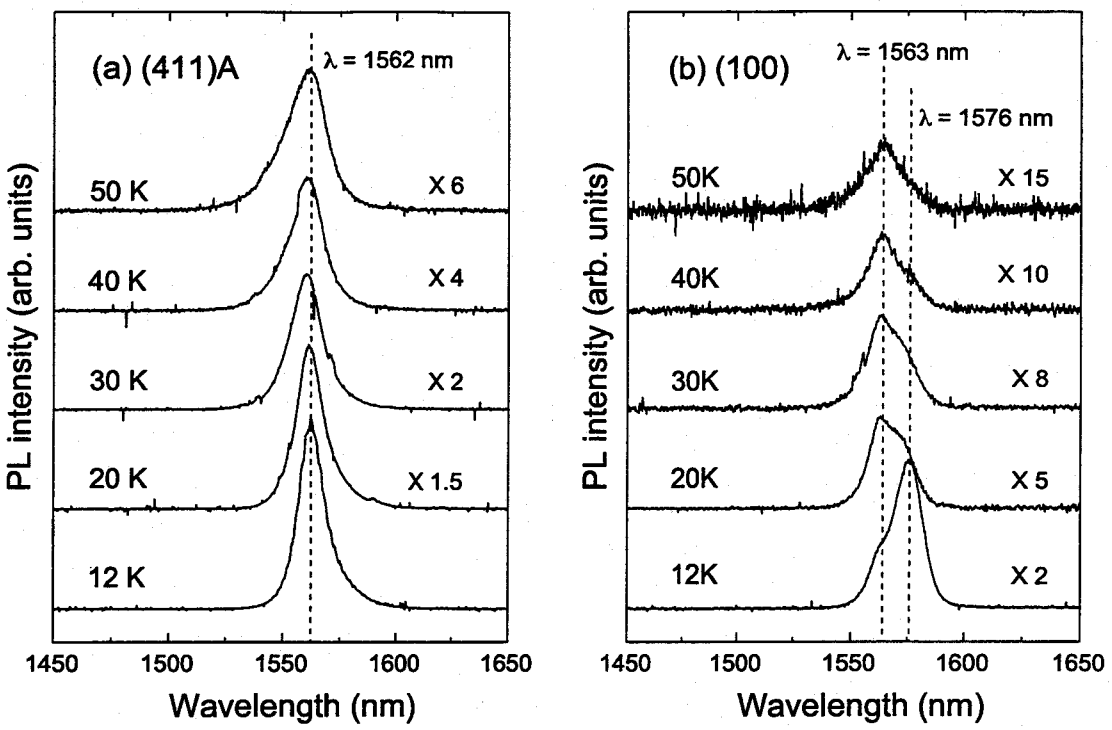


Figure 4.4: Temperature dependence of photoluminescence spectra of the $In_xGa_{1-x}As$ ($x$ = 0.53) layers grown at $T_s$ = 490°C and V/III = 10 on (a) (411)A and (b) (100) InP substrates.

to 50 K [Fig. 4.4(b)]. The low-energy PL peak ($\lambda$ = 1576 nm) from the (100) sample at 12 K is due to defect- or impurity-related luminescence, and the shoulder at the high-energy side ($\lambda$ = 1563 nm) is due to band-to-band luminescence. Further investigations are necessary to determine the exact origins of the luminescence peaks. The PL peak of the (411)A sample is considered to be mainly dominated by band-to-band luminescence, because the wavelength of the PL peak is almost the same as that (1563 nm) of the band-to-band luminescence of the (100) InGaAs layer, and these two samples have the same In content, which was confirmed by HRXRD measurements. FWHM of the PL peak of the (411)A sample at 12 K was 6.7 meV, which is about 20% smaller than that (8.4 meV at 12 K) of the (100) sample. Furthermore, integrated intensity of the PL peak from the (411)A InGaAs layer was about three–five times larger than that of the (100) InGaAs layer. These results imply that incorporation of impurities and non radiative centers such as defects into the (411)A InGaAs layer during MBE growth is significantly suppressed compared with the conventional (100) InGaAs layer.

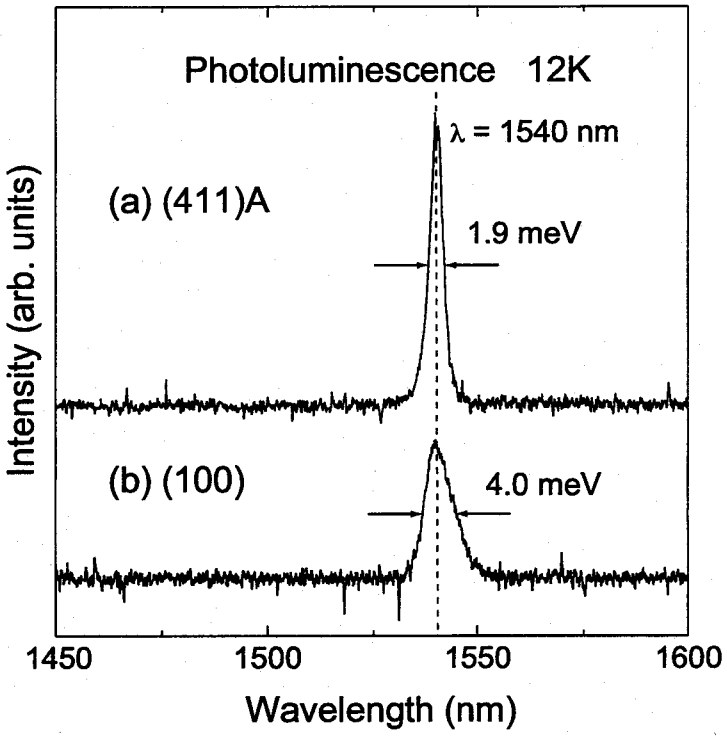


Figure 4.5: Photoluminescence spectra observed at 12 K for the $In_xGa_{1-x}As$ layers ($x$ = 0.505) grown at an elevated temperature $T_s$ of 520°C and V/III = 15 on (a) (411)A and (b) (100) InP substrates.

Figure 4.5 shows PL spectra observed at 12 K for the $In_xGa_{1-x}As$ layers ($x = 0.505$) grown at an elevated temperature ($T_s = 520$°C) and V/III = 15 on (411)A and the (100) InP substrates. Excitation power of the He-Cd laser was reduced to 0.5 mW for these PL spectra. PL peaks from the (411)A and the (100) InGaAs layers were observed at the same wavelength of 1540 nm, and these PL peaks are considered to be dominated by band-to-band luminescence because there was no difference among the PL line shapes at 12 K and elevated temperatures (12–50 K) for both the (411)A and the (100) samples. PL FWHM (1.9 meV) of the (411)A InGaAs layer was 52% smaller than that (4.0 meV) of the simultaneously grown (100) InGaAs layer, and almost the same as the optimum value (1.2–3.0 meV) reported for InGaAs layers grown on (100) InP substrates by MBE [2, 3] and chemical beam epitaxy (CBE) [4]. This result also indicates that incorporation of impurities or defects into an InGaAs layer grown on the (411)A InP substrate by MBE is suppressed more than that into a conventional (100) InGaAs layer, and high-quality InGaAs layers can be easily grown on the (411)A InP substrates.

### 4.1.4 Summary

High-quality $In_xGa_{1-x}As$ layers ($0.505 \leq x \leq 0.545$, about 800 nm thick) were grown on (411)A-oriented InP substrates by MBE. Observed residual strain in the (411)A $In_xGa_{1-x}As$ layers by HRXRD measurements showed good agreement with the calculated results based on the "constrained" model [1] for a pseudomorphic layer grown on the high index plane of a substrate, indicating that there were no relaxations of lattice mismatch in the (411)A InGaAs layers. Low-temperature photoluminescence measurements showed significantly improved optical properties of the (411)A InGaAs layers compared with those of simultaneously grown InGaAs layers on a (100) InP substrate; this improvement is probably due to reduced incorporation of impurities and/or defects in the (411)A samples during MBE growth. The observed PL FWHM (1.9 meV) of the (411)A $In_xGa_{1-x}As$ layer ($x = 0.505$) grown at 520°C and V/III = 15 was almost the same as the optimum value (1.2–3.0 meV) reported so far for InGaAs layers grown on the (100) InP substrates. These results imply that high-quality InGaAs layers can be easily obtained by MBE growth on (411)A InP substrates.

## 4.2 Properties of InAlAs layer on (411)A InP

MBE growth of a high quality InAlAs barrier layers is essential in order to achieve high quality InGaAs/InAlAs heterostructures. In this section, we investigated that MBE growth conditions of high quality InAlAs layers on (411)A-oriented InP substrates with the use of high resolution X-ray diffraction (HRXRD) and low-temperature (12 K) PL measurements.

### 4.2.1 MBE growth of InAlAs layers

The (411)A-oriented InP substrates were degreased and etched by $Br_2/CH_3OH$ to remove residual impurities on the substrate surfaces, and they were mounted side by side with (100) InP substrates on a 2-inch Mo holder with In solder. After loading into a growth chamber of a Nissin RB-2001G MBE system, native oxides of InP were desorbed by raising substrate temperature ($T_s$) up to 520°C under $As_4$ beam flux. 800 nm-thick $In_xAl_{1-x}As$ layers ($x = 0.49 \sim 0.52$) were grown on these substrates under two growth conditions of (1) $T_s$ = 520°C, V/III ($As_4$/(In+Al)) = 16 (in pressure) and (2) $T_s$ = 570°C, V/III = 9. A growth rate of the InAlAs layers was about 1 $\mu$m/h and the substrates were rotated at 30 rpm during MBE growth. Beam flux intensities of In and Al were adjusted with the use of a beam flux monitor, and In contents (x) of $In_xAl_{1-x}As$ layers were checked by high resolution X-ray diffraction (HRXRD) measurements.

### 4.2.2 Crystalline properties of InAlAs layers

Figure 4.6 shows surface morphologies of the InAlAs layers simultaneously grown on (411)A- [(a) and (b)] and (100)-oriented [(c) and (d)] InP substrates observed by a Nomarski interference microscope. Figs 4.6(a) and 4.6(c) are surface morphologies of the InAlAs layers grown at $T_s$ = 520°C, and Figs 4.6(b) and 4.6(d) are those of the InAlAs grown at $T_s$ = 570°C. Surface morphologies of the (100) InAlAs layers are quite featureless even for two different growth conditions. In case of the (411)A InAlAs layers, quite a featureless surface was observed for $T_s$ = 570°C, while a rough surface for $T_s$ = 520°C, indicating that enhancement of surface migration of group III atoms (In, Al) by a

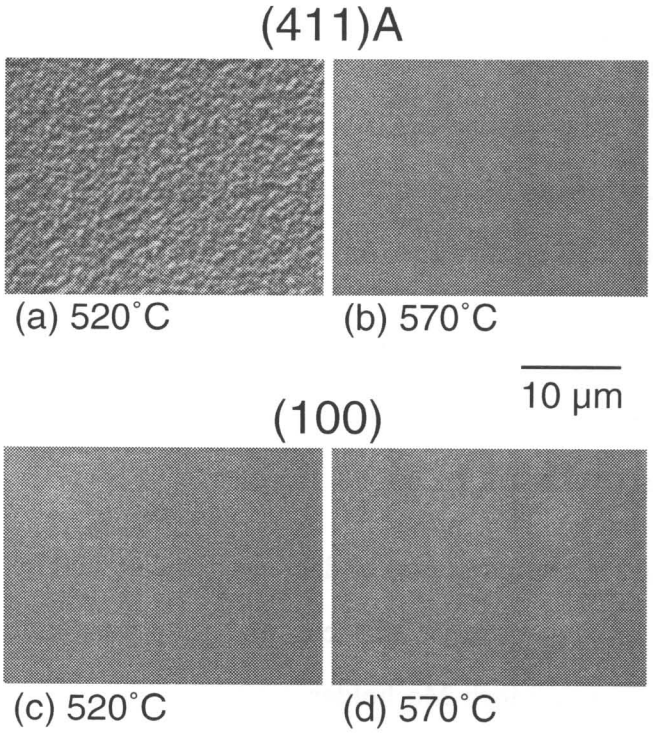


Figure 4.6: Surface morphologies of the InAlAs layers simultaneously grown at $T_s = 520$ and 570°C on (411)A- [(a) and (b), respectively] and (100)-oriented [(c) and (d)] InP substrates by MBE.

high substrate temperature is necessary to obtain flat surfaces of InAlAs layers grown on (411)A InP substrates.

Figure 4.7 shows HRXRD rocking curves around low-incidence (511) reflection of the InAlAs layers grown on (411)A InP substrates. An incident X-ray beam with a wavelength ($\lambda = 0.15406$ nm) of Cu K$\alpha$1 was obtained by a (220)-oriented Ge asymmetric four-crystal monochromator. InAlAs samples were mounted on a computer-controlled goniometer stage, and a diffracted X-ray intensity was counted as a function of the incident beam angle. A sharp peak from the (411)A InAlAs layer grown at $T_s = 570$°C is clearly seen at 104 sec apart from a (511) reflection peak of the InP substrate [full width at half maximum (FWHM) of 34 sec] in Fig. 4.7(a), while a broaden peak from the (411)A InAlAs grown at $T_s = 520$°C is observed at 775 sec apart from a substrate peak (FWHM of 450 sec) in Fig. 4.7(b). By comparing these reflection angles with calculated ones taking into account of the strain components of InAlAs layers on (411)A InP substrates [1], In contents (x) of the (411)A $In_xAl_{1-x}As$ layers grown at $T_s = 520$ and 570°C were determined to be 0.49

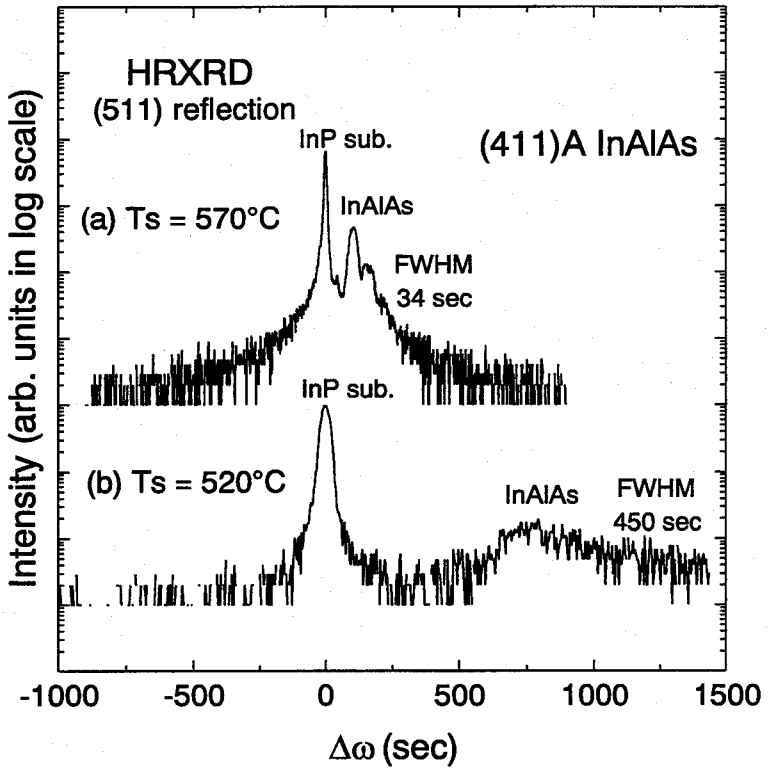


Figure 4.7: HRXRD rocking curves around (511) reflections of the InAlAs layers grown at $T_s = 570$°C (a) and $T_s = 520$°C (b) on (411)A InP substrates.

and 0.52, respectively. The difference of the In content between these two samples is due to different beam flux intensity ratio [In / (In + Al)]. Relaxation of lattice-mismatch did not occur in these two samples, which was confirmed by HRXRD measurements of high- and low-incidence asymmetric (511) reflections for these two samples. The InAlAs layers simultaneously grown on (100) InP substrates showed the same In contents as those of the (411)A InAlAs layers. HRXRD measurements around (400) reflections were used for the (100) samples. A most prominent feature in HRXRD rocking curves in Fig. 4.7 is that the linewidth of the (411)A InAlAs peak is much improved by increasing Ts from 520°C to 570°C. These results indicate that the high substrate temperature ($T_s = 570$°C) is very important for MBE growth of InAlAs layers with featureless surface morphology and high crystalline quality.

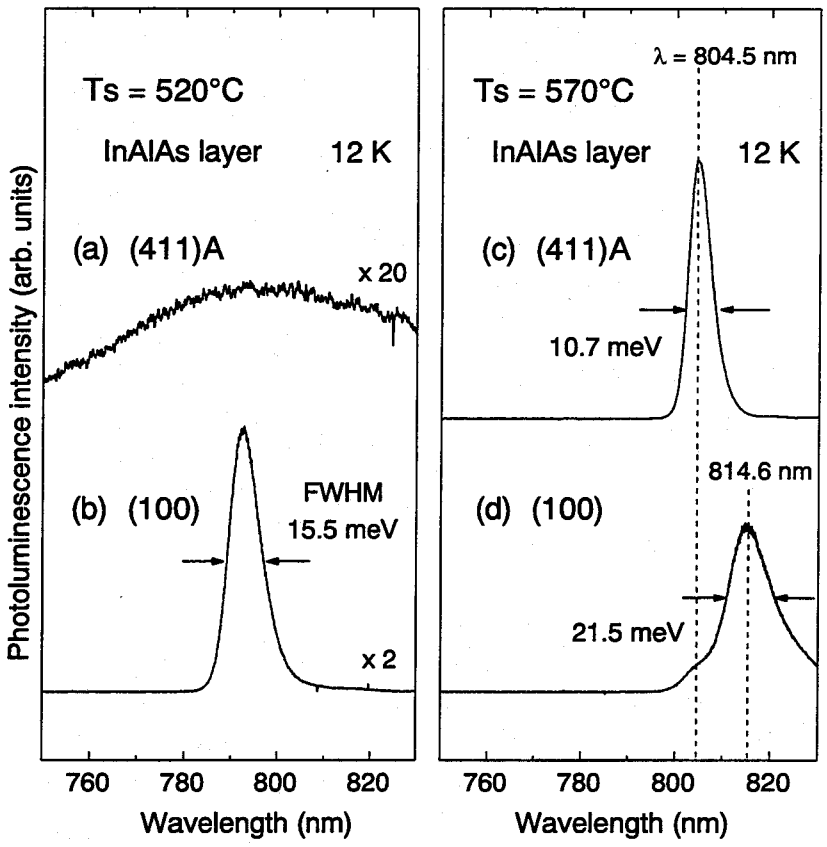


Figure 4.8: PL spectra (12 K) from InAlAs layers simultaneously grown at $T_s$ = 520 and 570°C on (411)A- [(a) and (c), respectively] and (100)-oriented [(b) and (d)] InP substrates.

### 4.2.3 Optical properties of InAlAs layers

Figure 4.8 shows PL spectra from InAlAs layers simultaneously grown on (411)A and (100) InP substrates at 12 K. An excitation laser was a He-Cd laser ($\lambda$ = 325 nm) with an excitation power of 2 mW. The excitation beam was focused on an area of about 200 $\mu$m diameter of the substrate surface. A much broadened PL peak was observed from the (411)A InAlAs layer grown at $T_s$ = 520°C, as shown in Fig. 4.8(a), while a sharp peak at 792.8 nm (FWHM = 15.5 meV) from the (100) InAlAs is clearly seen in Fig. 4.8(b). A broadened PL peak from the (411)A InAlAs grown at $T_s$ = 520°C is due to poor crystalline quality of the InAlAs layer, which is consistent with results of crystalline characterization by HRXRD. In contrast with this, a very sharp PL peak was observed at 804.5 nm (FWHM = 10.7 meV) from the (411)A InAlAs layer grown at $T_s$ = 570°C [Fig. 4.8(c)], while a broadened PL peak was observed at 814.6 nm (FWHM = 21.5

meV) from the (100) InAlAs [Fig. 4.8(d)]. It is worth to note that when the substrate temperature was increased from 520°C to 570°C, PL properties of the (411)A InAlAs layer were drastically improved, while those of the (100) InAlAs were slightly degraded. This result implies that MBE growth of the InAlAs layer at the high $T_s$ on the (411)A face is more stable than that on (100). The linewidth of the PL peak from the (411)A InAlAs layer is narrower than not only those of the (100) samples in this study but also those of (100) InAlAs layers grown by MBE reported so far (FWHM = 12.8 meV at 15 K [5], 15 meV at 4 K [6]). Therefore, the (411)A InAlAs layer grown at the high substrate temperature of 570°C has better optical quality compared with any conventional (100) InAlAs layers. Furthermore, the lineshape of the (411)A InAlAs is a single-peak at 804.5 nm [Fig. 4.8(c)], while that of the (100) InAlAs has a double-peak character, which consists of a main-peak at 814.6 nm with a high-energy side shoulder around 804.5 nm [Fig. 4.8(d)].

Figure 4.9 shows excitation power dependence of PL spectra from the (411)A and (100) InAlAs layers simultaneously grown at $T_s$ = 570°C. The lineshape of the PL peak from the (411)A InAlAs layer almost does not depend on the excitation power in the range of 0.05–2 mW as shown in Fig. 4.9(a). For the (100) InAlAs layer [Fig. 4.9(b)], the relative PL intensity of the high-energy side peak ($\lambda$ = 804.5 nm) against the main peak ($\lambda$ = 814.6 nm) are decreasing with decreases excitation power. The main PL peak at 814.6 nm of the (100) InAlAs layer is probably due to As-vacancy-related luminescence because of the high substrate temperature of 570°C, and the high energy side shoulder around 804.5 nm should be due to band-to-band luminescence. The PL peak from the (411)A InAlAs is due to band-to-band luminescence, because (1) the lineshape almost does not depend on the excitation power, and (2) the wavelength of the PL peak from the (411)A InAlAs layer ($\lambda$ = 804.5 nm) is the same as the high-energy side shoulder of the (100) InAlAs layer, which has the same In content (0.52) as that of the (411)A InAlAs layer. This result indicates that the incorporation of defects such as As vacancies in the InAlAs layer grown on a (411)A InP substrate is much suppressed compared with (100) InAlAs even at a high substrate temperature of 570°C.

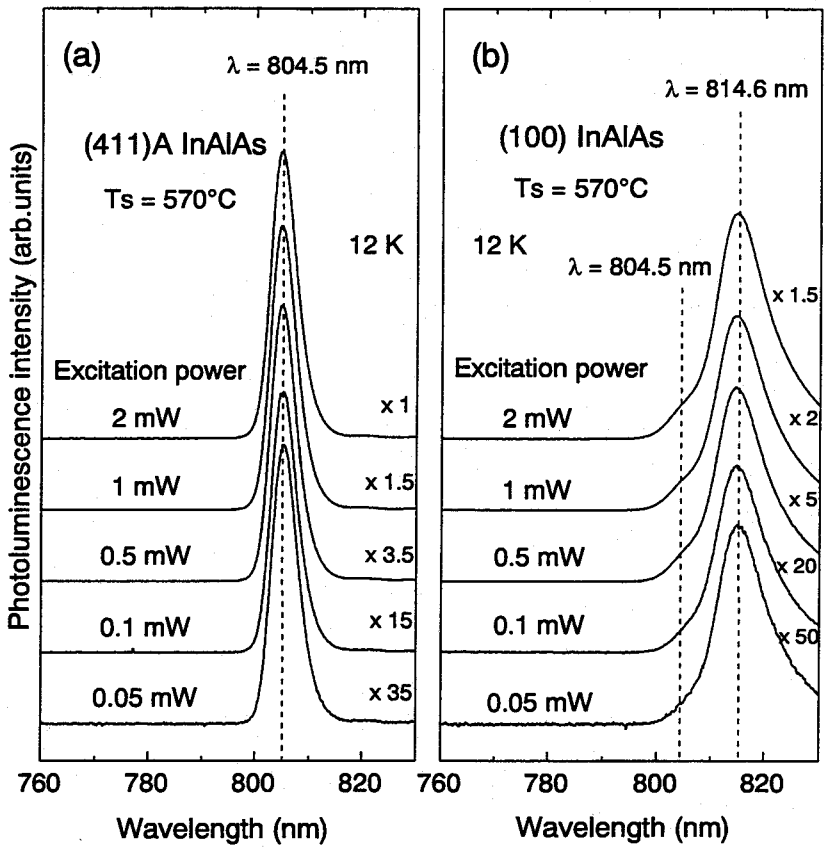


Figure 4.9: Excitation power dependence of PL spectra (12 K) from the InAlAs layers simultaneously grown on (411)A- (a) and (100)-oriented (b) InP substrates.

### 4.2.4 Summary

High quality InAlAs layers were successfully grown on (411)A-oriented InP substrates by MBE. Crystalline and optical properties of the (411)A InAlAs layers grown under different conditions revealed that a high substrate temperature of 570°C is very important for (411)A InAlAs layers with featureless surface morphology and good crystalline quality. Even at a high substrate temperature (570°C), the incorporation of defects such as As vacancies in the (411)A InAlAs layer is much suppressed compared with the simultaneously grown (100) InAlAs layer, which was characterized by PL measurements. Furthermore, a linewidth of the PL peak from the (411)A InAlAs layer (10.7 meV) is 16–29% narrower than those of conventional (100) InAlAs layers reported so far. [5, 6] Hence, MBE grown (411)A InGaAs/InAlAs heterostructures should be suitable for novel quantum devices such as HEMTs.

## 4.3 Interface flatness in InGaAs/InAlAs QWs on (411)A InP

Atomically flat interfaces of InGaAs/InAlAs heterostructures are very important for achieving better device performance, but there exists ± 1 monolayer fluctuation on atomically flat InGaAs/InAlAs interface formed by conventional molecular beam epitaxy (MBE) [7, 8]. In this section, we report that much improved PL linewidths of $In_{0.53}Ga_{0.47}As/In_{0.52}Al_{0.48}As$ QWs grown on (411)A InP substrates compared with those for conventional InGaAs/InAlAs QWs on (100) InP substrates.

### 4.3.1 MBE Growth of InGaAs/InAlAs QWs

The (411)A-oriented InP substrates were degreased and etched by $Br_2/CH_3OH$ to remove residual impurities on the substrate surfaces, and they were mounted side by side with (100) InP substrates on a 2-inch Mo substrate holder with the use of In solder. After loading into a growth chamber of a Nissin RB-2001G MBE system, native oxides of InP were desorbed by raising substrate temperature ($T_s$) up to 520°C under $As_4$ beam flux. After a buffer layer of a 500 nm thick InGaAs and a 4-periods $In_{0.52}Al_{0.48}As/In_{0.53}Ga_{0.47}As$ (20 nm / 50 nm) superlattice was grown on these substrates, $In_{0.53}Ga_{0.47}As/In_{0.52}Al_{0.48}As$ QWs were grown at $T_s$ = 570°C under V/III pressure ratio of 6. The substrates were rotated at 30 rpm during MBE growth. $In_{0.53}Ga_{0.47}As$ well widths ($L_w$) were 0.6, 1.2, 2.4, 3.6, 4.8, 7.2 and 12.0 nm, and $In_{0.52}Al_{0.48}As$ barrier layers were 20 nm thick. Growth rates of InGaAs and InAlAs were about 1 $\mu$m/h. Beam flux intensities of In, Ga and Al were adjusted with the use of a beam flux monitor, and In contents of the QWs were checked by high resolution X-ray diffraction (HRXRD) measurements. In contents of InGaAs and InAlAs layers in the QWs were 0.516 and 0.514, respectively. Layer thicknesses of $In_{0.53}Ga_{0.47}As$ layers were checked by cross-sectional atomic force microscope (AFM) images of the superlattice buffer layer of the sample.

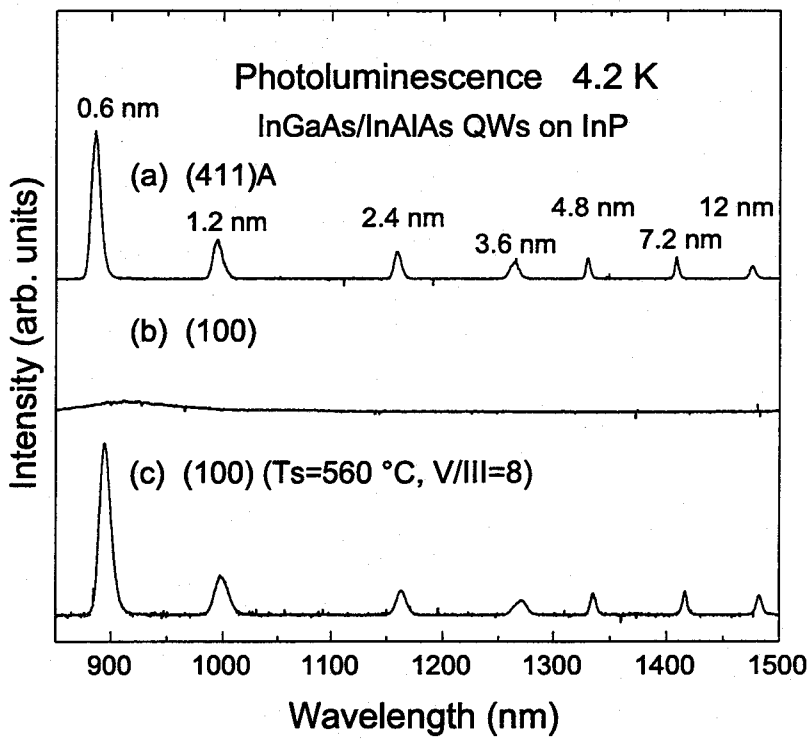


Figure 4.10: Photoluminescence spectra at 4.2 K from $In_{0.53}Ga_{0.47}As/In_{0.52}Al_{0.48}As$ QWs simultaneously grown on (a) (411)A and (b) (100) InP substrates at $T_s$ = 570°C under V/III = 6 and (c) from InGaAs/InAlAs QWs grown on (100) InP substrate at optimized condition ($T_s$ = 560°C, under V/III = 8).

### 4.3.2 Photoluminescence measurements

Figure 4.10 shows PL spectra at 4.2 K from the $In_{0.53}Ga_{0.47}As/In_{0.52}Al_{0.48}As$ QWs with well widths of 0.6–12 nm grown (a) on the (411)A InP substrate and (b) on the (100) InP substrate at $T_s$ = 570°C under V/III = 6. An excitation laser was a He-Cd laser with a wavelength of 325 nm and an excitation power of 4.5 mW. The excitation beam was focused on the substrate surface in an area of about 200 $\mu$m diameter. Narrow seven PL peaks at 885.4 nm (full width at half maximum (FWHM) of 15.5 meV), 994.4 nm (11.8 meV), 1158.9 nm (7.0 meV), 1264.5 nm (7.5 meV), 1329.8 nm (2.9 meV), 1408.6 nm (2.3 meV), and 1475.7 nm (3.2 meV) correspond to the luminescence from the (411)A QWs with $L_w$ = 0.6, 1.2, 2.4, 3.6, 4.8, 7.2 and 12 nm [Fig. 4.10(a)]. On the other hand, the luminescence from the (100) QWs was very weak, and a PL peak from each (100) QW could not be observed [Fig. 4.10(b)], indicating that crystalline structure of the (100) QWs was much degraded. Fig. 4.10(c) is a PL spectrum of (100) InGaAs/InAlAs QWs

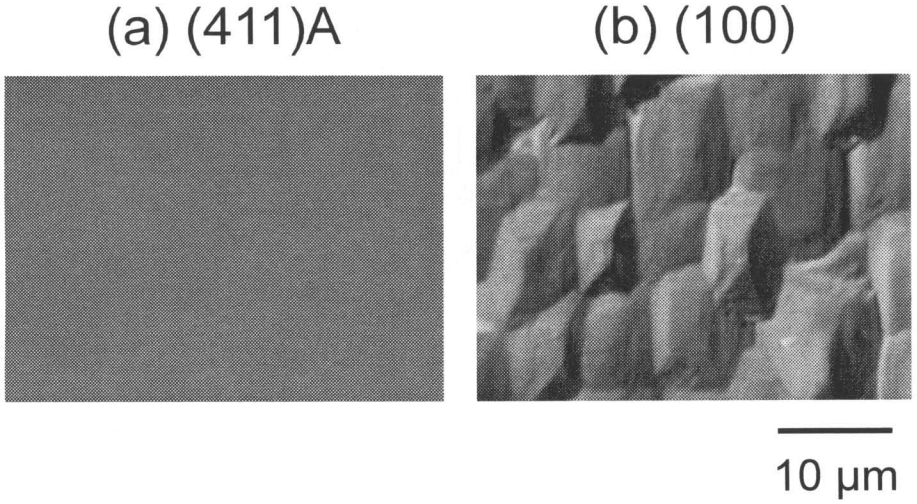


Figure 4.11: Surface morphology of the $In_{0.53}Ga_{0.47}As/In_{0.52}Al_{0.48}As$ QWs grown on (a) (411)A and (b) (100) InP substrates at $T_s = 570°C$ under V/III = 6.

grown at an optimized growth condition ($T_s = 560°C$, V/III = 8). FWHMs of the sample are about 20–30% larger than those of the (411)A QWs.

Surface morphology of the (411)A QWs sample was very smooth and featureless as shown in Fig. 4.11(a), in contrast with a rough surface of the simultaneously grown (100) QWs sample [Fig. 4.11(b)]. These surface roughing of the (100) QWs occurred at $T_s = 570°C$. Similar phenomenon had been reported for AlGaAs: surface morphology of 1.5 $\mu$m thick AlGaAs layers grown on (411)A GaAs substrates at $T_s = 580$–$700°C$ is very smooth, while rough surfaces of those simultaneously grown on (100) GaAs substrates are observed. [9] These results indicate that the (411)A plane is very stable during MBE growth not only for GaAs/AlGaAs QWs but also for $In_{0.53}Ga_{0.47}As/In_{0.52}Al_{0.48}As$ system at high substrate temperatures.

Figure 4.12 shows FWHMs of PL peaks from the (411)A $In_{0.53}Ga_{0.47}As/In_{0.52}Al_{0.48}As$ QWs plotted as a function of luminescence wavelength. FWHMs of the (100) $In_{0.53}Ga_{0.47}As/In_{0.52}Al_{0.48}As$ QWs grown at the optimized condition ($T_s = 560°C$, V/III = 8) in this study and the best values reported for (100) QWs [7, 8] are also plotted together. Wavelengths of PL peaks from the (100) QWs were slightly red-shift compared with those

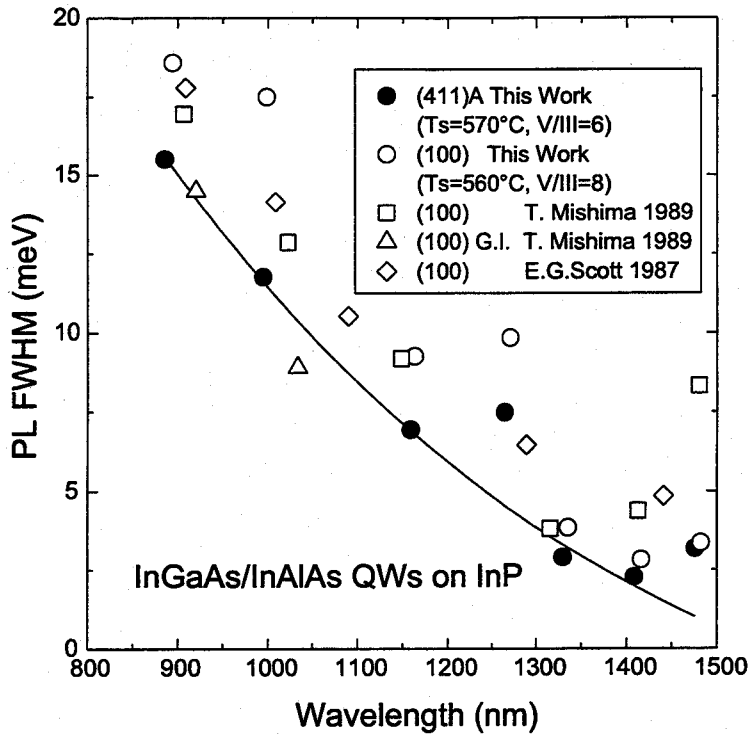


Figure 4.12: FWHMs of PL peaks (4.2 K) from the $In_{0.53}Ga_{0.47}As/In_{0.52}Al_{0.48}As$ QWs grown on (411)A (solid circles) and (100) (open circles) InP substrate as a function of wavelength. Data reported so far for the (100) InGaAs/InAlAs QWs (open squares [7] and diamonds [8]) and the (100) growth interrupted InGaAs/InAlAs QWs (open triangles [7]) are also plotted.

of the (411)A QWs, because In content of the (100) InGaAs QWs was 2.6% larger than that of the (411)A InGaAs QWs, which was observed by HRXRD measurements. FWHMs for the (411)A QWs (•) are 20–30% narrower than those of the (100) QWs grown in this study (○) and the reported values of (100) QWs (□ [7] and ◇ [8]), indicating that superior flatness of heterointerfaces are achieved in the (411)A $In_{0.53}Ga_{0.47}As/In_{0.52}Al_{0.48}As$ QWs. FWHMs for the (411)A QW ($\lambda$ = 1264.5 nm) and the (100) QW ($\lambda$ = 1270.9 nm) with $L_w$ = 3.6 nm are rather large compared with the reported value, which is probably due to coexistence of free excitons and bound excitons in these QWs. FWHMs for the (411)A QWs with $L_w$ = 0.6 and 1.2 nm are almost as small as those of the reported (100) QWs (△ [7]) grown by the growth interruption technique. In these very thin QWs ($L_w$ = 0.6, 1.2 nm), broading of PL peaks are mainly due to crystal quality of $In_{0.52}Al_{0.48}As$ barriers, in addition to the interface fluctuation, because a wavefunction of an electron confined in these QWs much more penetrates into the InAlAs barrier regions. The most prominent

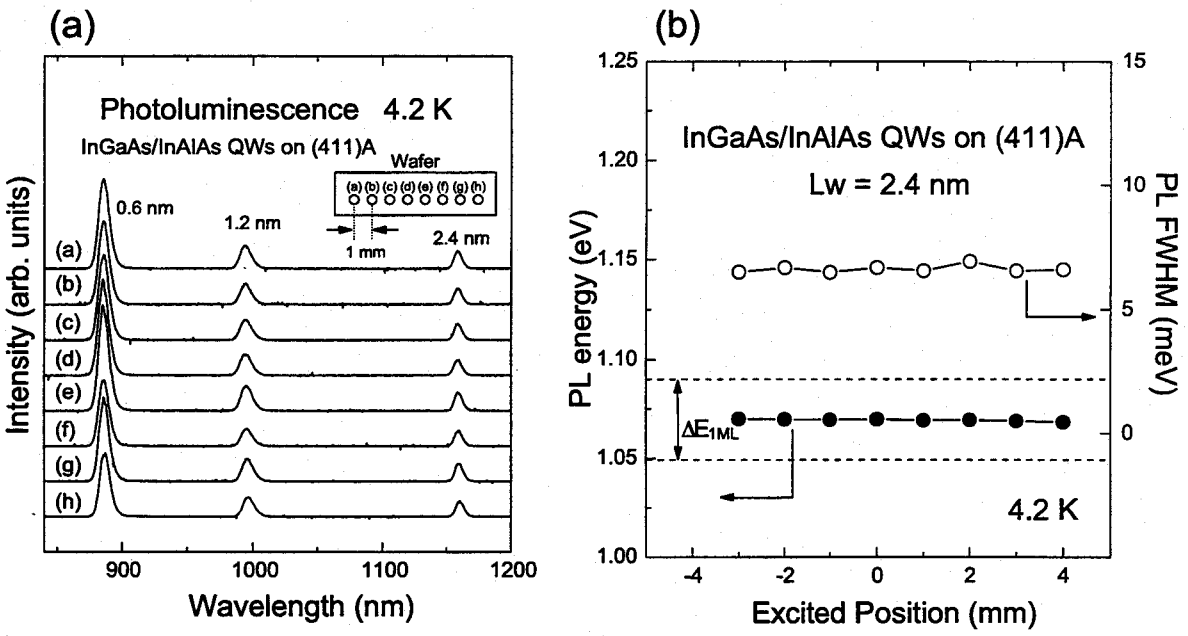


Figure 4.13: Excited position dependence of (a) PL spectra (4.2 K) from the (411)A $In_{0.53}Ga_{0.47}As/In_{0.52}Al_{0.48}As$ QWs with $L_w$ = 0.6, 1.2, and 2.4 nm, and (b) PL peak energy and FWHM of the (411)A QW with $L_w$ = 2.4 nm. $\Delta E_{1ML}$ indicates a calculated PL energy difference for 1 ML fluctuation of the QW.

feature is that only one PL peak with very narrow FWHM is observed from each (411)A QW as shown in Fig. 4.10(a), while a two- or three- splitted peaks were observed from each (100) growth-interrupted QW due to small size of atomically flat interface region of about a few $\mu m^2$. This result suggests that effectively atomically flat interfaces are formed in the (411)A $In_{0.53}Ga_{0.47}As/In_{0.52}Al_{0.48}As$ QWs over at least an area of the excited region ($\simeq$ 200 $\mu m^2$).

In order to confirm the formation of the effectively atomically flat interfaces over a substrate size area in the (411)A QWs, we observed lateral variation of PL peaks. Figure 4.13(a) shows excited position dependence of PL spectra from the (411)A QWs with $L_w$ = 0.6, 1.2, and 2.4 nm. Luminescence was observed at every 1 mm from the edge of the (411)A sample surface. The lineshape of each luminescence peak shows almost no lateral variation over a distance of as long as 7 mm. PL peak energy and FWHM of the (411)A QW with $L_w$ = 2.4 nm are plotted as a function of excited position in Fig. 4.13(b). PL peak energy continuously varied from 1069.9 meV to 1068.3 meV, and this variation (1.6 meV) of the PL peak energy is much smaller than a calculated energy

difference ($\Delta E_{1ML}$) of 40.7 meV for 1 ML thickness fluctuation of the 2.4 nm InGaAs well. Furthermore, FWHMs of PL peaks from the (411)A QWs are very narrow and almost constant (6.5–6.9 meV). These results indicate that effectively atomically flat interfaces over a large distance of 7 mm (the (411)A super-flat interfaces) are realized in the (411)A $In_{0.53}Ga_{0.47}As/In_{0.52}Al_{0.48}As$ QWs.

### 4.3.3 Summary

The (411)A super-flat interfaces were formed in $In_{0.53}Ga_{0.47}As/In_{0.52}Al_{0.48}As$ QWs on (411)A InP substrates by MBE. Excellent surface morphology of the (411)A $In_{0.53}Ga_{0.47}As/In_{0.52}Al_{0.48}As$ QWs obtained at higher $T_s$ shows that (411)A plane is more stable than (100) plane under MBE growth conditions. Single and narrow PL peaks were observed from the (411)A $In_{0.53}Ga_{0.47}As/In_{0.52}Al_{0.48}As$ QWs over a large distance of 7 mm compared with conventional (100) QWs. Hence, the (411)A $In_{0.53}Ga_{0.47}As/In_{0.52}Al_{0.48}As$ heterostructures are expected to improved performance of novel quantum devices.

## 4.4 Improved heterointerface flatness by using $(InGaAs)_2(InAlAs)_m$ SPS barrier

Flatness of InGaAs/InAlAs heterointerfaces in the (411)A QWs strongly depends on a substrate temperature ($T_s$) during MBE growth, because the growing surface flatness of InAlAs barrier layers strongly depends on $T_s$. This indicates that heterointerface flatness of the (411)A InGaAs/InAlAs QW is dominated by flatness of InAlAs layers during MBE growth. In this section, we report that improved interface flatness in the (411)A QWs grown by MBE can be achieved by using $(InGaAs)_2(InAlAs)_m$ short-period superlattice (SPS) barriers ($m \leq 4$) instead of thick InAlAs barriers.

### 4.4.1 MBE growth

The (411)A-oriented InP substrate was prepared by conventional methods and mounted on a 3 in Mo substrate holder with the use of In solder. After loading into a growth chamber of a VG semicon V80H MK-II MBE system, native oxides of InP were desorbed by raising substrate temperature ($T_s$) up to 520°C under $As_4$ beam flux. After a buffer layer of a 500 nm thick InGaAs and a 4-periods $In_{0.52}Al_{0.48}As$ (20 nm)/$In_{0.53}Ga_{0.47}As$ (50 nm) superlattice was grown on this substrate, InGaAs/InAlAs or InGaAs/$(InGaAs)_2(InAlAs)_m$ (m = 2–8) QWs with well widths ($L_w$) of 1.2–12 nm were grown at $T_s$ = 480°C or 540°C under V/III pressure ratio of 8. Thickness of the InAlAs layer in the InGaAs/InAlAs QW was 23 nm, and periods of the SPS layer in the InGaAs/$(InGaAs)_2(InAlAs)_m$ QWs (m = 2–8) were adjusted so that thickness of each SPS barrier layer might be almost the same as that (23 nm) of the InAlAs barrier. The substrate was rotated at 30 rpm during MBE growth. Growth rates of InGaAs and InAlAs were 1 $\mu$m/h.

### 4.4.2 Photoluminescence measurements

Figure 4.14 shows PL spectra at 12 K from the (411)A InGaAs/InAlAs QWs grown at $T_s$ = (a) 480°C and (b) 540°C, and the (411)A InGaAs/$(InGaAs)_2(InAlAs)_2$ QWs grown at $T_s$ = (c) 480°C and (d) 540°C. An excitation laser was a He-Cd laser with a wavelength of 325 nm and an excitation power of 4.5 mW. The excitation beam was

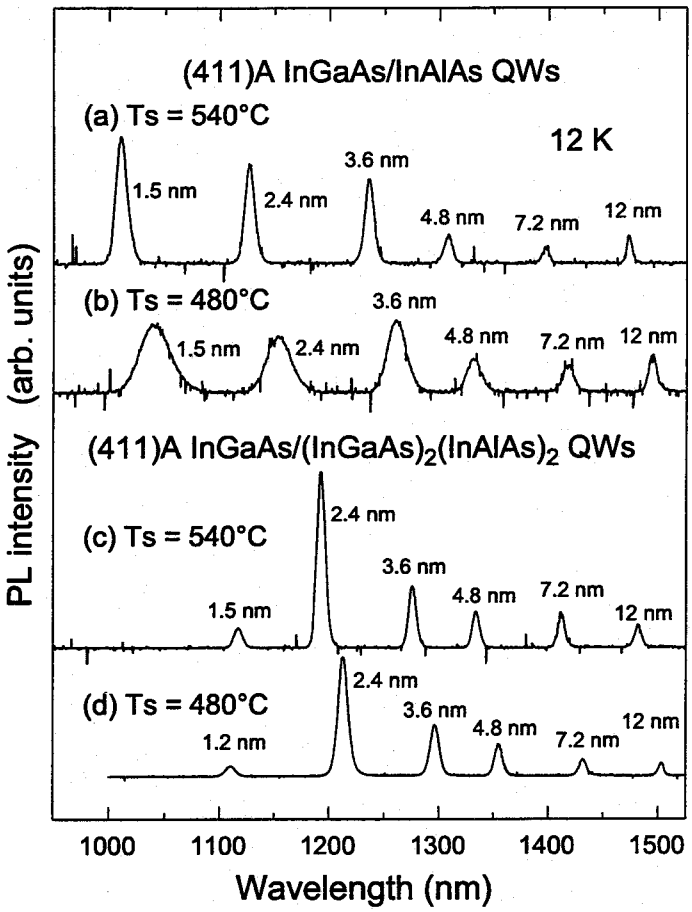


Figure 4.14: PL spectra at 12 K from the (411)A InGaAs/InAlAs QWs grown at $T_s$ = (a) 540°C and (b) 480°C, and the (411)A InGaAs/$(InGaAs)_2(InAlAs)_2$ QWs grown at $T_s$ = (c) 540°C and (d) 480°C.

focused on the substrate surface in an area of about 200 $\mu$m diameter. Six PL peaks corresponding to the (411)A QWs with six different well widths ($L_w$ = 1.2–12 nm) can be clearly seen for all of the samples in Fig. 4.14. Slight blue shift of PL peaks were observed for both the InGaAs/InAlAs and InGaAs/$(InGaAs)_2(InAlAs)_m$ QWs grown at $T_s$ = 540°C compared with those for $T_s$ = 480°C. This is due to slight desorption of In atoms during MBE growth of InGaAs layers at a high $T_s$ of 540 °C. High resolution X-ray diffraction (HRXRD) measurements of the samples showed that In contents ($x$) in $In_xGa_{1-x}As$ grown at $T_s$ = 480°C and 540°C were 0.547 and 0.540, respectively, indicating that 1.3% desorption of In atoms was occurred during MBE growth of InGaAs at $T_s$ = 540°C compared with that for $T_s$ = 480°C. PL linewidths from the InGaAs/InAlAs QWs were much broader with decreasing $T_s$ from 540°C to 480°C as shown in Figs. 4.14(a)

and 4.14(b). This broadening of PL peaks was more significant for the InGaAs/InAlAs QW with a small $L_w$ than that for a large $L_w$, indicating that the (411)A InGaAs/InAlAs heterointerface flatness degrades with decreasing $T_s$. This degradation of heterointerface flatness is mainly caused by a lower heterointerface (*InGaAs on InAlAs* interface), because a rough surface was observed for a 800 nm thick InAlAs layer grown on the (411)A InP substrate at a low $T_s$ [11], while that was not observed for a 800 nm thick InGaAs layer [12]. In contrast with this, PL linewidths of (411)A InGaAs/$(InGaAs)_2(InAlAs)_2$ QWs grown at $T_s$ = 480°C are almost the same as those for $T_s$ = 540°C as shown in Figs. 4.14(c) and 4.14(d). This result indicates that the lower heterointerface of the InGaAs/$(InGaAs)_2(InAlAs)_2$ QW are much improved compared with that of the InGaAs/InAlAs QW even for a low $T_s$ of 480°C, because roughness of a two monolayer thick InAlAs growing surface on the (411)A InP substrate at $T_s$ = 480°C should be smoothed by MBE growth of a two monolayer thick InGaAs layer.

Figure 4.15 shows PL spectra at 12 K from InGaAs/$(InGaAs)_2(InAlAs)_m$ QWs [m = (a) 4 and (b) 8] and (c) InGaAs/InAlAs QWs grown at $T_s$ = 540°C. Wavelengths of PL peaks from the InGaAs/$(InGaAs)_2(InAlAs)_m$ QWs (m = 8) were almost the same as those of the InGaAs/InAlAs QWs, while slight red-shifts were observed for the InGaAs/$(InGaAs)_2(InAlAs)_m$ QWs (m = 4). These red-shifts for InGaAs/$(InGaAs)_2(InAlAs)_m$ QWs (m = 4) were due to a decrease in effective barrier height with decreasing InAlAs thickness (m) in the $(InGaAs)_2(InAlAs)_m$ SPS barrier. Wavelengths of PL peaks from the (411)A InGaAs/$(InGaAs)_2(InAlAs)_m$ QWs (m = 2–8) with $L_w$ = 1.5–12 nm were good agreements with calculated ones, which were given by electron- and hole-energy levels in finite square well potential profiles. It is worth to note that effective barrier height in the (411)A InGaAs QWs can be easily controlled by changing thickness (m) of InAlAs layers in $(InGaAs)_2(InAlAs)_m$ SPS barriers. Full width at half maximum (FWHM) of PL peak from the InGaAs/$(InGaAs)_2(InAlAs)_m$ QWs (m = 4) with $L_w$ = 2.4 nm is 7.6 meV, which is 24% smaller than that of the corresponding QW for m = 8 (FWHM = 10.7 meV) and the InAlAs barriers (FWHM = 10.0 meV). This result indicates that heterointerface flatness in the (411)A QWs can be improved by using $(InGaAs)_2(InAlAs)_m$ barriers with

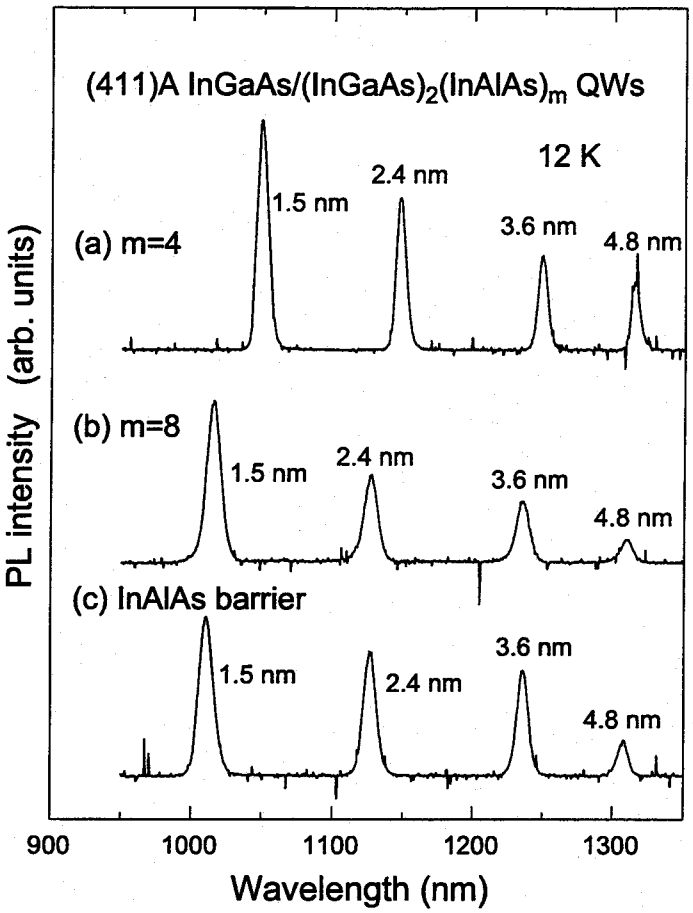


Figure 4.15: PL spectra at 12 K from the (411)A InGaAs/$(InGaAs)_2(InAlAs)_m$ QWs [(a) m = 4 and (b) m = 8] and (c) the (411)A InGaAs/InAlAs QWs grown at $T_s$ = 540°C.

m = 4 instead of thick InAlAs barriers even for a high $T_s$ of 540°C.

Figure 4.16 shows FWHMs of PL peaks at 12 K from the (411)A InGaAs/$(InGaAs)_2(InAlAs)_m$ QWs (m = 2–8) and InGaAs/InAlAs QWs grown at $T_s$ = 540°C are plotted as a function of luminescence wavelength. FWHMs of PL peaks from the (411)A InGaAs/$(InGaAs)_2(InAlAs)_m$ QWs with m = 6 and 8 are almost the same as those of the (411)A InGaAs/InAlAs QWs, while PL FWHMs are slightly improved for m = 2 and 4. This result indicates that flatness of the lower heterointerface in the (411)A QWs with the $(InGaAs)_2(InAlAs)_m$ barriers is almost the same as those for thick InAlAs barriers, while the flatness can be improved by using $(InGaAs)_2(InAlAs)_m$ barriers with m $\leq$ 4. As a result, roughness of a growing surface of the InAlAs layer can not be smoothed by MBE growth of a two monolayer thick InGaAs layer for m $\geq$ 6, while that can be smoothed for m $\leq$ 4. FWHMs of PL peaks from the (411)A InGaAs/InAlAs QWs in this study

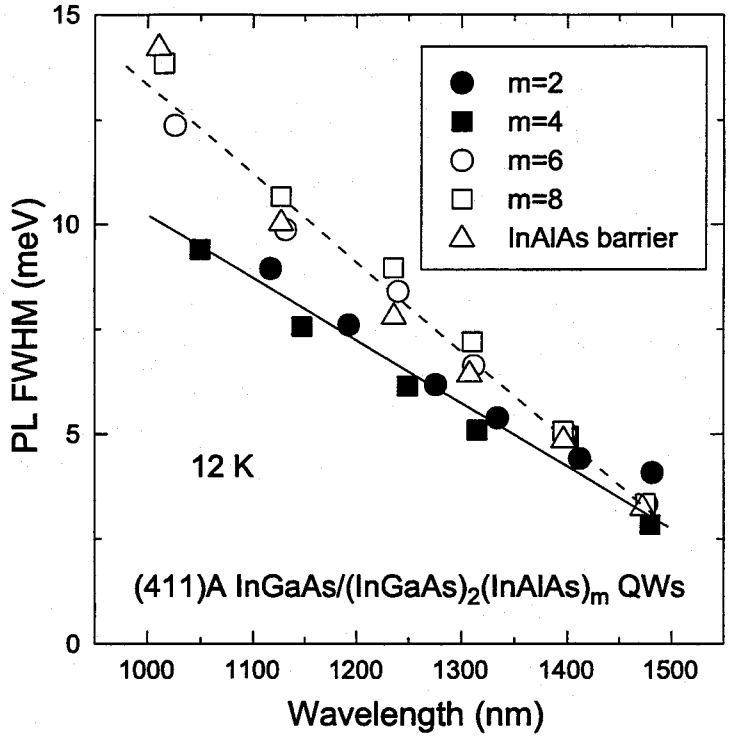


Figure 4.16: FWHMs of PL peaks at 12 K from the (411)A InGaAs/$(InGaAs)_2(InAlAs)_m$ QWs [m = 2 (closed circles), 4 (closed squares), 6 (open circles) and 8 (opens squares)] and the (411)A InGaAs/InAlAs QWs (open triangles) grown at $T_s$ = 540°C.

are slightly larger than those for previously reported ones [10]. This is probably due to the (411)A InGaAs/InAlAs QWs grown at not so optimized conditions. This implies that much smaller FWHMs of PL peaks would be observed for the InGaAs QWs with $(InGaAs)_2(InAlAs)_m$ SPS barriers ($m \leq 4$) if the QWs are grown at much better MBE growth conditions.

### 4.4.3 Summary

In summary, we have investigated that flatness of heterointerfaces in InGaAs/$(InGaAs)_2(InAlAs)_m$ QWs (m = 2–8) grown on (411)A InP substrates by MBE. Linewidths of PL (12 K) peaks from (411)A InGaAs/InAlAs QWs grown at a low $T_s$ of 480°C were significantly degraded due to rough growing surfaces of 23 nm thick InAlAs barriers, while much narrow PL linewidths were observed from (411)A InGaAs/$(InGaAs)_2(InAlAs)_2$ QWs grown even at $T_s$ = 480°C. PL FWHMs of the (411)A InGaAs/$(InGaAs)_2(InAlAs)_m$ QWs grown at $T_s$ = 540°C were the same as those of the (411)A

InGaAs/InAlAs QWs for m = 6 and 8, while the PL FWHMs were slightly improved for m = 2 and 4, indicating that heterointerface flatness in the (411)A QWs can be improved by using $(InGaAs)_2(InAlAs)_m$ SPS barriers ($m \leq 4$) instead of 23 nm thick InAlAs barriers. These improved interface flatness in the (411)A InGaAs/$(InGaAs)_2(InAlAs)_m$ QWs with $m \leq 4$ can be expected to achieve improved performance of (411)A InP-based quantum effect devices.

# Bibliography


[1] K. Yang, T. Anan and L. J. Schowalter: Appl. Phys. Lett. **65** (1994) 2789.

[2] V. Swaminathan, R. A. Stall, A. T. Macrander and R. J. Wunder: J. Vac. Sci. & Technol. **B3** (1985) 1631.

[3] R. P. Leavitt and J. L. Bradshaw: J. Appl. Phys. **76** (1994) 3429.

[4] W. T. Tsang, A. H. Dayem, T. H. Chiu, J. E. Cunningham, E. F. Schubert, J. A. Ditzenberger, J. Shah, J. L. Zyskind and N. Tabatabaie: Appl. Phys. Lett. **49** (1986) 170.

[5] A. Chin, P. Bhattacharya, W. P. Hong and W. Q. Li: J. Vac. Sci. & Technol. **B6** (1988) 665.

[6] S. Monéger, A. Tabata, C. Bru, G. Guillot, A. Georgakilas, K. Zekentes and G. Halkias: Appl. Phys. Lett. **63** (1993) 1654.

[7] T. Mishima, J. Kasai, Y. Uchida, and S. Takahashi: J. Cryst. Growth **95** (1989) 338.

[8] E. G. Scott, S. T. Davey, and G. J. Davies: Electron. Letters **23** (1987) 761.

[9] S. Shimomura, S. Kaneko, T. Motokawa, K. Shinohara, A. Adachi, Y. Okamoto, N. Sano, K. Murase, and S. Hiyamizu: J. Cryst. Growth **150** (1995) 409.

[10] T. Kitada, T. Saeki, M. Ohashi, S. Shimomura, A. Adachi, Y. Okamoto, N. Sano and S. Hiyamizu: J. Electron. Mater. **27** (1998) 1043.

[11] T. Kitada, K. Nii, T. Hiraoka, S. Shimomura and S. Hiyamizu: to be published in J. Vac. Sci. & Technol.

[12] T. Kitada, M. Ohashi, S. Shimomura and S. Hiyamizu: to be published in Jpn. J. Appl. Phys.

# Chapter 5

# Pseudomorphic InGaAs/InAlAs modulation-doped quantum wells on (411)A InP substrates

InP-based pseudomorphic InGaAs/InAlAs modulation-doped quantum wells (MD-QWs) with higher two dimensional electron (2DEG) mobilities and carrier concentrations promise for high-frequency and low-noise device applications with better performances. Higher In content (x) in a pseudomorphic $In_xGa_{1-x}As$ channel layer much improves electric properties of the InGaAs/InAlAs MD-QW because of a light electron effective mass in the channel layer and a large conduction band offset. However, thickness of the pseudomorphic InGaAs channel layer is limited by a critical thickness of $In_xGa_{1-x}As$. In order to enhance 2DEG mobilities in the pseudomorphic MD-QWs with thin channel thicknesses, reduced roughness at InGaAs/InAlAs heterointerfaces is necessary to suppress interface roughness scattering. In this chapter, we have investigated 2DEG mobilities in $In_{0.7}Ga_{0.3}As/In_{0.52}Al_{0.48}As$ MD-QWs grown on (411)A InP substrates by MBE and they were analyzed by calculated mobilities based on a 2DEG elastic scattering theory.

## 5.1 InGaAs/InAlAs MD-QW structures

The (411)A-oriented InP substrate was prepared by conventional methods and mounted on a 3 in Mo substrate holder with the use of In solder. After loading into a growth chamber of a VG semicon V80H MK-II MBE system, the native oxide of InP was desorbed by raising substrate temperature ($T_s$) up to 520°C under $As_4$ beam flux. After a buffer

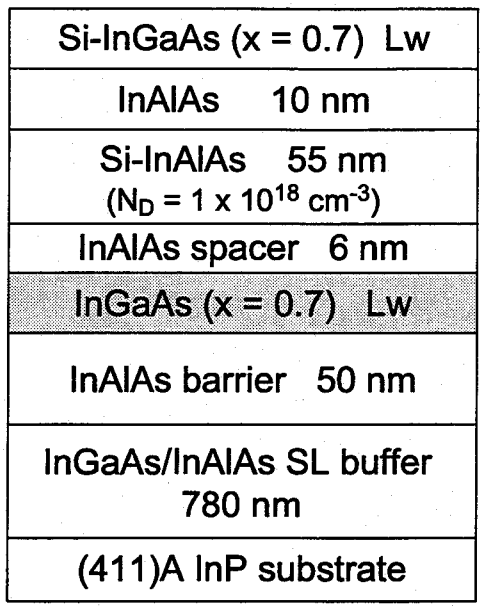


Figure 5.1: Schematic illustration of the $In_{0.7}Ga_{0.3}As/In_{0.52}Al_{0.48}As$ MD-QW structures.

layer of a 500 nm thick InGaAs and a 4-periods $In_{0.52}Al_{0.48}As$ (20 nm)/$In_{0.53}Ga_{0.47}As$ (50 nm) superlattice were grown on this substrate, the $In_{0.7}Ga_{0.3}As/In_{0.52}Al_{0.48}As$ MD-QW was grown at $T_s$ = 540°C under V/III pressure ratio of 8. Figure 5.1 shows a schematic illustration of the $In_{0.7}Ga_{0.3}As/In_{0.52}Al_{0.48}As$ MD-QW structures. The MD-QW structures consist of a 50-nm-thick undoped $In_{0.52}Al_{0.48}As$ barrier, an undoped $In_{0.7}Ga_{0.3}As$ QW channel layer with a well width ($L_w$) of 12, 14, 16 or 18 nm, a 6-nm-thick undoped $In_{0.52}Al_{0.48}As$ spacer layer and a 55-nm-thick Si-doped $In_{0.52}Al_{0.48}As$ with donor concentration ($N_D$) of $1 \times 10^{18}$ $cm^{-3}$. Finally, a 10-nm-thick undoped InAlAs layer and an $In_{0.7}Ga_{0.3}As$ cap layer with thickness $L_w$ were grown on the MD-QW structures, in order to observe surface morphology of the $In_{0.7}Ga_{0.3}As$ layer by atomic force microscope (AFM). The same MD-QW structures were grown on a (100)-oriented InP substrate at optimized conditions of $T_s$ = 480°C and V/III pressure ratio of 14. In contents in the pseudomorphic $In_{0.7}Ga_{0.3}As$ QW channel layers were checked by high resolution X-ray diffraction (HRXRD) measurements and they were almost the same for the (411)A and (100) samples. Growth rates of the $In_{0.7}Ga_{0.3}As$ channel layer and $In_{0.52}Al_{0.48}As$ layers were 0.76 and 1 $\mu$m/h.

Hall effects of the (411)A and (100) MD-QW samples were measured by the con-

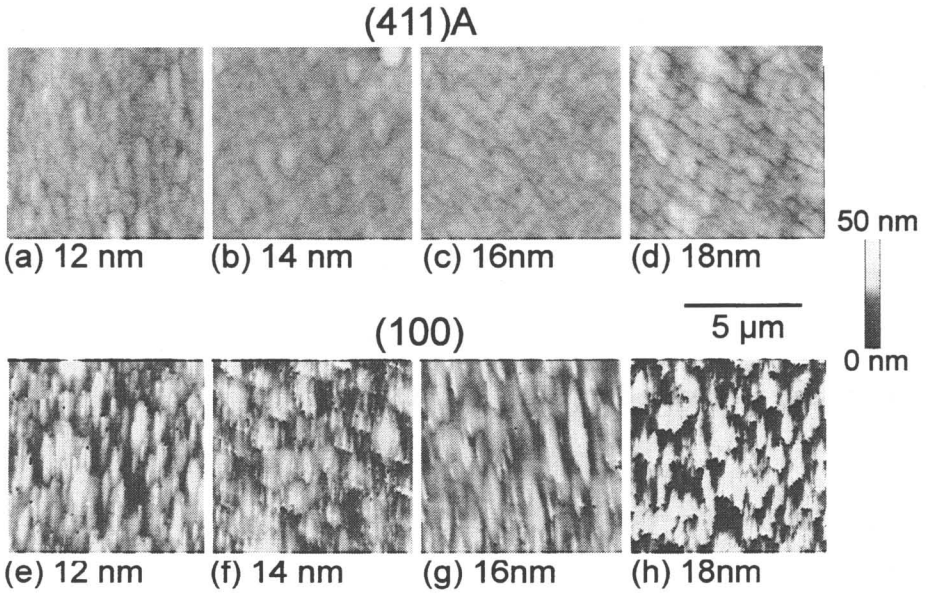


Figure 5.2: Surface morphologies of $In_{0.7}Ga_{0.3}As$ layers grown on the (411)A [(a)–(d)] and (100) [(e)–(h)] MD-QW structures observed by AFM measurements.

ventional van der Pauw method under a magnetic field of 0.5 T. Ohmic contacts to the MD-QWs were formed by AuGeNi metals. The samples were cooled to a temperature range of 24–300 K by using a helium-gas closed cycle cryostat or liquid nitrogen.

## 5.2 Surface morphologies of $In_{0.7}Ga_{0.3}As$ layers

Figure 5.2 shows surface morphologies of $In_{0.7}Ga_{0.3}As$ layers grown on the (411)A and (100) MD-QW structures observed by AFM measurements. These surface morphologies reflect interface roughness in *InGaAs on InAlAs* heterointerfaces. No cross-hatched patterns were observed for all of the (411)A and (100) InGaAs layers. However, the surface morphology of the (100) InGaAs with thickness ($L_{InGaAs}$) of 18 nm [Fig. 5.2(h)] is much rough compared with the (100) InGaAs with $L_{InGaAs}$ = 12–16 nm [Figs. 5.2(e)–(g)]. An average amplitude of roughness ($\Delta$) of the (100) InGaAs is approximately 10 nm for $L_{InGaAs}$ = 12–16 nm, and drastically increases to 30 nm for $L_{InGaAs}$ = 18 nm. This is due to three-dimensional growth mode of the (100) InGaAs for $L_{InGaAs} > 16$ nm caused by a strain relaxation. In contrast with this, a drastic increase of $\Delta$ can not be seen for the (411)A InGaAs with $L_{InGaAs}$ = 12–18 nm [Figs. 5.2(a)–(d)], suggesting that larger

critical thickness of the pseudomorphic (411)A $In_{0.7}Ga_{0.3}As$ layers compared with the (100) $In_{0.7}Ga_{0.3}As$. Larger critical thickness on the (411)A substrate was also observed in a pseudomorphic $In_{0.25}Ga_{0.75}As$/AlGaAs QW grown on a (411)A GaAs substrate [3]. Roughness of the (411)A InGaAs layer ($\Delta$ = 3 nm) is much smaller than the corresponding (100) InGaAs layer for all the InGaAs thickness. This indicates that superior flatness is achieved in the InGaAs/InAlAs heterointerfaces for the (411)A MD-QWs compared with those for the corresponding (100) MD-QWs.

## 5.3 Transport properties at 77 K

Figure 5.3 shows 2DEG mobilities and sheet carrier concentrations of the (411)A and (100) InGaAs/InAlAs MD-QWs as a function of well width. The 2DEG mobility of the (100) sample drastically decreases with an increase in $L_w$ from 16 nm to 18 nm. Furthermore, the sheet carrier concentrations of the (100) samples were almost constant at $N_s = 1.6 \times 10^{12}$ cm$^{-2}$ for the (100) MD-QW with $L_w$ = 12–16 nm, while 25% decrease of the sheet carrier concentration was observed for the (100) MD-QW with $L_w$ = 18 nm ($N_s$ = $1.2 \times 10^{12}$ cm$^{-2}$). This is due to the $In_{0.7}Ga_{0.3}As$ QW thickness exceeding their critical layer thickness for the (100) samples. In contrast with this, a drastic decrease of the 2DEG mobility was not observed for the (411)A sample with an increase in $L_w$ from 16 nm to 18 nm. This result indicates larger critical thickness of the pseudomorphic $In_{0.7}Ga_{0.3}As$ layer on the (411)A InP substrate compared with that for (100) substrate, which is consistent with results of the surface morphologies of the $In_{0.7}Ga_{0.3}As$ layers, as described in 5.2. The slightly smaller sheet carrier concentrations for the (411)A samples are observed for $L_w$ = 12–16nm, which is probably due to a slightly higher compensation ratio of Si-dopants in the N-$In_{0.52}Al_{0.48}As$ layer on the (411)A InP substrate. A similar result was observed for a Si-doped GaAs layer on a (411)A GaAs substrate [2]. Enhancement of the 2DEG mobilities in the (411)A MD-QWs compared with the corresponding (100) MD-QWs is also observed for $L_w$ = 12–16 nm, which is probably due to superior interface flatness in the (411)A MD-QWs.

Figure 5.4 shows 2DEG mobilities of the (411)A and (100) InGaAs/InAlAs MD-QWs

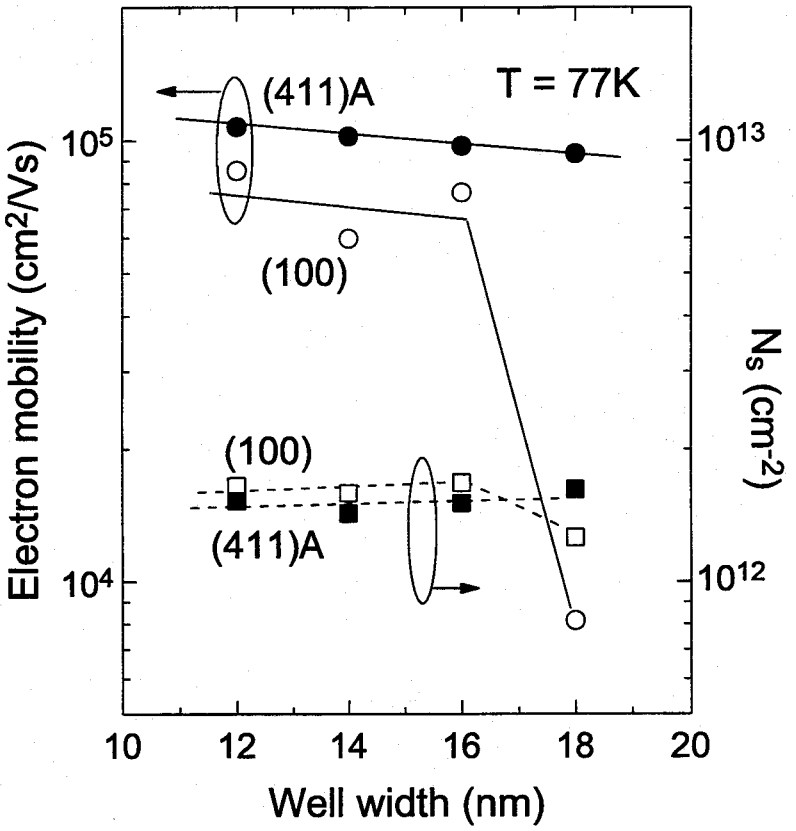


Figure 5.3: 2DEG mobilities and sheet carrier concentrations (T = 77 K) of the (411)A and (100) $In_{0.7}Ga_{0.3}As/In_{0.52}Al_{0.48}As$ MD-QWs plotted as a function of well width.

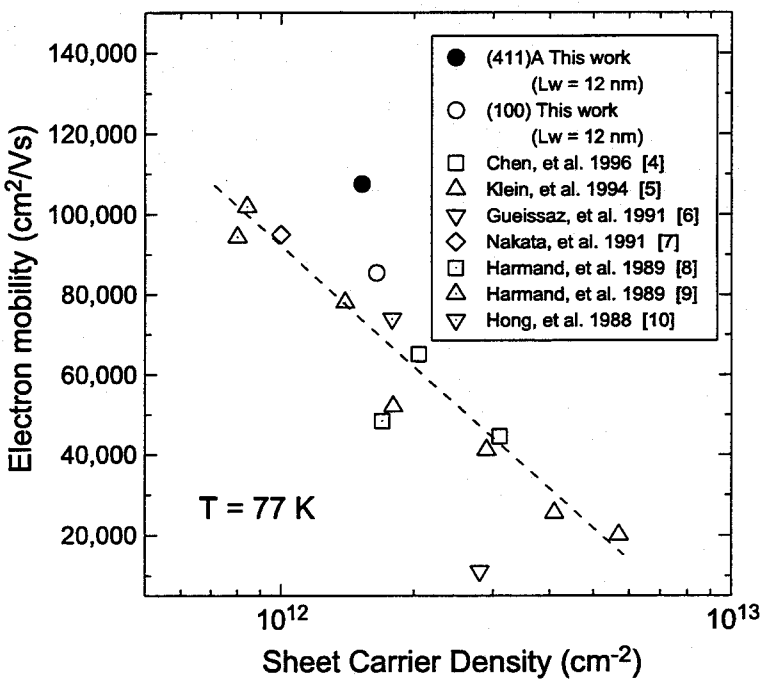


Figure 5.4: 2DEG mobilities at T = 77 K of the (411)A and (100) MD-QWs with $L_w$ = 12 nm plotted as a function of sheet carrier concentration. 2DEG mobilities at T = 77 K reported so far [4–10] is also plotted.

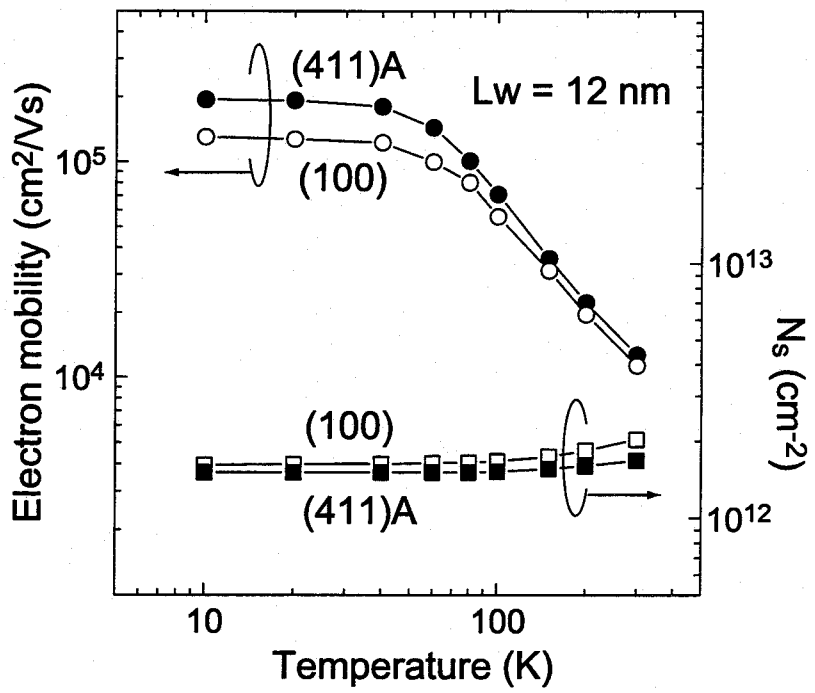


Figure 5.5: Temperature dependence of 2DEG mobilities and sheet carrier concentrations of the (411)A and (100) $In_{0.7}Ga_{0.3}As/In_{0.52}Al_{0.48}As$ MD-QWs with $L_w$ = 12 nm.

with $L_w$ = 12 nm plotted as a function of sheet carrier concentration. 2DEG mobilities at T = 77 K reported so far [4–10] is also plotted in Fig. 5.4. The 2DEG in the (411)A MD-QW with $L_w$ = 12 nm shows 27% higher mobility ($\mu$ = 108,000 cm$^2$/Vs) than that ($\mu$ = 85,000 cm$^2$/Vs) of the corresponding (100) MD-QW in this study, and the $\mu$ of the (411)A MD-QW is the highest mobility in the previously reported ones. This result indicates that superior interface flatness in the (411)A InGaAs/InAlAs MD-QWs is an important factor to achieve the highest 2DEG mobility.

## 5.4 Low-temperature 2DEG mobility

Figure 5.5 shows temperature dependence of the sheet carrier concentrations and 2DEG mobilities in the (411)A and (100) pseudomorphic InGaAs/InAlAs MD-QWs with $L_w$ = 12 nm. The sheet carrier concentrations are almost constant for both the (411)A ($N_s$ = 1.5 × 10$^{12}$ cm$^{-2}$) and (100) ($N_s$ = 1.6 × 10$^{12}$ cm$^{-2}$) samples below T = 100 K. The 2DEG mobilities at T = 10 K of the (411)A and (100) samples are 194,000 cm$^2$/Vs and 130,000 cm$^2$/Vs, respectively, and they are almost constant at T = 10–40 K. Rapid decreases of

Table 5.1: 2DEG mobilities and sheet carrier concentrations of the (411)A and (100) $In_{0.7}Ga_{0.3}As/In_{0.52}Al_{0.48}As$ MD-QWs measured at T = 24 K.

| $L_w$ (nm) | $\mu$ ($cm^2/Vs$) | | $N_s$ ($cm^{-2}$) | |
|---|---|---|---|---|
| | (411)A | (100) | (411)A | (100) |
| 12 | 181,000 | 131,000 | $1.5 \times 10^{12}$ | $1.6 \times 10^{12}$ |
| 14 | 179,000 | 87,000 | $1.4 \times 10^{12}$ | $1.6 \times 10^{12}$ |
| 16 | 163,000 | 112,000 | $1.5 \times 10^{12}$ | $1.6 \times 10^{12}$ |
| 18 | 140,000 | 8,500 | $1.5 \times 10^{12}$ | $1.2 \times 10^{12}$ |

the 2DEG mobilities with increasing temperature at T > 40 K were observed for both the (411)A and (100) samples because of increasing optical phonon scattering. Enhancement of the 2DEG mobility of the (411)A sample compared with that of the (100) sample is much significant at low-temperatures, indicating that dominant factor of scattering at the low-temperature such as interface roughness scattering is reduced for the (411) MD-QW.

The 2DEG mobilities and sheet carrier concentrations of the (411)A and (100) MD-QW samples measured at T = 24 K are summarized in Table 5.1. A drastic decrease of the 2DEG mobility was also observed at T = 24 K for the (100) MD-QW with $L_w$ = 18 nm, not for the corresponding (411)A MD-QW due to the larger critical thickness of $In_{0.7}Ga_{0.3}As$ on the (411)A InP substrate. Enhancement of the electron mobility in the (411)A MD-QW was significantly observed for all the well widths ($L_w$ = 12–16 nm) compared with the corresponding (100) MD-QW.

## 5.5 Theoretical analysis

The observed low-temperature 2DEG mobilities in the (411)A and (100) InGaAs/InAlAs MD-QWs were analyzed by calculated ones based on a 2DEG elastic scattering theory [12–15]. The electronic states and sheet carrier concentration of the MD-QW at T = 0 K were calculated by a conventional self-consistent method [11], and the 2DEG mobility at T = 0 K, which is limited by ionized impurity scattering, alloy disorder scattering and interface roughness scattering, was calculated by using the self-consistent results.

### 5.5.1 Electronic states

The wave function and energy of the electron with a 2D wave vector $\boldsymbol{k} = (k_x, k_y)$ parallel to heterointerfaces in the $n$th subband are given by

$$\Psi_n(\boldsymbol{k}, \boldsymbol{r}, z) = f_n(z) \exp(i\boldsymbol{k} \cdot \boldsymbol{r}), \tag{5.1}$$

$$E_n(\boldsymbol{k}) = E_n + \hbar^2 k^2 / 2m^*, \tag{5.2}$$

where $f_n(z)$ and $E_n$ is the quantized wave function and energy level of the electron in the $n$th subband, $m^*$ is the effective mass of the $In_{0.7}Ga_{0.3}As$ channel layer and $\hbar$ is the reduce Planck constant. The quantized wave function satisfies a following one-dimensional shrödinger equation,

$$\left[ -\frac{\hbar^2}{2m_z^*} \frac{d^2}{dz^2} + V(z) \right] f_n(z) = E_n f_n(z), \tag{5.3}$$

where $m_z^*$ is $m^*$ for $0 < z \leq L_w$ and the effective mass of the InAlAs barrier layer, $m_b^*$ for otherwise. The potential $V(z)$ is written as

$$V(z) = -e\phi(z) + V_0 H(z), \tag{5.4}$$

where $e$ is the elemental charge and $V_0$ is the barrier height. The function $H(z)$ is 0 for $0 < z \leq L_w$ and 1 for otherwise. The potential $\phi(z)$ satisfies a following Poisson equation,

$$\kappa(z)\epsilon_0 \frac{d^2}{dz^2}\phi(z) = -\left[ \rho_{\mathrm{depl}}(z) - e \sum_n N_n |f_n(z)|^2 \right], \tag{5.5}$$

where $\kappa(z)\epsilon_0$ is the static dielectric constant, $\rho(z)$ is the charge concentration in the depletion layer and $N_n$ is the sheet carrier concentration in the $n$th subband, which is given by

$$N_n = \frac{m^*}{\pi\hbar^2}(E_F - E_n), \tag{5.6}$$

where $E_F$ is the Fermi energy. The sheet carrier concentration $N_s$ can be evaluated from the sum of $N_n$ over the subbands. Thickness of the depletion layer can be determined by the electrical neutral condition and the condition that the $E_F$ is constant in space. By using eqs. (5.1)–(5.6), we calculated the energy levels and the sheet carrier concentrations of 0th, 1st and 2nd subbands as a function of the well width. Parameter values used in the calculation are summarized in Table. 5.2.

Table 5.2: Parameter values used in the calculation of the electric states and the 2DEG mobility for the $In_{0.7}Ga_{0.3}As/In_{0.52}Al_{0.48}As$ MD-QW.

| | | |
|---|---|---|
| Electron effective mass of InGaAs: | $m^*$ | $0.0356m_0$ |
| Electron effective mass of InAlAs: | $m_b^*$ | $0.0715m_0$ |
| Conduction band offset: | $V_0$ (meV) | 580 |
| Static dielectric constant of InGaAs: | $\kappa$ | 13.9 |
| Static dielectric constant of InAlAs: | $\kappa_b$ | 12.65 |
| Impurity concentration in undoped-layer: | $N_a - N_d$ ($cm^{-3}$) | $1 \times 10^{14}$ |

Figure 5.6 shows calculated energy levels and sheet carrier concentration at T = 0 K as a function of the well width. Experimental sheet carrier concentrations of the (411)A and (100) samples measured at T = 24 K are also plotted in Fig. 5.6. The energy of the 0th subband ($E_0$) drastically increases with decreasing well width when $L_w$ < 10 nm, indicating that a quantum size effect cause by the lower-side InAlAs barrier is much effective for the MD-QW with $L_w$ < 10 nm. The 1st subband appears at $L_w \simeq 8$ nm, however, there are no electrons in this subband when $L_w$ < 15 nm. At small well widths below 15 nm, difference between the Fermi energy ($E_F$) and $E_0$, $E_F$ - $E_0$ increases consistently with the well width, because of the decrease of $E_0$ with increasing well width. The total sheet carrier concentration of the InGaAs/InAlAs MD-QW slightly increases consistently with the well width when $L_w$ > 15 nm, however, $E_F$ - $E_0$ slightly decreases with increasing well width. This is because population of electrons in the 2nd subbands appears at $L_w \simeq 15$ nm, and it increases consistently with the well width when $L_w$ > 15 nm. The experimental sheet carrier concentrations measured at T = 24 K are good agreements with the calculated results.

### 5.5.2 2DEG mobility

We calculated the 2DEG mobility of the MD-QW at T = 0 K based on a 2DEG elastic scattering theory. At low-temperatures, the 2DEG mobility in the InGaAs/InAlAs MD-QW is limited by (1) ionized impurity scattering, (2) alloy disorder scattering and (3) interface roughness scattering. We calculate the mobility of the 2DEG in the 0th subband, for simplicity. The 2DEG mobility $\mu$ at T = 0 K can be determined from the sum of the

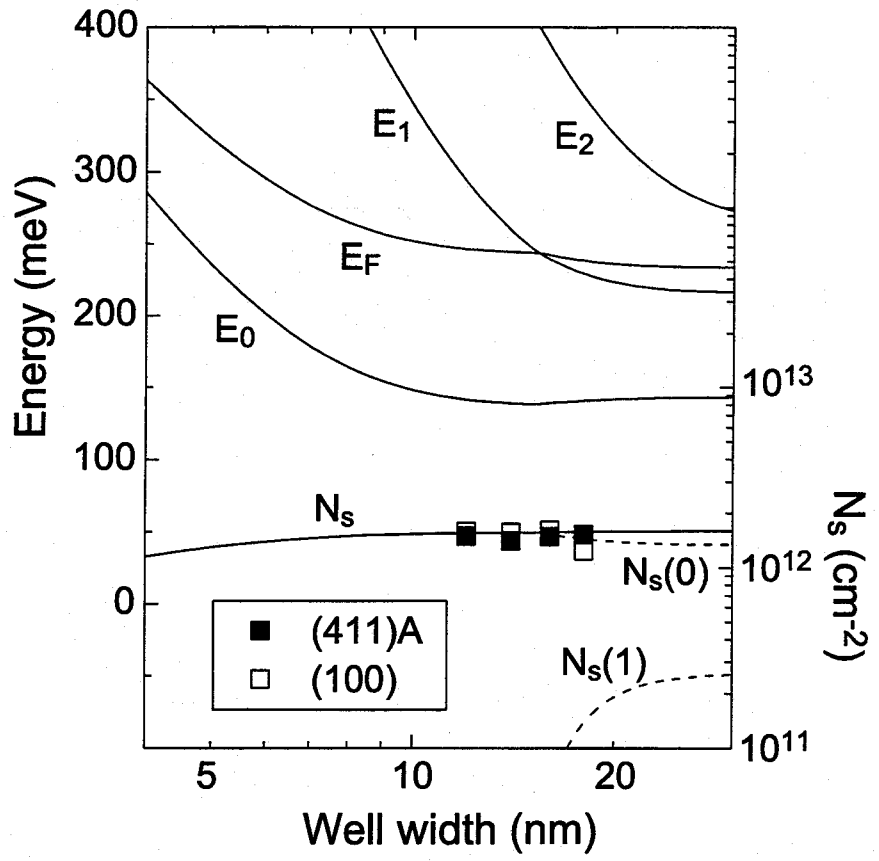


Figure 5.6: Calculated energy levels (solid lines), sheet carrier concentrations (dotted lines) of 0th, 1st and 2nd subbands and the total sheet carrier concentration (a solid line) at T = 0 K in the $In_{0.7}Ga_{0.3}As/In_{0.52}Al_{0.48}As$ MD-QW plotted as a function of the well width. Measured sheet carrier concentration of the (411)A (closed squares) and (100) (open squares) samples at T = 24 K are also plotted.

inverse of the mobility $\mu_i$ limited by each scattering mechanism, which is written as,

$$\frac{1}{\mu} = \sum_i \frac{1}{\mu_i} = \sum_i \frac{m^*}{e} \frac{1}{\tau_i(k_F)}, \tag{5.7}$$

where $\tau_i(k)$ is the momentum relaxation time of an electron with wave vector $\boldsymbol{k}$ for each scattering mechanism and $\boldsymbol{k_F}$ is the Fermi wave vector. The inverse of the momentum relaxation time is given by [15]

$$\frac{1}{\tau_i(k)} = \frac{1}{(2\pi)^2}\left(\frac{2\pi}{\hbar}\right)\int d^2\boldsymbol{k'}\left[\frac{M_i}{S(q,T)}\right]^2 (1-\cos\theta)\delta(E_{k'}-E_k), \tag{5.8}$$

where $M_i$ is the 2D scattering matrix element for each scattering mechanism, $\boldsymbol{q}(=\boldsymbol{k}-\boldsymbol{k'})$ is the 2D scattering wave vector and $q = |\boldsymbol{q}|$. $\theta$ is angle between $\boldsymbol{k}$ and $\boldsymbol{k'}$. $S(q,T)$ is the screening factor, which depends on q and temperature T [16].

At low-temperatures, ionized impurity scattering plays an important role even for

modulation-doped structures. The inverse of momentum relaxation time $\tau_{ion}(k)$ for ionized impurity scattering is given by [12, 13, 14]

$$\frac{1}{\tau_{ion}(k)} = \frac{m^* e^4}{4\pi\hbar^3\kappa^2{\epsilon_0}^2}\int_0^\pi d\theta \int_{-\infty}^{\infty} dz_i \left[\frac{F(q,z_i)}{qS(q,T)}\right]^2 g(z_i)(1-\cos\theta), \tag{5.9}$$

where $g(z_i)$ is the impurity distribution, which is determined from the self-consistent results of the MD-QW. The form factor $F(q,z_i)$ is defined as

$$F(q,z_i) \equiv \int_{-\infty}^{\infty} dz |f_0(z)|^2 \exp\left(-q|z_i - z|\right). \tag{5.10}$$

Alloy disorder scattering is dominant scattering mechanism at low-temperatures for the InGaAs/InAlAs MD-QW, because the channel region consists of a ternary random alloy of InAs and GaAs. We assumed that a potential of In and Ga is a short-range $\delta$-potential with the strength $(1-x)\Delta U(a^3/4)$ and $-x\Delta U(a^3/4)$, respectively, where $x$ is the In content, $a$ is a lattice constant and $\Delta U$ is the difference of the conduction band minima of InAs and GaAs. [12, 14] The inverse of momentum relaxation time $\tau_{alloy}(k)$ for alloy disorder scattering is given by

$$\frac{1}{\tau_{alloy}(k)} = \frac{m^*(\Delta U)^2 a^3}{4\pi\hbar^3}\int_0^\pi d\theta \int_{-\infty}^{\infty} dz x(1-x)|f_0(z)|^4 \frac{1-\cos\theta}{S(q,T)^2}. \tag{5.11}$$

For simplicity, $\Delta U$ of InAlAs layer is the same as that of InGaAs, because alloy disorder scattering in the InAlAs barrier layer is much smaller than that in the InGaAs channel layer.

Interface roughness scattering is also important for low-temperature 2DEG mobility. We assumed that interface roughness can be characterized by the height $\Delta$ and the lateral size $\Lambda$ of the Gaussian fluctuations of the interface, which is written by

$$< \Delta(\boldsymbol{r})\Delta(\boldsymbol{r}') >= \Delta^2 \exp\left(-\frac{|\boldsymbol{r}-\boldsymbol{r}'|^2}{\Lambda^2}\right). \tag{5.12}$$

The inverse of momentum relaxation time $\tau_{int}(k)$ for interface roughness scattering is given by [14, 15]

$$\frac{1}{\tau_{int}(k)} = \frac{m^*\Delta^2\Lambda^2}{\hbar^3}\int_0^\pi d\theta \left[\left(\frac{\partial E_0}{\partial L_w}\right)^2 + F_{eff}^2\right] \exp\left(-\frac{q^2\Lambda^2}{4}\right)\frac{1-\cos(\theta)}{S(q,T)^2}. \tag{5.13}$$

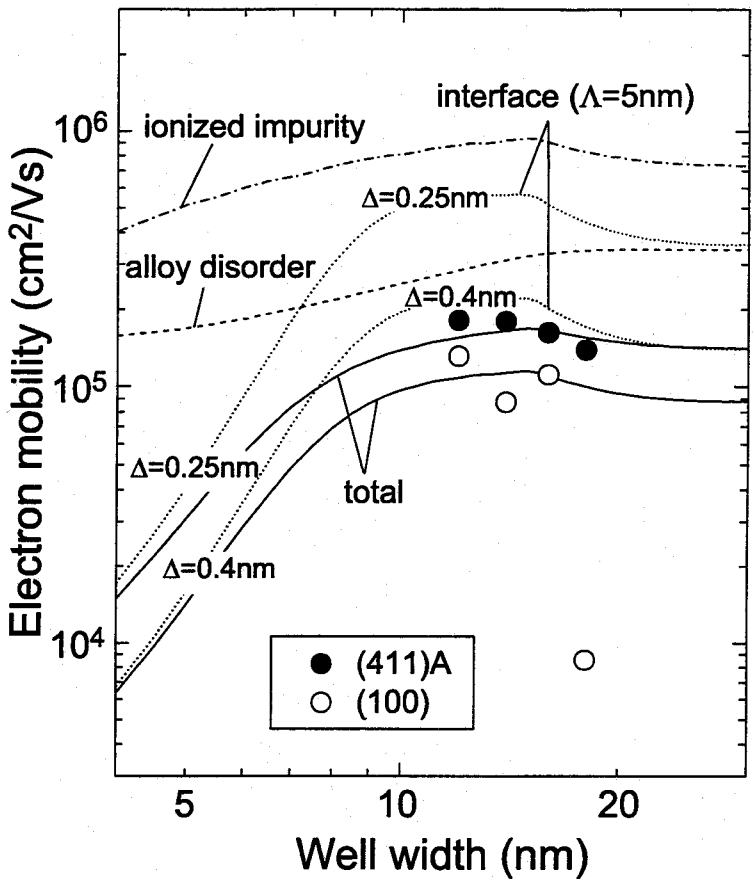


Figure 5.7: Calculated 2DEG mobilities limited by ionized impurity scattering (a dotted-broken line), alloy disorder scattering (a broken line), interface roughness scattering (dotted lines) and total 2DEG mobilities (solid lines) at T = 0 K plotted as a function of the well width. Experimental 2DEG mobilities at T = 24 K are well fitted by $\Delta = 0.25$ nm for the (411)A samples and $\Delta = 0.4$ nm for the (100) samples, assuming $\Lambda = 5$ nm.

Here, we have defined the effective field $F_{eff}$, which is written by

$$F_{eff} \equiv \int_{-\infty}^{\infty} dz |f_0(z)|^2 \frac{\partial \phi(z)}{\partial z}, \tag{5.14}$$

where $\phi(z)$ is the electrostatic potential, which is determined from eq. (5.5).

Calculated 2DEG mobility $\mu$ and the mobility limited by each scattering mechanism ($\mu_{ion}$, $\mu_{alloy}$ and $\mu_{int}$) at T = 0 K are plotted as a function of well width in Fig. 5.7. Experimental 2DEG mobilities at T = 24 K of the (411)A (closed circles) and (100) (open circles) samples are also plotted. When $L_w < 15$ nm, $\mu_{ion}$ and $\mu_{alloy}$ decrease consistently with the well width. This is because sheet carrier concentration decreases consistently with the well width, which cause a decrease of the mobility due to a screening effect. When $L_w > 15$ nm, all of the mobility decreases with increasing well width. This is due to an increase of the screening effect caused by a decrease of $E_F$ - $E_0$ with increasing

well width. However, we did not take into account of the screening effect of the electrons in the 2nd subband for this calculation, therefore, a future investigation is necessary for the 2DEG mobility of the QW with $L_w > 15$ nm. Below the well width of 10 nm, $\mu_{int}$ falls very rapidly as the well width is reduced. This is due to the term proportional to $(\partial E_0/\partial L_w)^2$ in eq. (5.13), which is much larger for the smaller well width. When $L_w >$ 10 nm, therefore, $\mu_{int}$ is limited by the term proportional to $F_{eff}^2$ in eq. (5.13). Assuming that $\Lambda$ is equal to 5 nm, the experimental 2DEG mobilities measured at T = 24 K can be well fitted by $\Delta = 0.25$ nm for the (411)A samples, and $\Delta = 0.4$ nm for the (100) samples. This suggests that enhancement of the 2DEG mobilities of the (411)A MD-QWs with $L_w$ = 12–16 nm compared with the corresponding (100) MD-QWs is due to superior interface flatness of the (411)A MD-QWs. However, the lateral size assumed in this calculation ($\Lambda$ = 5 nm) is the case that electrons are scattered very strongly by the interface roughness, because a half of the Fermi wavelength ($\lambda_F = 20$ nm) is almost the same as an average period of interface roughness ($2\Lambda$). The validity of the values of $\Delta$ and $\Lambda$ is discussed in 5.5.3.

### 5.5.3 Comparison with photoluminescence data

In order to confirm the validity of the values of $\Delta$ and $\Lambda$ used in the 2DEG mobility calculations for the (411)A and (100) MD-QWs, low-temperature (4.2 K) PL linewidths of undoped-$In_{0.53}Ga_{0.47}As/In_{0.52}Al_{0.48}As$QWs with $L_w$ = 0.6, 1.2, 2.4, 3.6, 4.8 and 12 nm grown on the (411)A and (100) InP substrates [1] were analyzed.

The low-temperature PL linewidth $\Gamma$ of the QW can be expressed as

$$\Gamma = \Gamma_{int} + \Gamma_0, \tag{5.15}$$

where $\Gamma_{int}$ and $\Gamma_0$ are the linewidths caused by interface roughness and the other factor such as alloy disorder of InGaAs, respectively. $\Gamma_{int}$ is given by

$$\Gamma_{int} = \left(\frac{\partial E}{\partial L_w}\right) \Delta L_w, \tag{5.16}$$

where $E$ is the PL transition energy and $\Delta L_w$ is local well width fluctuation over an exciton size. Assuming that interface fluctuation is made up of valleys and hills with

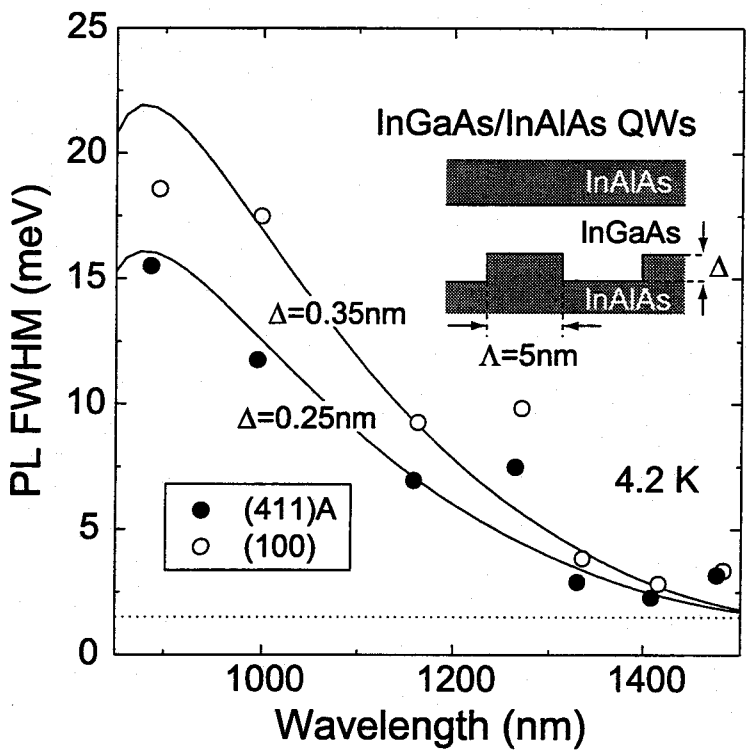


Figure 5.8: Photoluminescence FWHMs of the low-temperature (4.2 K) PL peaks from undoped-$In_{0.53}Ga_{0.47}As/In_{0.52}Al_{0.48}As$ QWs grown on the (411)A and (100) InP substrates. Solid lines are calculated ones. Experimental PL FWHMs can be well fitted by $\Delta = 0.25$ nm for the (411)A QWs and $\Delta = 0.35$ nm for the (100) QWs. The inset is an illustration of the interface structure used for calculation.

height $\Delta$ and lateral size $\Lambda$ (see the inset of Fig. 5.8), $\Delta L_{\rm w}$ is given by [17]

$$\Delta L_{\rm w} = \sqrt{\frac{\ln 2}{\pi}} \frac{\Delta\Lambda}{r_{ex}}, \tag{5.17}$$

where $r_{ex}$ is the exciton radius.

Figure 5.8 shows PL FWHMs of undoped-$In_{0.53}Ga_{0.47}As/In_{0.52}Al_{0.48}As$ QWs and calculated ones as a function of the luminescence wavelength. The PL FWHMs of the (411)A QWs are 20–30% smaller than those of the (100)QWs, indicating that superior interface flatness can be achieved in the (411)A QWs, as previously reported [1]. For calculation of the PL FWHMs, $\Gamma_0$ was assumed to be a constant value of 2 meV, which is determined from PL FWHM of a InGaAs bulk layer, because $\Gamma_0$ is much smaller than $\Gamma_{int}$ for the QW with a small well width, and it has almost no dependence on the well width. $\Gamma_{int}$ was calculated by using eqs. (5.16) and (5.17). $\partial E/\partial L_{\rm w}$ is determined from calculated electron- and hole-energy levels in a finite square well profiles, and $r_{ex}$ is assumed to be 10 nm. Experimental PL FWHMs can be well fitted by $\Delta = 0.25$ nm for the (411)A

QWs and $\Delta = 0.35$ nm for the (100) QWs, assuming $\Lambda = 5$ nm. These values of $\Delta$ are almost the same as those used for the 2DEG mobility calculation. If $\Lambda$ is assumed to be a different value, values of $\Delta$ determined by results of 2DEG mobility calculation can not be consistent with those for PL FWHMs of the undoped-InGaAs/InAlAs QWs. Therefore, it is reasonable to use these parameter values of interface roughness [$\Delta = 0.25$ nm and $\Lambda = 5$ nm for (411)A samples, and $\Delta = 0.4$ nm and $\Lambda = 5$ nm for (100) samples] in the calculation of the low-temperature 2DEG mobility.

## 5.6 Summary

We have investigated the 2DEG mobilities in the pseudomorphic $In_{0.7}Ga_{0.3}As$/ $In_{0.52}Al_{0.48}As$ MD-QWs with $L_w = 12$–$18$ nm grown on (411)A and (100) InP substrates by MBE. A drastic decrease of the 2DEG mobility was observed for the (100) MD-QW with $L_w = 18$ nm, not for the corresponding (411)A MD-QW, indicating the larger critical thickness of $In_{0.7}Ga_{0.3}As$ on the (411)A InP substrate. The surface morphologies of the (411)A and (100) $In_{0.7}Ga_{0.3}As$ layers observed by AFM also suggest that the critical thickness of the (411)A $In_{0.7}Ga_{0.3}As$ is larger than that of the (100) $In_{0.7}Ga_{0.3}As$. The 2DEG in the (411)A MD-QW with $L_w = 12$ nm shows 27% higher mobility ($\mu =$ 108,000 $cm^2/Vs$) with 2DEG concentration of $1.5 \times 10^{12}$ $cm^{-2}$ at T = 77 K than that ($\mu =$ 85,000 $cm^2/Vs$) of the corresponding (100) MD-QW in this study, and the $\mu$ of the (411)A MD-QW is the highest mobility in the previously reported ones. The low-temperature (24 K) 2DEG mobilities were analyzed by calculated mobilities taking into account of ionized impurity scattering, alloy disorder scattering and interface roughness scattering by using self-consistent results of the MD-QWs. Enhanced 2DEG mobilities in the (411)A MD-QWs can be well explained by reduced interface roughness scattering due to the (411)A super-flat interfaces. The validity of parameter values of interface roughness (height $\Delta = 0.25$ nm and lateral size $\Lambda = 5$ nm) used in the 2DEG mobility calculation was confirmed by photoluminescence data at 4.2 K of undoped-InGaAs/InAlAs QWs grown on the (411)A InP substrate by MBE. These results indicate that pseudomorphic InGaAs/InAlAs MD-QWs with (411)A super-flat interfaces are very suitable for

InP-based HEMT devices because of their high 2DEG mobilities.

# Bibliography


[1] T. Kitada, T. Saeki, M. Ohashi, S. Shimomura, A. Adachi, Y. Okamoto, N. Sano and S. Hiyamizu: J. Electron. Mater. **27** (1998) 1043.

[2] K. Shinohara, T. Motokawa, K. Kasahara, S. Shimomura, N. Sano, A. Adachi and S. Hiyamizu: Semicond. Sci. Technol. **11** (1996) 125.

[3] K. Nii, R. Kuriyama, T. Hiraoka, T. Kitada, S. Shimomura and S. Hiyamizu: to be published in J. Vac. Sci. & Technol. **B** (1999).

[4] J. X. Chen, A. Z. Li, Y. C. Ren, M. Qi and Y. G. Chang: J. Cryst. Growth **164** (1996) 460.

[5] W. Klein, G. Böhm, M. Sexl, S. Grigull, H. Heiss, G. Tränkle and G. Weimann: J. Vac. Sci. & Technol. **B12** (1994) 1306.

[6] F. Gueissaz, R. Houdre and M. Ilegems: J. Cryst. Growth **111** (1991) 470.

[7] Y. Nakata, O. Ueda and T. Fujii: Jpn. J. Appl. Phys. **30** (1991) L249.

[8] J. C. Harmand, T. Matsuno and K. Inoue: Jpn. J. Appl. Phys. **28** (1989) L1101.

[9] J. C. Harmand, T. Matsuno and K. Inoue: J. Appl. Phys. **66** (1989) 2633.

[10] W. P. Hong, G. I. Ng, P. K. Bhattacharya, D. Pavlidis and S. Willing: J. Appl. Phys. **64** (1988) 1945.

[11] T. Ando: J. Phys. Soc. Jpn. **51** (1982) 3893.

[12] T. Ando: J. Phys. Soc. Jpn. **51** (1982) 3900.

[13] K. Hirakawa and H. Sakaki: Phys. Rev. **B33** (1986) 8291.

[14] T. Matsuoka, E. Kobayashi, K. Taniguchi, C. Hamaguchi and S. Sasa: Jpn. J. Appl. Phys. **29** (1990) 2017.

[15] H. Sakaki, T. Noda, K. Hirakawa, M. Tanaka and T. Matsusue: Appl. Phys. Lett. **51** (1987) 1934.

[16] F. Stern: Phys. Rev. Lett **44** (1980) 1469.

[17] J. Singh, K. K. Baja and S. Chaudhuri: Appl. Phys. Lett **44** (1984) 805.

# Chapter 6

# Conclusions

InGaAs-related III-V heterostructures with "(411)A super-flat interfaces" are expected to have a high potential for fabrication of low-noise and high-frequency devices with better performance. In order to know characteristics of pseudomorphic InGaAs-related III-V heterostructures grown on (411)A-oriented substrates, at first, structural and optical properties of pseudomorphic InGaAs/AlGaAs heterostructures grown on (411)A-oriented GaAs substrates by MBE were investigated with the use of low-temperature PL, HRXRD and AFM. Following results were obtained.

1. "(411)A super-flat interfaces" can be successfully formed in pseudomorphic InGaAs/AlGaAs QWs with In content up to 0.27. PL peaks from the (411)A $In_xGa_{1-x}As$/$Al_yGa_{1-y}As$ QWs ($y = 0.28$–$0.3$) with $L_w = 2.4$ nm (1.9 nm), which are very sensitive to interface roughness, are 30–40% smaller than those of the (100) QWs for $x$ up to 0.27 over a wafer-size area. (**3.1**)
2. An $In_{0.08}Ga_{0.92}As$/GaAs strained-layer superlattice (SLS) with (411)A super-flat interfaces exhibits superior crystalline quality. HRXRD measurements revealed that fluctuation of tilting angles of local crystal planes in the (411)A SLS was much reduced than that of a simultaneously grown (100) SLS, which is due to difference of relaxation of lattice-mismatch between InGaAs and GaAs layers for these two SLSs. PL properties of the (411)A and (100) SLSs also support these results of HRXRD measurements. (**3.2**)
3. Much larger critical thickness (approximately 20 nm) of a (411)A $In_{0.25}Ga_{0.75}As$ layer was observed compared with that ($\sim$ 12 nm) of a simultaneously grown (100)

$In_{0.25}Ga_{0.75}As$, which were determined by PL (11 K) FWHMs of $In_{0.25}Ga_{0.75}As$/$Al_{0.32}Ga_{0.68}As$ SQWs. We believe that this lager critical thickness should be another advantage of the (411)A pseudomorphic InGaAs/AlGaAs QWs besides the (411)A super-flat interfaces for device applications of this material. (**3.3**)

4. Enhanced In surface segregation during MBE growth of InGaAs was observed in (411)A InGaAs/(Al)GaAs SLSs and QWs by HRXRD and PL measurements compared with that of the (100) SLSs and QWs, which is probably due to larger surface migration of group III atoms. Much narrower PL linewidths of the (411)A QWs have almost no dependence on the substrate temperature, indicating that superior interface flatness does not degrade even if In surface segregation is enhanced by an increase in the substrate temperature. Therefore, In surface segregation uniformly proceeds in the (411)A growth-layer plane and (411)A super-flat InGaAs/AlGaAs interfaces can be formed at a wide substrate temperature range of $T_s$ = 450–540°C. (**3.4**)

In order to apply "(411)A super-flat interfaces" to InP-based InGaAs/InAlAs system grown on InP substrates, crystalline and optical properties of InGaAs and InAlAs epitaxial layers and InGaAs/InAlAs QWs lattice-matched to (411)A-oriented InP substrates by MBE were investigated with the use of low-temperature PL and HRXRD. Following results were obtained.

1. High-quality $In_xGa_{1-x}As$ layers ($0.505 \leq x \leq 0.545$) were successfully grown at $T_s$ = 480–520°C on (411)A InP substrates by MBE. Observed residual strain in the (411)A InGaAs layers by HRXRD measurements are well explained by the "constrained" model for a pseudomorphic layer grown on the high-index substrate. The observed PL FWHM (1.9 meV) of the (411)A InGaAs layer was almost the same as the optimum value (1.2–3.0 meV) reported so far for InGaAs layers grown on the (100) InP substrates. (**4.1**)
2. High substrate temperature is very important for (411)A InAlAs layers with featureless surface morphology and good crystalline quality. Linewidth of the PL peak from the (411)A InAlAs layer grown at $T_s$ = 570°C (10.7 meV) was 16–29% nar-

rower than those of conventional (100) InAlAs layers reported so far, indicating that high-quality InAlAs layers can be grown on (411)A InP substrates. (**4.2**)

3. "(411)A super-flat interfaces" were successfully formed in InGaAs/InAlAs QWs lattice-matched to (411)A InP substrates grown by MBE. Excellent surface morphology of the (411)A QWs observed at high substrate temperature shows that (411)A plane is more stable than (100) plane under MBE growth conditions. Single and narrow PL peaks were observed from the (411)A QWs over a large distance of 7 mm, and their linewidths are almost comparable to those of splitted PL peaks of the growth-interrupted (100) QWs. (**4.3**)
4. Heterointerface flatness in the (411)A InGaAs QWs can be improved by using $(InGaAs)_2(InAlAs)_m$ SPS barriers ($m \leq 4$) instead of 23 nm thick InAlAs barriers. Linewidths of PL (12 K) peaks from (411)A InGaAs/InAlAs QWs grown at a low $T_s$ of 480°C were significantly degraded due to rough growing surfaces of 23 nm thick InAlAs barriers, while much narrow PL linewidths were observed from (411)A InGaAs/$(InGaAs)_2(InAlAs)_2$ QWs grown even at $T_s$ = 480°C. PL FWHMs of the (411)A InGaAs/$(InGaAs)_2(InAlAs)_m$ QWs grown at $T_s$ = 540°C were the same as those of the (411)A InGaAs/InAlAs QWs for m = 6 and 8, while the PL FWHMs were slightly improved for m = 2 and 4. (**4.4**)

Based on the results as mentioned above, the pseudomorphic $In_{0.7}Ga_{0.3}As$/$In_{0.52}Al_{0.48}As$ MD-QWs with "(411)A super-flat interfaces" were successfully grown on InP substrates by MBE. (Chapter **5**) Higher 2DEG mobilities were observed in the (411)A MD-QWs with well widths of $L_w$ = 12–18 nm compared with the corresponding (100) MD-QWs due to (1) the (411)A super-flat interfaces for $L_w$ = 12–16 nm and (2) larger critical thickness of the (411)A $In_{0.7}Ga_{0.3}As$ for $L_w$ = 18 nm. The 2DEG in the (411)A MD-QW with $L_w$ = 12 nm shows 27% higher mobility ($\mu$ = 108,000 $cm^2/Vs$) with 2DEG concentration of $1.5 \times 10^{12}$ $cm^{-2}$ at T = 77 K than that ($\mu$ = 85,000 $cm^2/Vs$) of the corresponding (100) MD-QW in this study, and the $\mu$ of the (411)A MD-QW is the highest mobility in the previously reported ones. The low-temperature (24 K) 2DEG mobilities were analyzed by calculated mobilities taking into account of ionized impurity scatter-

ing, alloy disorder scattering and interface roughness scattering by using self-consistent results of the MD-QWs. Enhanced 2DEG mobility in the (411)A MD-QWs can be well explained by reduced interface roughness scattering, and parameter values of interface roughness (height $\Delta = 0.25$ nm and lateral size $\Lambda = 5$ nm) used in the 2DEG mobility calculation are good agreement with PL data at 4.2 K of undoped-InGaAs/InAlAs QWs with the (411)A super-flat interfaces.

These results indicate that the (411)A super-flat interfaces can be successfully formed not only in pseudomorphic InGaAs/AlGaAs heterostructures but also in InGaAs/InAlAs system lattice-matched to InP. These InGaAs-related III-V heterostructures grown on (411)A-oriented substrates have a high potential for fabrication of novel quantum devices such as HEMTs because of their superior physical properties due to effectively atomically flat heterointerfaces over a wafer-size area.

# Acknowledgments

The author would like to express the sincerest gratitude to Professor Satoshi Hiyamizu for the thoughtful guidance, the warm encouragement and for offering the wonderful opportunity. He would like to thank especially Associate Professor Satoshi Shimomura for the helpful and thoughtful discussions and the warm encouragement.

He wishes to express deep thanks to Professor Hisao Nakashima and Professor Naoshi Suzuki for their critical reading of the manuscript.

He wishes to express his thanks to Dr. Nobuyuki Tomita, Dr. Keisuke Shinohara and Dr. Masataka Higashiwaki for the interesting and thoughtful discussions. His special thanks are also given to all collaborators, Mr. Tatsuya Saeki, Mr. Masanobu Ohashi, Mr. Keisuke Nii, Mr. Masato Ueno, Mr. Tetsuya Hiraoka, Mr. Toyohiro Aoki and Mr. Naoki Saka for their assistance on the experiment. All members in Hiyamizu Laboratory are thanked for their help and supportive atmosphere. He also would like to express his deep thanks to Ms. Ikuko Uchida for her hearty supports and all members in Department of Physical Science for their encouragement.

He is indebted to Mr. Shinya Tsujikura and Mr. Seiji Ikawa in Kubota Corporation for their technical supports in PL measurements.

He is grateful to Professor Naokatsu Sano in Kwansei-Gakuin University.

This work is supported in part by a Grant-in-Aid for Scientific Research (A) from the Ministry of Education, Science, Sports and Culture.

Finally, he would like to express his special thanks to all of his family for the warm encouragement.

# Publication list

1. "Extremely flat interfaces in $In_xGa_{1-x}/Al_{0.3}Ga_{0.7}As$ quantum wells grown on (411)A GaAs substrates by molecular beam epitaxy"

   T. Saeki, T. Motokawa, T. Kitada, S. Shimomura, A. Adachi, Y. Okamoto, N. Sano and S. Hiyamizu:

   Jpn. J. Appl. Phys. **36** (1997) 1786.

2. "Super-flat interfaces in $In_{0.53}Ga_{0.47}As/In_{0.52}Ga_{0.48}As$ quantum wells grown on (411)A InP substrates by molecular beam epitaxy"

   T. Kitada, T. Saeki, M. Ohashi, S. Shimomura, A. Adachi, Y. Okamoto and S. Hiyamizu:

   J. Electron. Mater. **27** (1998) 1043.

3. "Extremely uniform $In_{0.08}Ga_{0.92}As$/GaAs superlattice grown on (411)A GaAs substrate by molecular beam epitaxy"

   T. Kitada, T. Saeki, M. Ohashi, S. Shimomura and S. Hiyamizu:

   Solid-State Electron. **42** (1998) 1575.

4. "Super-flat interfaces in pseudomorphic $In_xGa_{1-x}/Al_{0.3}Ga_{0.7}As$ quantum wells with high In contents ($x = 0.15$) grown on (411)A GaAs substrates by molecular beam epitaxy"

   M. Ohashi, T. Saeki, T. Kitada, S. Shimomura, Y. Okamoto and S. Hiyamizu:

   Jpn. J. Appl. Phys. **37** (1998) 4515.

5. "High-quality InGaAs layers grown on (411)A-oriented InP substrates by molecular beam epitaxy"

   T. Kitada, M. Ohashi, S. Shimomura and S. Hiyamizu:

   Jpn. J. Appl. Phys. **38** (1999) 1888.

6. "Larger critical thickness determined by photoluminescence measurements in pseudomorphic $In_{0.25}Ga_{0.75}As/Al_{0.32}Ga_{0.68}As$ quantum wells grown on (411)A GaAs substrates by molecular beam epitaxy"

   K. Nii, R. Kuriyama, T. Hiraoka, T. Kitada, S. Shimomura and S. Hiyamizu:

   to be published in J. Vac. Sci. & Technol. **B** (1999).

7. "High-quality InAlAs layers grown on (411)A-oriented InP substrates by molecular beam epitaxy"

   T. Kitada, K. Nii, T. Hiraoka, S. Shimomura and S. Hiyamizu:

   to be published in J. Vac. Sci. & Technol. **B** (1999).

**Related papers**

1. "Lateral variation of indium content in InGaAs grown on GaAs channeled substrates by molecular beam epitaxy"

   A. Wakejima, A. Inoue, T. Kitada, N. Tomita, S. Shimomura, M. Fujii, T. Yamamoto, K. Kobayashi, N. Sano and S. Hiyamizu:

   J. Vac. Sci. & Technol. **B12** (1994) 1102.

2. "Preferential migration of indium atoms on the (411)A plane in InGaAs grown on GaAs channeled substrates by molecular beam epitaxy"

   T. Kitada, A. Wakejima, N. Tomita, S. Shimomura, A. Adachi, N. Sano and S. Hiyamizu:

   J. Cryst. Growth **150** (1995) 487.

3. "Much improved interfaces in GaAs/AlAs quantum wells grown on (411)A GaAs substrates by molecular beam epitaxy"

   S. Shimomura, K. Shinohara, T. Kitada, Y. Tsuda, A. Adachi, Y. Okamoto, N. Sano and S. Hiyamizu:

   J. Vac. Sci. & Technol. **B13** (1995) 696.

4. "Extremely flat interfaces in $In_{0.04}Ga_{0.96}As/Al_{0.3}Ga_{0.7}As$ quantum wells grown on (411)A $In_{0.04}Ga_{0.96}As$ substrates by MBE"

   S. Hiyamizu, T. Saeki, T. Motokawa, S. Shimomura, T. Kitada, A. Adachi, Y. Okamoto, T. Kusunoki, K. Nakajima and N. Sano:

Superlattices and Microstructures **21** (1997) 107.

5. "GaAs/$GaAs_{0.8}P_{0.2}$ quantum wells grown on ($n$11)A GaAs substrates by molecular beam epitaxy"

   Y. Tatsuoka, H. Kamimoto, Y. Kitano, T. Kitada S. Shimomura and S. Hiyamizu: to be published in J. Vac. Sci. & Technol. **B** (1999).

**International conference**

1. "Preferential migration of indium atoms on the (411)A plane in InGaAs grown on GaAs channeled substrates by molecular beam epitaxy"

   T. Kitada, A. Wakejima, N. Tomita, S. Shimomura, A. Adachi, N. Sano and S. Hiyamizu:

   8th International Conference on Molecular Beam Epitaxy (MBE-8), Osaka, Japan, August (1994).

2. "Much improved interfaces in GaAs/AlAs quantum wells grown on (411)A GaAs substrates by molecular beam epitaxy"

   S. Shimomura, K. Shinohara, T. Kitada, Y. Tsuda, A. Adachi, Y. Okamoto, N. Sano and S. Hiyamizu:

   14th North American Conference on Molecular Beam Epitaxy (NAC-MBE), Illinois, USA, October (1994).

3. "Extremely flat interfaces in $In_{0.04}Ga_{0.96}As/Al_{0.3}Ga_{0.7}As$ quantum wells grown on (411)A $In_{0.04}Ga_{0.96}As$ substrates by MBE"

   S. Hiyamizu, T. Saeki, T. Motokawa, S. Shimomura, T. Kitada, A. Adachi, Y. Okamoto, T. Kusunoki, K. Nakajima and N. Sano:

   9th International Conference on Superlattices, Microstructures and Microdevices, Liege, Belgium, July (1996).

4. "Extremely flat interfaces in $In_xGa_{1-x}/Al_{0.3}Ga_{0.7}As$ quantum wells grown on (411)A GaAs substrates by MBE"

   T. Saeki, T. Motokawa, T. Kitada, S. Shimomura, A. Adachi, Y. Okamoto, N. Sano and S. Hiyamizu:

   1996 International Conference on Solid State Devices and Materials (SSDM'96), Yokohama, Japan, August (1996).

5. "Super-flat interfaces in $In_{0.53}Ga_{0.47}As/In_{0.52}Ga_{0.48}As$ quantum wells grown on (411)A InP substrates by molecular beam epitaxy"

   T. Kitada, T. Saeki, M. Ohashi, S. Shimomura, A. Adachi, Y. Okamoto and S. Hiyamizu:

1997 Electronic Materials Conference (EMC'97), Colorado, USA, June (1997).

6. "Extremely uniform $In_{0.08}Ga_{0.92}As$/GaAs superlattice grown on (411)A GaAs substrate by molecular beam epitaxy"
   T. Kitada, T. Saeki, M. Ohashi, S. Shimomura and S. Hiyamizu:
   International Workshop on Nano-Physics and Electronics (NPE'97), Tokyo, Japan, September (1997).
7. "GaAs/$GaAs_{0.8}P_{0.2}$ quantum wells grown on ($n$11)A GaAs substrates by molecular beam epitaxy"
   Y. Tatsuoka, H. Kamimoto, Y. Kitano, T. Kitada S. Shimomura and S. Hiyamizu:
   17th North American Conference on Molecular Beam Epitaxy (NAC-MBE), Pennsylvania, USA, October (1998).
8. "Critical thickness of pseudomorphic $In_{0.25}Ga_{0.75}As/Al_{0.32}Ga_{0.68}As$ quantum wells grown on (411)A GaAs substrates by molecular beam epitaxy"
   K. Nii, R. Kuriyama, T. Hiraoka, T. Kitada, S. Shimomura and S. Hiyamizu:
   17th North American Conference on Molecular Beam Epitaxy (NAC-MBE), Pennsylvania, USA, October (1998).